ROTOR DOWNWASH VELOCITIES ABOUT THE UH-1M HELICOPTER - FLIGHT TEST MEASUREMENTS AND THEORETICAL CALCULATIONS

B. Z. Jenkins, et al

Army Missile Research, Development and Engineering Laboratory
Redstone Arsenal, Alabama

1 January 1975

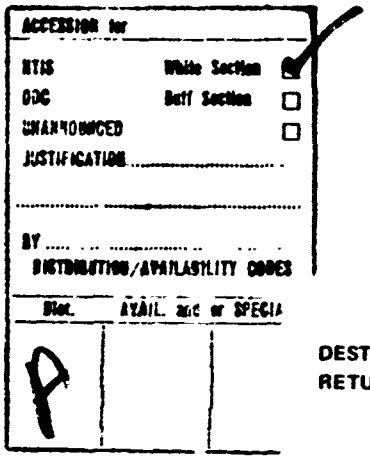

DISPOSITION INSTRUCTIONS

DESTROY THIS REPORT WHEN IT IS NO LONGER NEEDED. DO NOT RETURN IT TO THE ORIGINATOR.

DISCLAIMER

THE FINDINGS IN THIS REPORT ARE NOT TO BE CONSTRUED AS AN OFFICIAL DEPARTMENT OF THE ARMY POSITION UNLESS SO DESIGNATED BY OTHER AUTHORIZED DOCUMENTS.

TRADE NAMES

USE OF TRADE NAMES OR MANUFACTURERS IN THIS REPORT DOES NOT CONSTITUTE AN OFFICIAL INDORSEMENT OR APPROVAL OF THE USE OF SUCH COMMERCIAL HARDWARE OR SOFTWARE.

UNCLASSIFIED

SECURITY CLASSIFICATION OF THIS PAGE (When Data Entered)

REPORT DOCUMENTATION PAGE

READ INSTRUCTIONS BEFORE COMPLETING FORM

1. REPORT NUMBER: RD-75-27	2. GOVT ACCESSION NO.
3. RECIPIENT'S CATALOG NUMBER: AD-A008 965	
4. TITLE (and Subtitle): ROTOR DOWNWASH VELOCITIES ABOUT THE UH-1M HELICOPTER - FLIGHT TEST MEASUREMENTS AND THEORETICAL CALCULATIONS	5. TYPE OF REPORT & PERIOD COVERED: Technical Report
	6. PERFORMING ORG. REPORT NUMBER: RD-75-27
7. AUTHOR(s): B. Z. Jenkins and S. Marks	8. CONTRACT OR GRANT NUMBER(s): (DA) 1M262303A214 AMCMS Code 232303.11.21405
9. PERFORMING ORGANIZATION NAME AND ADDRESS: Commander, US Army Missile Command, Attn: AMSMI-RD, Redstone Arsenal, Alabama 35809	10. PROGRAM ELEMENT, PROJECT, TASK AREA & WORK UNIT NUMBERS
11. CONTROLLING OFFICE NAME AND ADDRESS	12. REPORT DATE: 1 January 1975
	13. NUMBER OF PAGES: 107
14. MONITORING AGENCY NAME & ADDRESS(if different from Controlling Office)	15. SECURITY CLASS. (of this report): UNCLASSIFIED
	15a. DECLASSIFICATION/DOWNGRADING SCHEDULE

16. DISTRIBUTION STATEMENT (of this Report)

Approved for public release; distribution unlimited.

17. DISTRIBUTION STATEMENT (of the abstract entered in Block 20, if different from Report)

18. SUPPLEMENTARY NOTES

19. KEY WORDS (Continue on reverse side if necessary and identify by block number)

Downwash velocity data
UH-1M helicopter
Rotor wake
Anenometers

20. ABSTRACT (Continue on reverse side if necessary and identify by block number)

Downwash velocity data from a flight test of the UH-1M helicopter are presented in comparison with calculated values. Hot film anenometers were used to measure flow velocities at five points in the downwash for a variety of aircraft forward velocities and hover. The theoretical predictions were made using a mathematical model of sources and sinks to simulate the fuselage and vortex filaments to simulate the rotor wake. Problems peculiar to the flight test are discussed.

DD FORM 1 JAN 73 1473 EDITION OF 1 NOV 65 IS OBSOLETE

UNCLASSIFIED

SECURITY CLASSIFICATION OF THIS PAGE (When Data Entered)

CONTENTS

1. Introduction

The requirement to achieve high accuracy with free rockets fired from rotary wing aircraft has been thwarted to a great extent by launch transients attributable to the aircraft. These transients, principally vibration, rotor downwash, and translation and rotation of the launch platform, have not been properly investigated as sources of rocket dispersion. In an effort to assess the importance of rotor downwash on the dynamics of the round during its first few feet of flight, an experiment to survey the induced velocity field about a helicopter in flight was planned. Knowing the properties of the environment which the rocket must traverse, one may then use aerodynamic forces derived therefrom in simulating the rocket's trajectory. The flight test plan called for a detailed velocity survey near the helicopter for a variety of flight and vehicle conditions. This survey was to cover the region through which missiles launched from the helicopter must fly. Computer codes also exist which are intended to provide a theoretical capability to define the helicopter downwash fluid mechanical properties. One such code is currently in use at MICOM and has been used to evaluate the effect of downwash on rocket motion. The flight test also serves as a means of substantiating (or refuting) the accuracy of the computer program. This report is intended as a concise presentation of the flight test results and a comparison with theory as predicted by the computer code in use at MICOM. Reference 1 presents in great detail the flight test results, instrumentation, and procedure.

2. Description of Experiments

The position of the boundaries of the rotor wake is strongly influenced by the aircraft's airspeed. For rockets launched from the helicopter in a conventional fashion, there exists a maximum airspeed for which the rotor downwash intersects the rocket's flight path. It was desirable to determine these downwash boundaries as a function of forward velocity before proceeding with the velocity survey in order to more efficiently allocate the flight time available to meaningful explorations, and to better interpret the measurements once completed. This wake boundary survey was conducted in April 1973 and the results are compared with theory in this report.

Virtually all the experimental data presented here can also be found in reference 1. Some is repeated here for completeness or comparison purposes and so that a more detailed representation can be seen.

a. Aircraft and Range

The flight tests were carried out by the US Army Aviation Engineering Flight Activity located at Edwards Air Force Base, California. Based primarily on aircraft availability, a UH-1M helicopter was selected as the test vehicle. A drawing of the aircraft showing the coordinate system used is presented in Figure 1.

b. Instrumentation and Procedure

The wake boundary surveys were made using an Elliott dual-axis low airspeed system. The Elliott system was mounted at Y = -65, Z = 29 for various X positions and at Y = -65, Z = 88 for various X positions. The flow angularity in the helicopter pitch plane was noted for various forward speeds of the aircraft. As the foremost boundary of the rotor wake passed the Elliott probe a pronounced change in the flow angularity occurred, allowing one to determine the X coordinate of the wake boundary as a function of airspeed for two outboard stations. This function is presented in Figure 2. It is seen that the weapon mount location, typically forward of fuselage station 120, will be free of downwash effects for true airspeeds greater than 45 feet per second.

The flow field velocity survey was carried out using an array of seven split film 3-component anemometers mounted linearly on a lateral rack (Figures 1 and 3) 8.5 inches apart. Plans were to make successive flights, repositioning the rack between flights until the entire volume of interest had been covered. During each flight a number of data records were to be taken at a predetermined set of flight conditions. The appendix briefly lists the instrumentation and data conditioning and collecting procedure. Complete descriptions and specifications are given in reference 1.

No further details will be given here concerning the complete test plan because the survey was conducted at the first rack position only. Due to the adverse vibration environment, the sensors failed on the first flight and the test progressed no further. The probe locations for the first rack position are given in Table 1. During this test flight, data were taken for a variety of forward velocities. Table 2 presents a summary of the 15 data records taken. As Table 1 indicates, only five of the seven sensors were fully operative throughout the flight.

TABLE 1. PROBE LOCATIONS

Probe No.	X (in.)	Y (in.)	Z (in.)	Comments
1	111.885	-109.56	58.928	
2	111.885	-101.06	58.928	Operative in one axis only
3	111.885	-92.56	58.928	
4	111.885	-84.06	58.928	
5	111.885	-75.56	58.928	Inoperative
6	111.885	-67.06	58.928	
7	111.885	-58.56	58.928	Data noisy (perhaps due to turbulence)

TABLE 2. FLIGHT RECORD SUMMARY

Flight Record	VF (ft/sec)	Aircraft Gross wt (lb)	α_T (deg)	$\frac{\rho}{\rho_0}$	Velocity-time data included in this report
1	152.2	7495	5.44	0.839	√
2	153.5	7494	5.54	0.839	
3	136.5	7483	4.10	0.840	√
4	132.7	7480	4.52	0.839	
5	112.8	7474	1.38	0.841	√
6	113.7	7470	1.35	0.843	
7	92.5	7456	1.00	0.841	√
8	93.1	7454	1.04	0.841	
9	73.8	7439	5.07	0.838	√
10	54.5	7410	-2.52	0.838	
11	54.0	7418	-2.40	0.838	√
*					
13	7.7	7374	0.4	0.832	√
14	19.3	7359	-0.3	0.832	
15	17.9	7355	-0.2	0.832	√

Rotor speed - 324 rpm

*Flight Record 12 was unusable due to flight transients

c. Experimental Results

Velocity-time curves for each component, sensor, and flight record are presented for the entire measurement interval in reference 1. This time interval is large compared to the period of the fluctuating velocity, making it hard to distinguish details of the curve shape over only one period (≈ 0.095 second). Figures 4 through 36 depict the velocity-time curves for selected flight records through only six periods. When two flight records were taken at practically the same velocity, only one is shown (Table 2). In these graphs, the scatter in data, repeatability from cycle to cycle, and variability of data quality from flight record to flight record are readily seen. In one case, flight record number 1, the behavior of the signals for sensor number 7 are shown. It has been suggested that the dispersion occurring in data from sensor number 7 is due to turbulence caused by being near the fuselage. Data from the inoperative sensors, numbers 2 and 5, are not presented.

3. Description of Analytical Technique

The computer program being used at MICOM and the analysis upon which it is based are described in references 3, 4, and 5. Basically, the resultant flow in the domain of interest is assumed to be a superposition of three elements: the freestream, the fuselage represented by a distribution of sources and sinks, and the rotor wake represented by line vortices shed from each blade. Obviously, the representation of the fuselage and the representation of the rotor downwash are interdependent and both should be periodic functions of time. In the program, the initial representation of the wake is chosen to be helical (one for each blade) and slanted aft in accordance with momentum theory. The fuselage representation is initially taken to be that resulting from the freestream only. The rotor representation is then advanced by marching timewise for several revolutions of the rotor. The fuselage representation is then recalculated using the time average values for the downwash effect in accounting for flow nonuniformity. This procedure is then repeated until a nearly periodic flow is established - usually approximately four complete passes. It is seen that the solution found is not completely interactive - the fuselage representation resulting is the one that would result from the time average of the periodic flow. The influence of the fuselage is relatively small compared to the other sources and this shortcoming is not very important. There is another shortcoming which is potentially more serious. The shed vortex sheet from all along the blades is ignored or lumped into the vortex filaments being shed by the blade tips. More recent downwash simulation programs which account for this effect indicate that it is quite important.

4. Comparison of Theory and Experiment

Theoretical simulations were carried out for flight records 1, 10, 13, and 15 corresponding to airspeeds of 152.2, 54.5, 7.7, and 17.9 feet per second respectively. Because each computer run requires approximately 30 minutes of CDC 6600 computer time, four simulations were deemed sufficient.

One of the critical input variables is the incidence of the rotor tip path plane to the freestream (α_T). This quantity varies with airspeed and aircraft weight and center of gravity location and was not directly measured during the experiment but inferred from aircraft attitude measurements. Since rotor flapping angle was not measured, the angle of the tip plane relative to the aircraft coordinate system was unknown. For the values of α_T derived from experiment, the flapping angle was assumed to be zero; therefore, α_T may be in error by the amount of the true flapping angle. If one uses the available data for aircraft weight and drag, α_T may be calculated by balancing forces at the rotor hub. The comparison of the values obtained in these two different ways

is presented in Figure 37. We may then expect to find disagreements between theory and experiment which correspond to up to 4 degrees of flow incidence in the pitch plane.

a. Wake Boundaries

Wake boundaries were determined from all but the highest speed simulation. Instead of examining flow angularity at a given point as a function of airspeed, as described in Paragraph 2, flow angularity was plotted as a function of X (with Y and Z constant) at a given velocity. Either way, an abrupt change in pitch plane flow angle indicates passage of the wake leading boundary and from this wake boundary station (X) can be crossplotted as a function of airspeed. The points found by applying the theory are indicated in Figure 2 together with the experimental data.

b. Time Dependent Data Comparison

Velocity-time data were calculated for each of the seven sensor positions and for each of the four simulations. Comparisons are shown in Figures 38 through 88 for the sensors which were fully operational, numbers 1, 3, 4, and 6. For flight record 13, sensor number 7 is also included. Since the period of the velocity fluctuations is governed by the rotation of the rotor, the time coordinate was replaced with rotor position. For a two-bladed rotor, such as that of the UH-1M, each blade contributes to the flow velocity experienced by a point in the wake, therefore, the period is 2 per revolution or 180 degrees of rotation of the rotor. Instead of plotting rotor position as an ever increasing angle for successive periods, it was plotted modulo 180 degrees. In this way all the periods are superimposed on each other in the same 0 to 180 degree range. This is called a folded plot. For flight record 1, the absolute value of rotor position was measured with 0 and 180 degrees corresponding to alignment of the rotor with the fuselage centerline. This measurement subsequently became inoperative; therefore, for flight records 10, 13, and 15, the experimental values for rotor position are known relative to each other but not with respect to any reference position as was the case for flight record 1. As a result, in comparing theory with experiment using Figures 38 through 88, one must realize that theory and experiment can be arbitrarily displaced relative to each other along the abscissa for flight records 10, 13, and 15.

During the course of the experiment, the rotational velocity of the rotor was nominally 324 rpm which would correspond to a period of 0.0926 second. However, in plotting the folded data it was found that slightly higher values for the period gave much better results, in that there was less scatter in the data. The value used for the period is indicated on each graph of Figures 38 through 88.

Instead of plotting flow velocity components along the three coordinate axes (Figures 4 through 36), velocity magnitude and direction are

shown in Figures 38 through 88. θ_Y and θ_Z are the angles between the flow velocity vector and the Y and Z axes respectively. In this manner differences in flow direction between theory and experiment are put in proper perspective whereas in plotting VX, VY, and VZ a small error in flow direction can overwhelm a small component, such as VY, making it scattered to the point of being useless.

c. Time Averaged Data

In many cases the frequency of the flow fluctuation ($\approx$ 10 Hz) is high enough that objects of interest which are immersed in the flow cannot respond to it. In this case time dependent details of the wake flow can be ignored and the time averaged flow velocity and direction can be used to determine the behavior of the object.

For each of the four flight records simulated, theoretical and experimental flow magnitude and direction were time averaged and plotted as a function of Y for fixed X and Z locations corresponding to the sensor rack position (Figure 89). Gaps in the experimental data correspond to positions of the malfunctioning sensors numbers 2, 5, and 7.

5. Conclusions and Recommendations

Based upon experience gained from the flight test discussed, new experiments will be run which should achieve what this one did not, a complete survey of the flow field about the helicopter traversed by air launched weapons. In these new experiments, a rotor position and blade flapping angle will be determined to make valid comparisons. The planned flight tests will be conducted on the Cobra helicopter which is the Army's attack helicopter.

The comparisons presented here are inconclusive. Although it is certain that the analytical model needs improvement, it is also quite likely that differences between theory and experiment reflect, to a certain degree, errors in measurement. Until an improved prediction capability is available, the results of the program in use should be better than stream tube approximations.

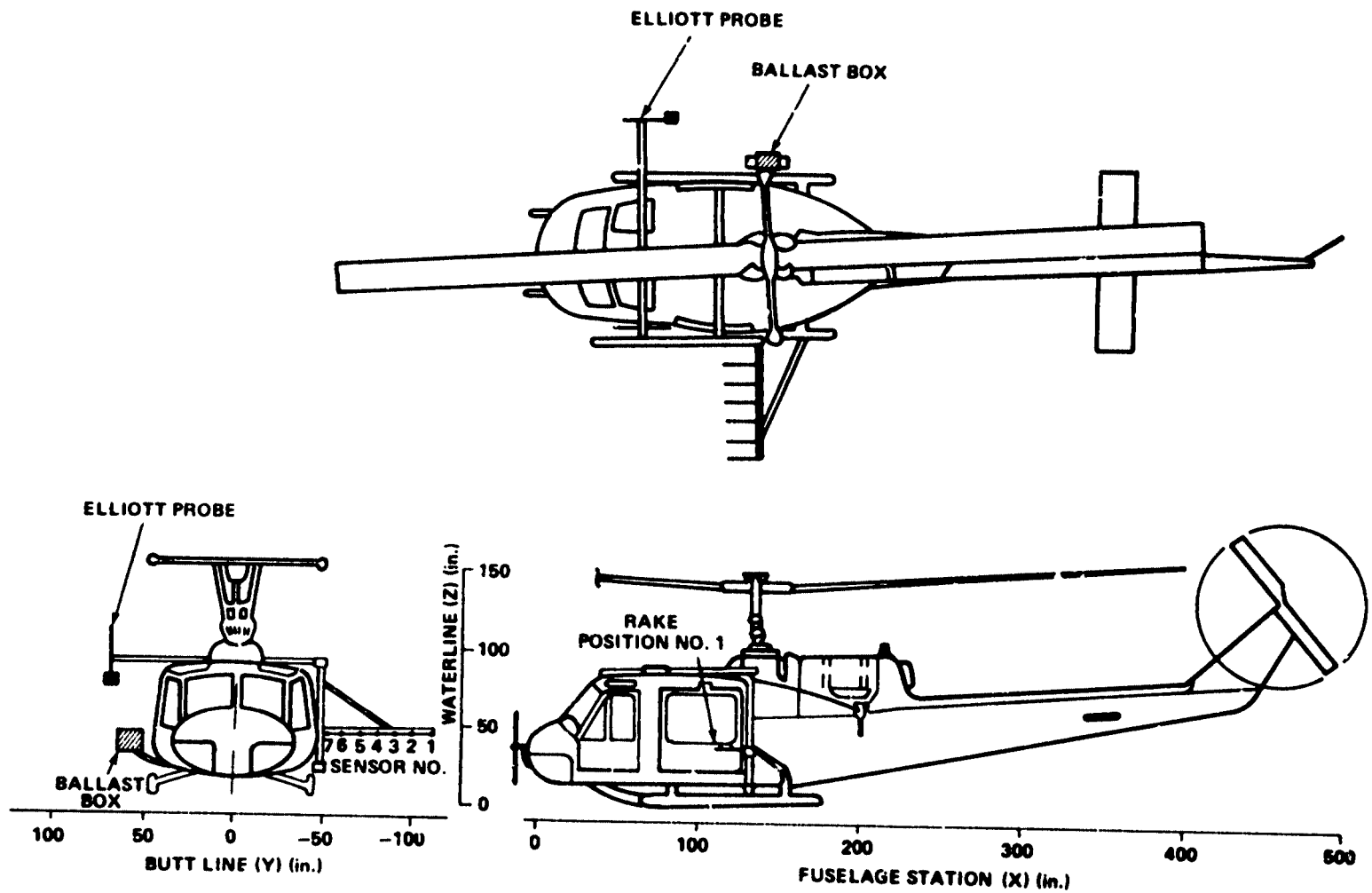

Figure 1. Aircraft coordinate system and probe installation.

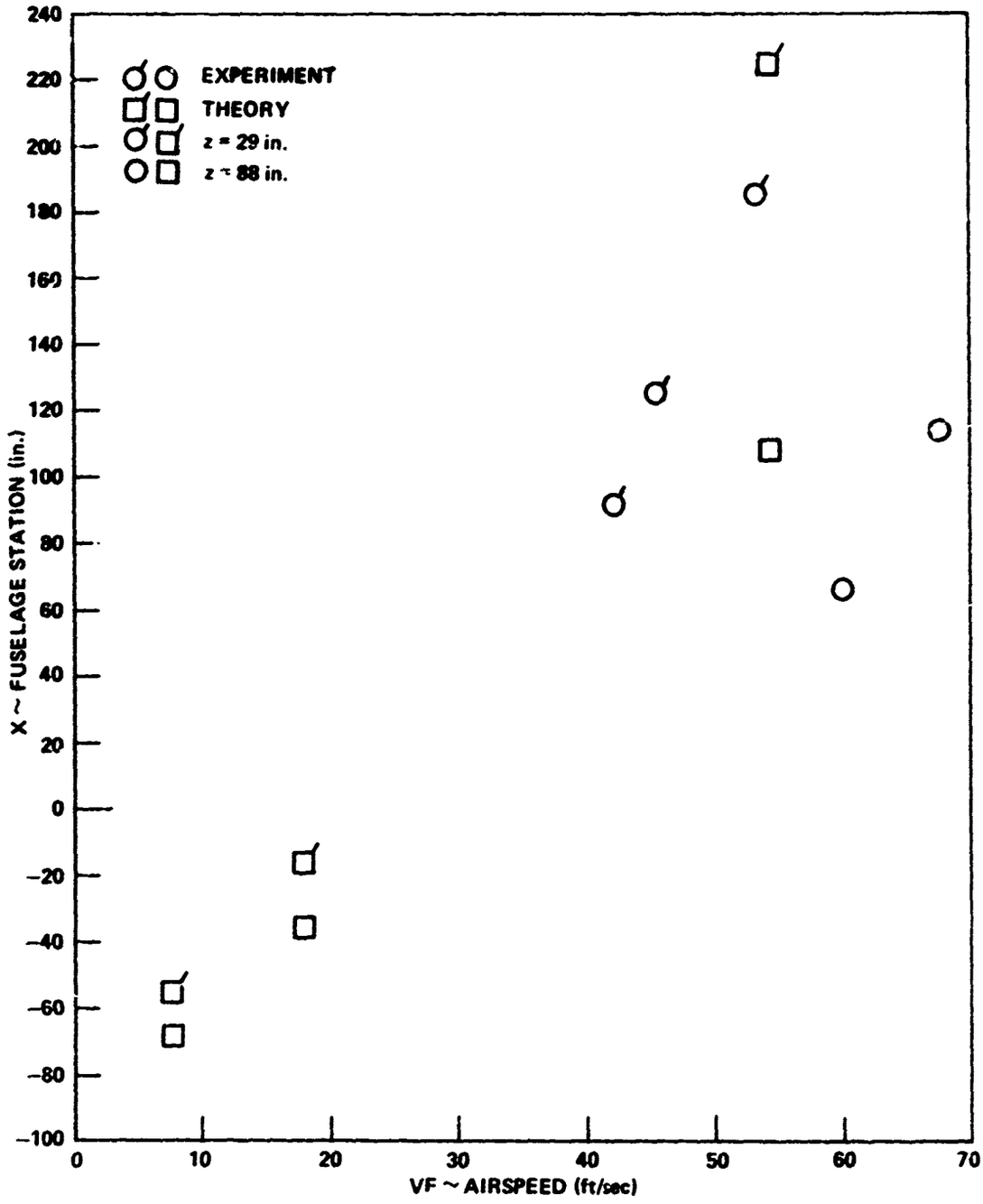

Figure 2. Rotor wake boundary in forward flight for buttline (Y) = -65 inches.

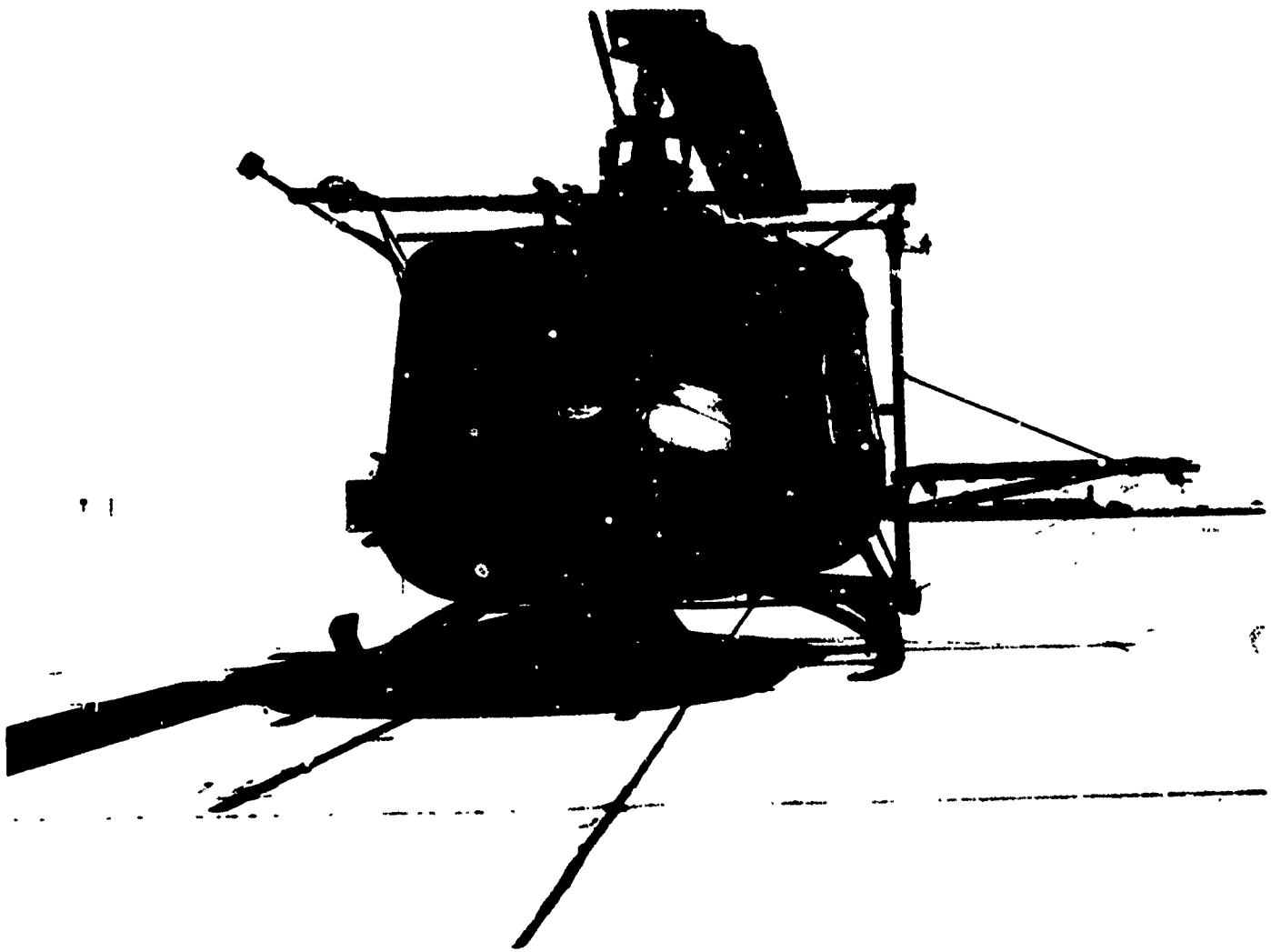

Figure 3. Aircraft with sensor rack in place.

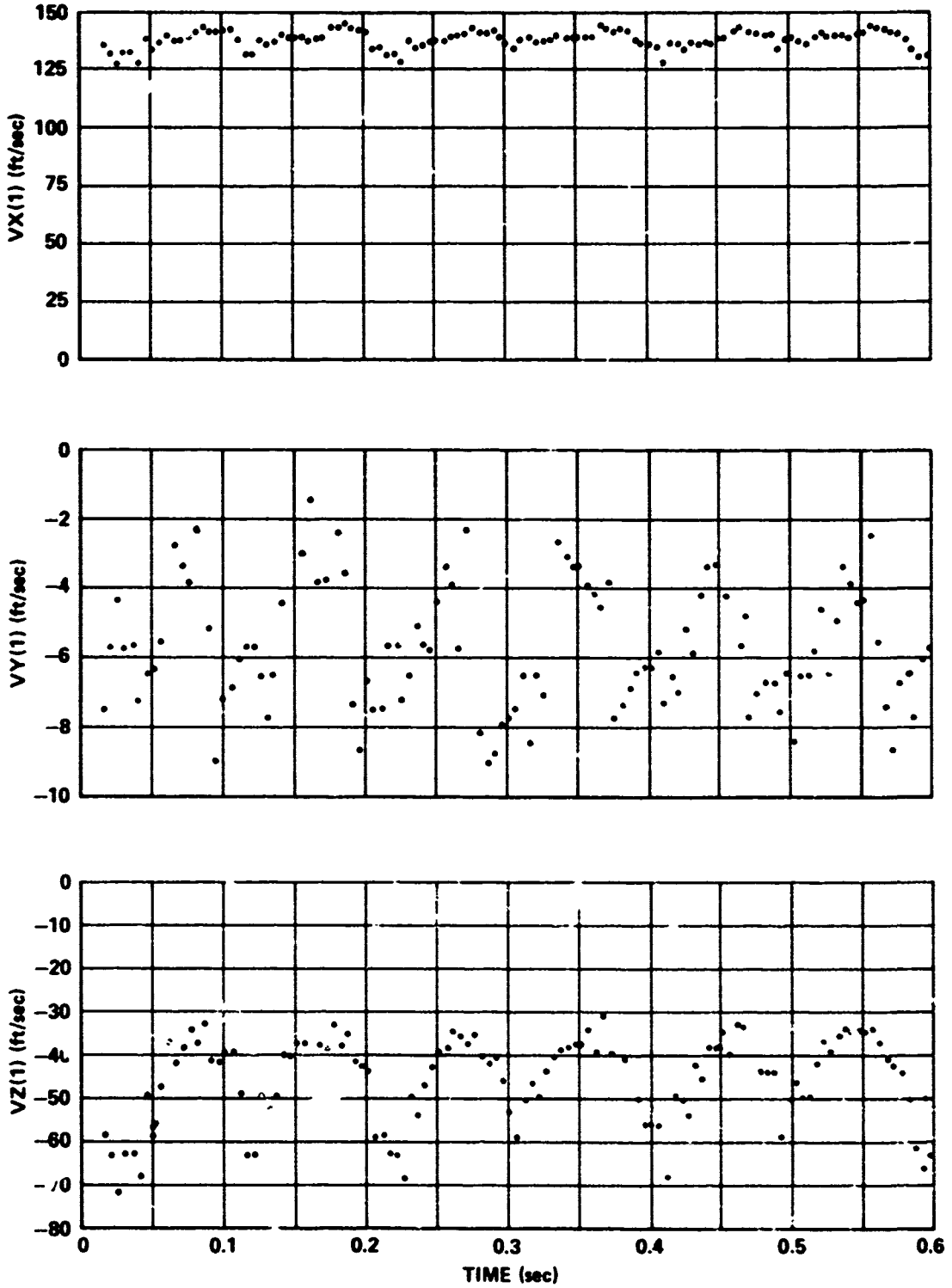

Figure 4. UH-1M helicopter flow field velocity components - flight record 1 and sensor No. 1.

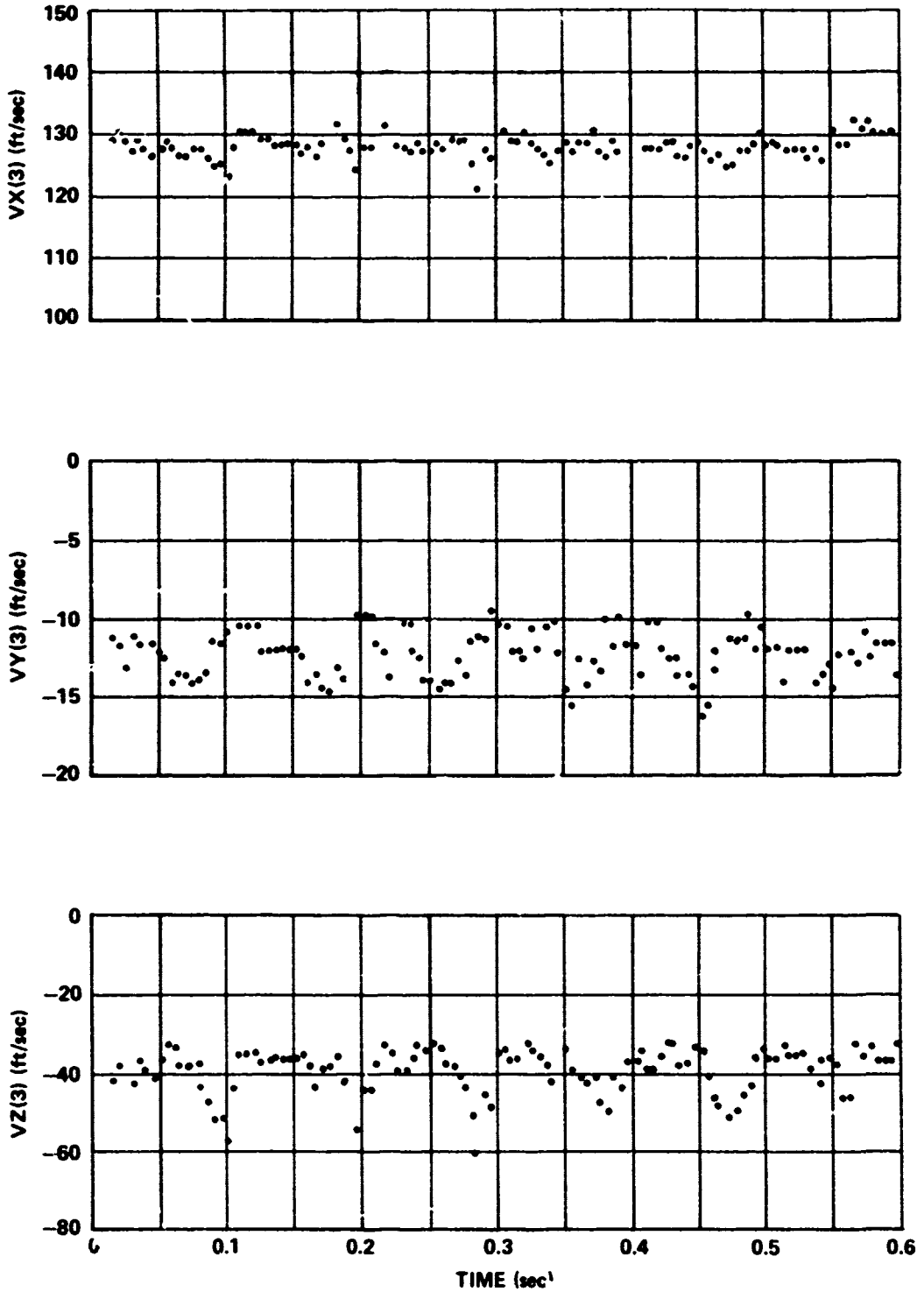

Figure 5. UH-1M helicopter flow field velocity components - flight record 1 and sensor No. 3.

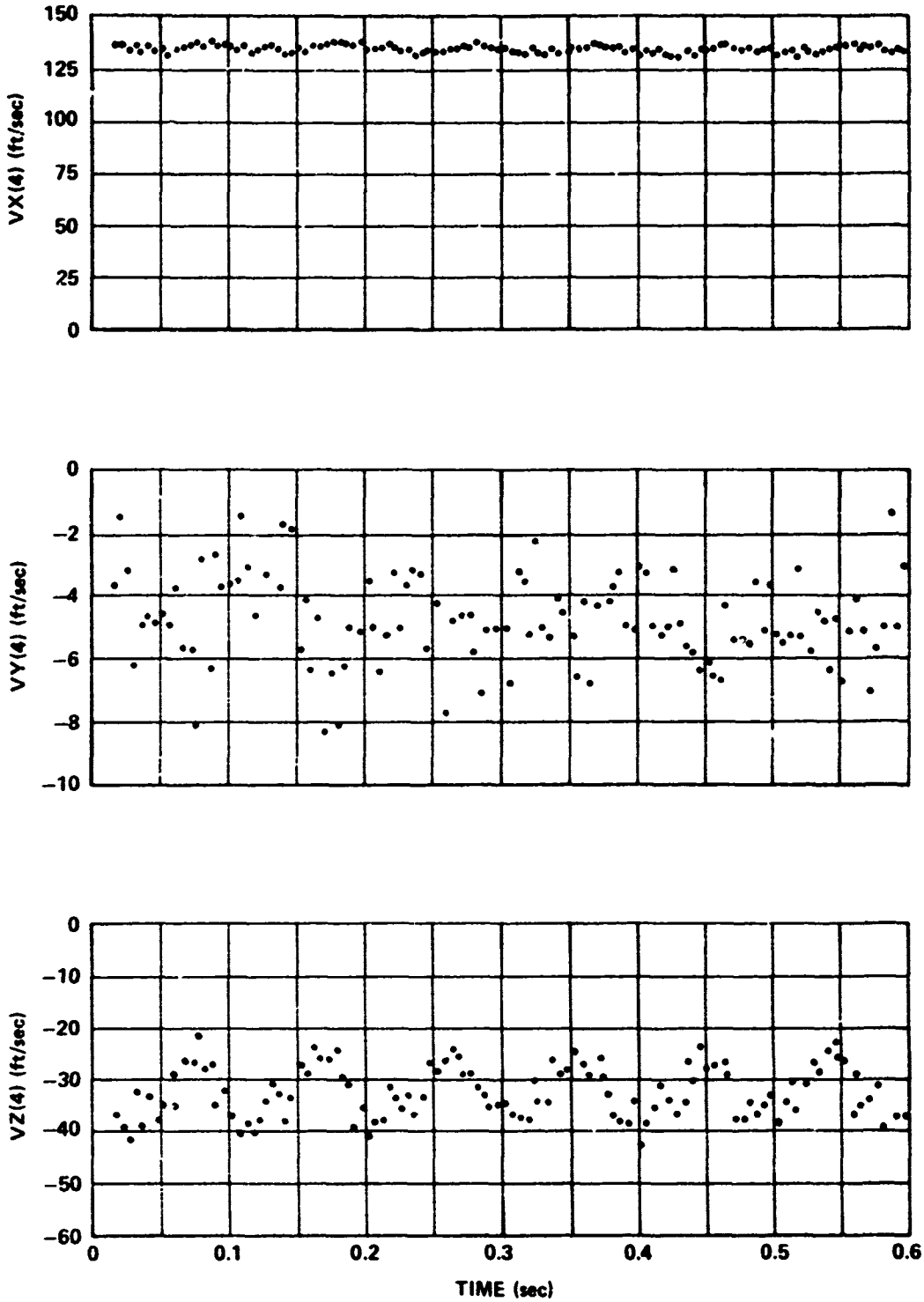

Figure 6. UH-1M helicopter flow field velocity components - flight record 1 and sensor No. 4.

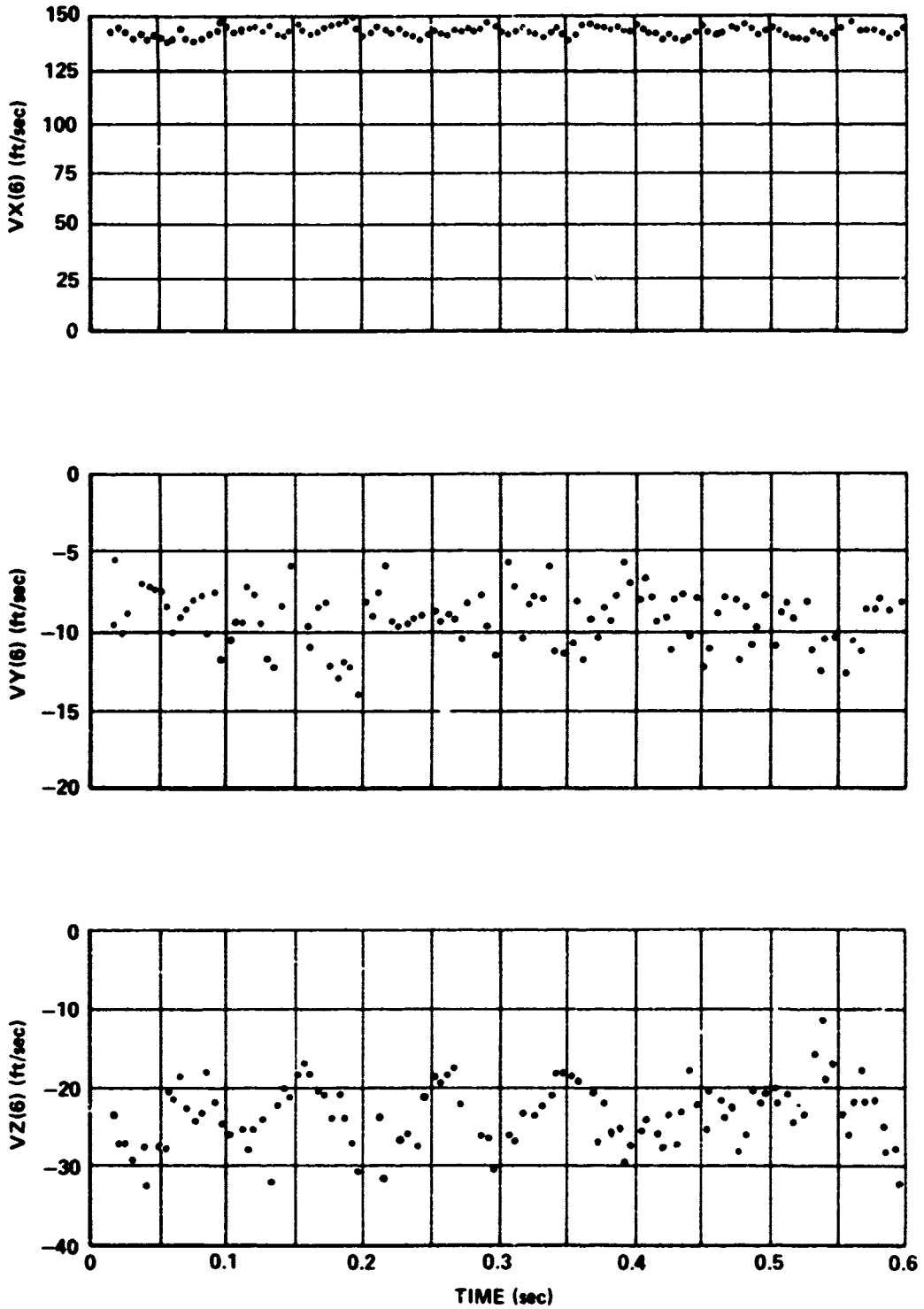

Figure 7. UH-1M helicopter flow field velocity components - flight record 1 and sensor No. 6.

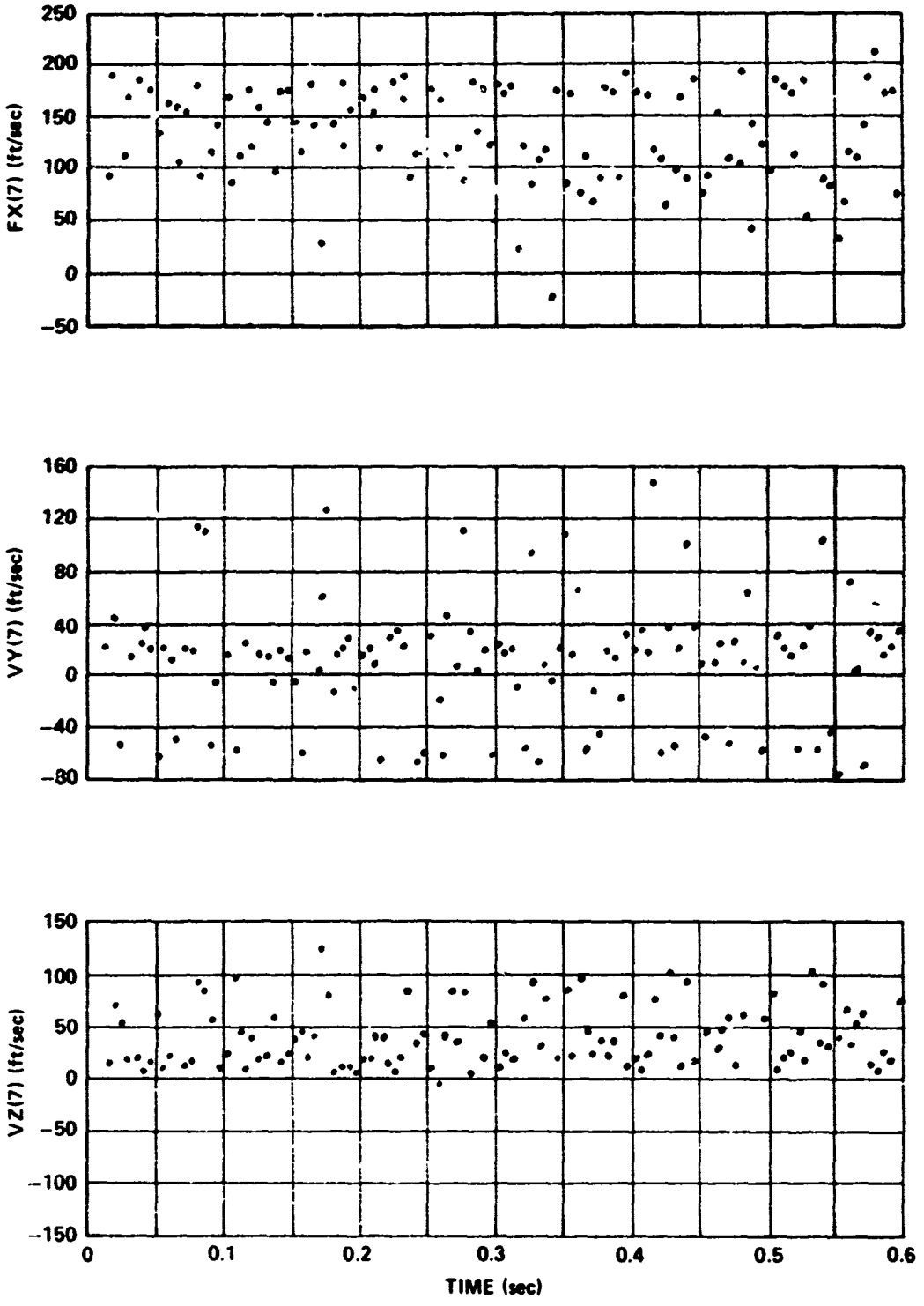

Figure 8. UH-1N helicopter flow field velocity components - flight record 1 and sensor No. 7.

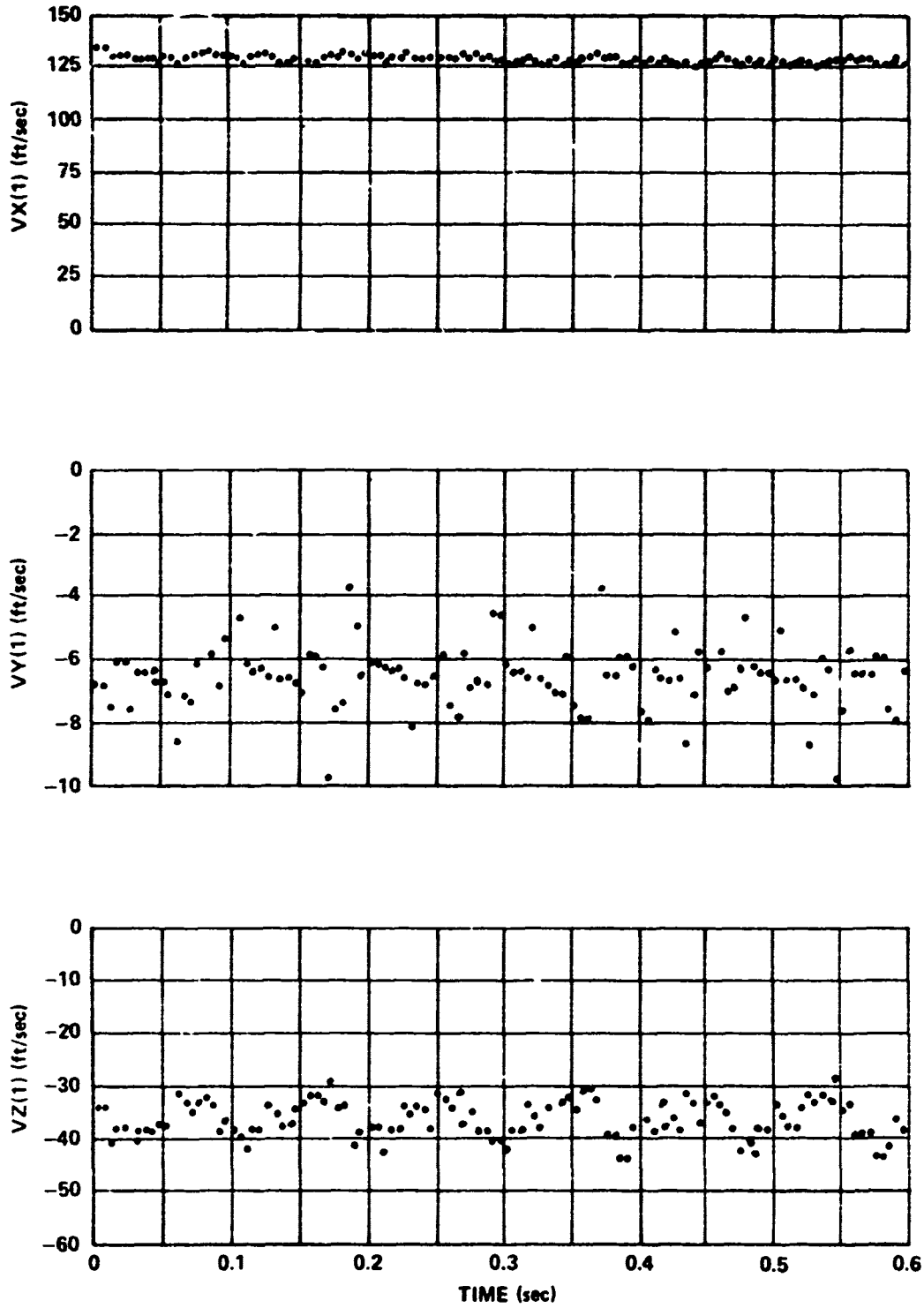

Figure 9. UH-1M helicopter flow field velocity components - flight record 3 and sensor No. 1.

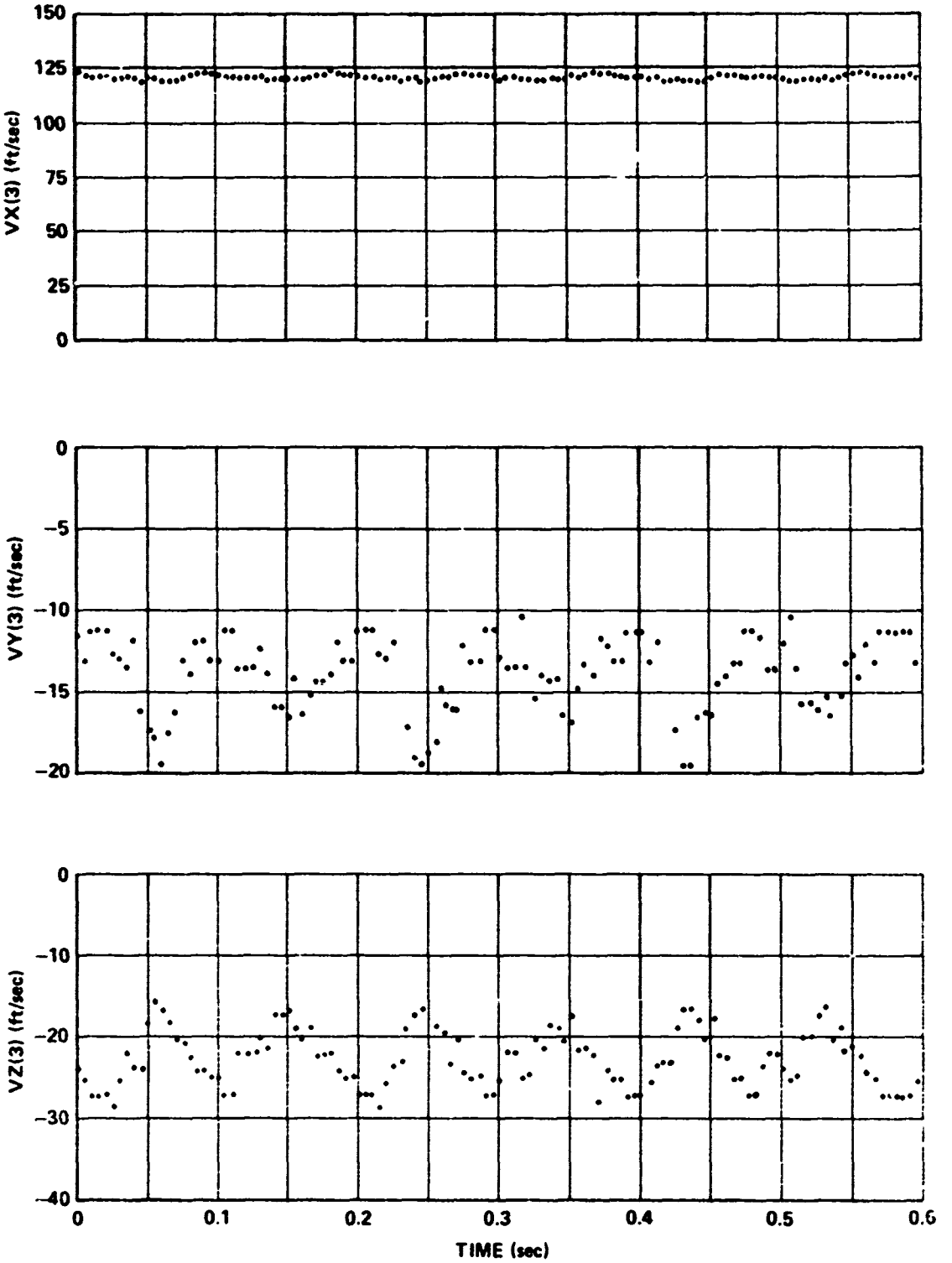

Figure 10. UH-1M helicopter flow field velocity components - flight record 3 and sensor No. 3.

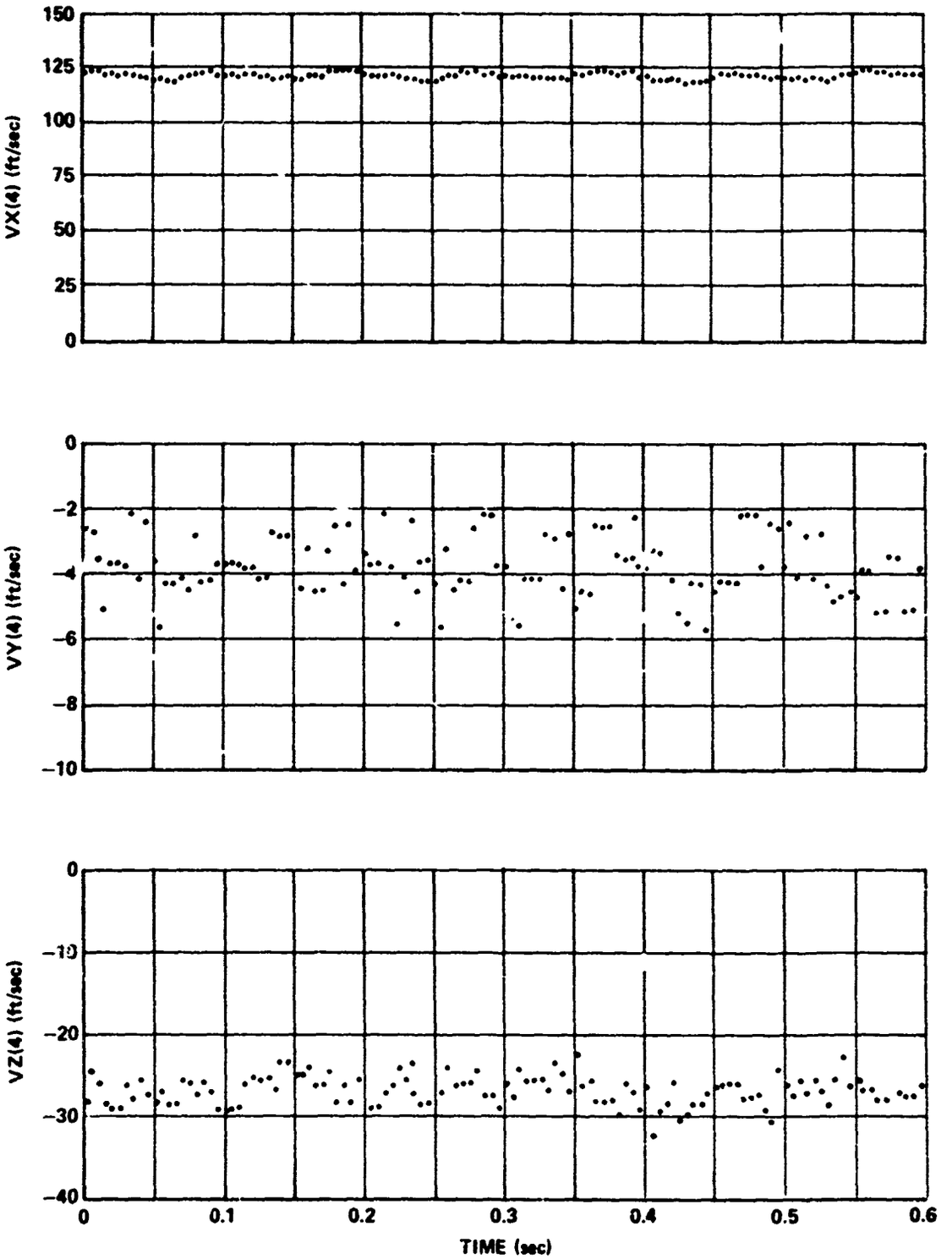

Figure 11. UH-1M helicopter flow field velocity components - flight record 3 and sensor No. 4.

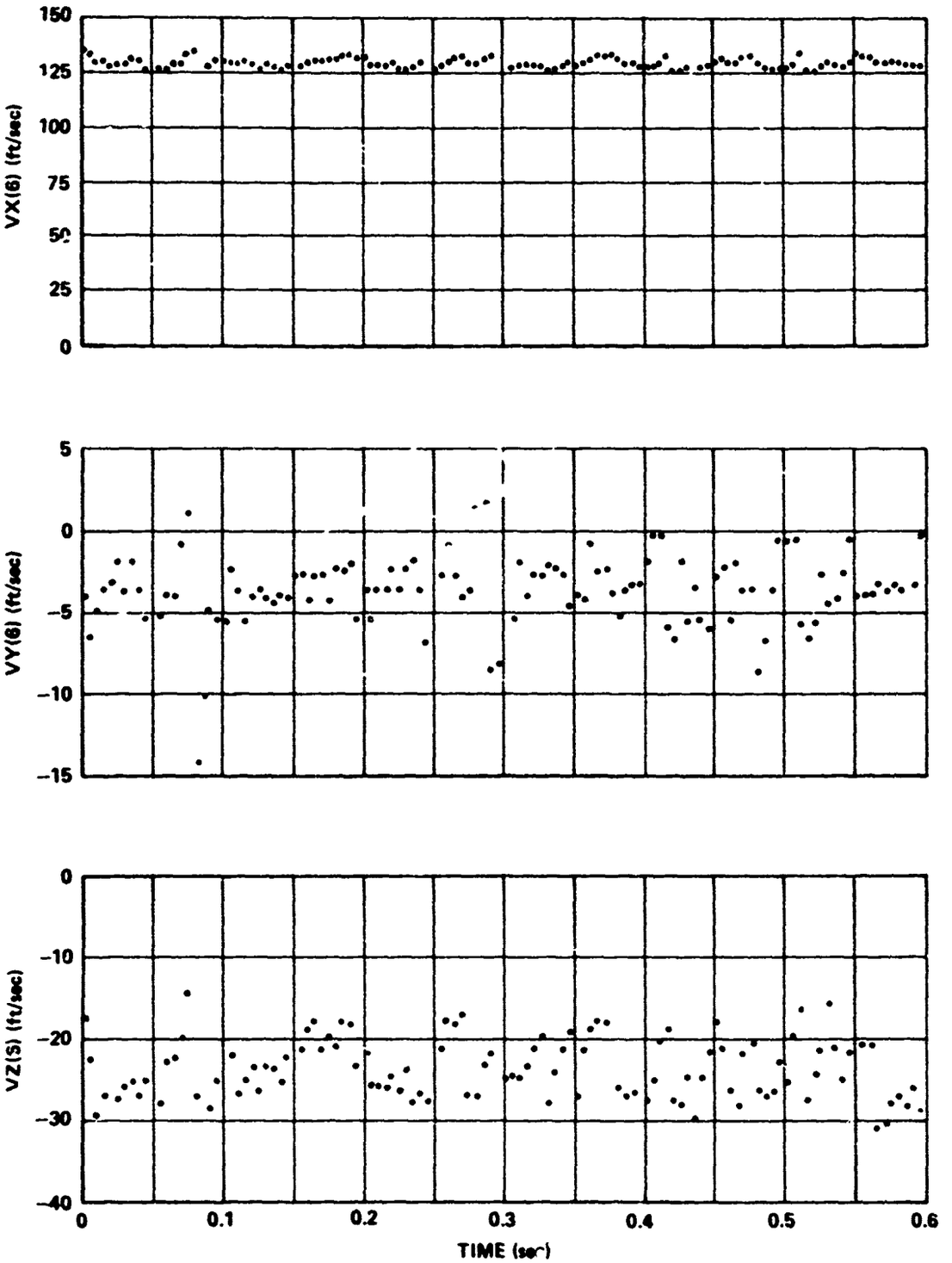

Figure 12. UH-1M helicopter flow field velocity components - flight record 3 and sensor No. 6.

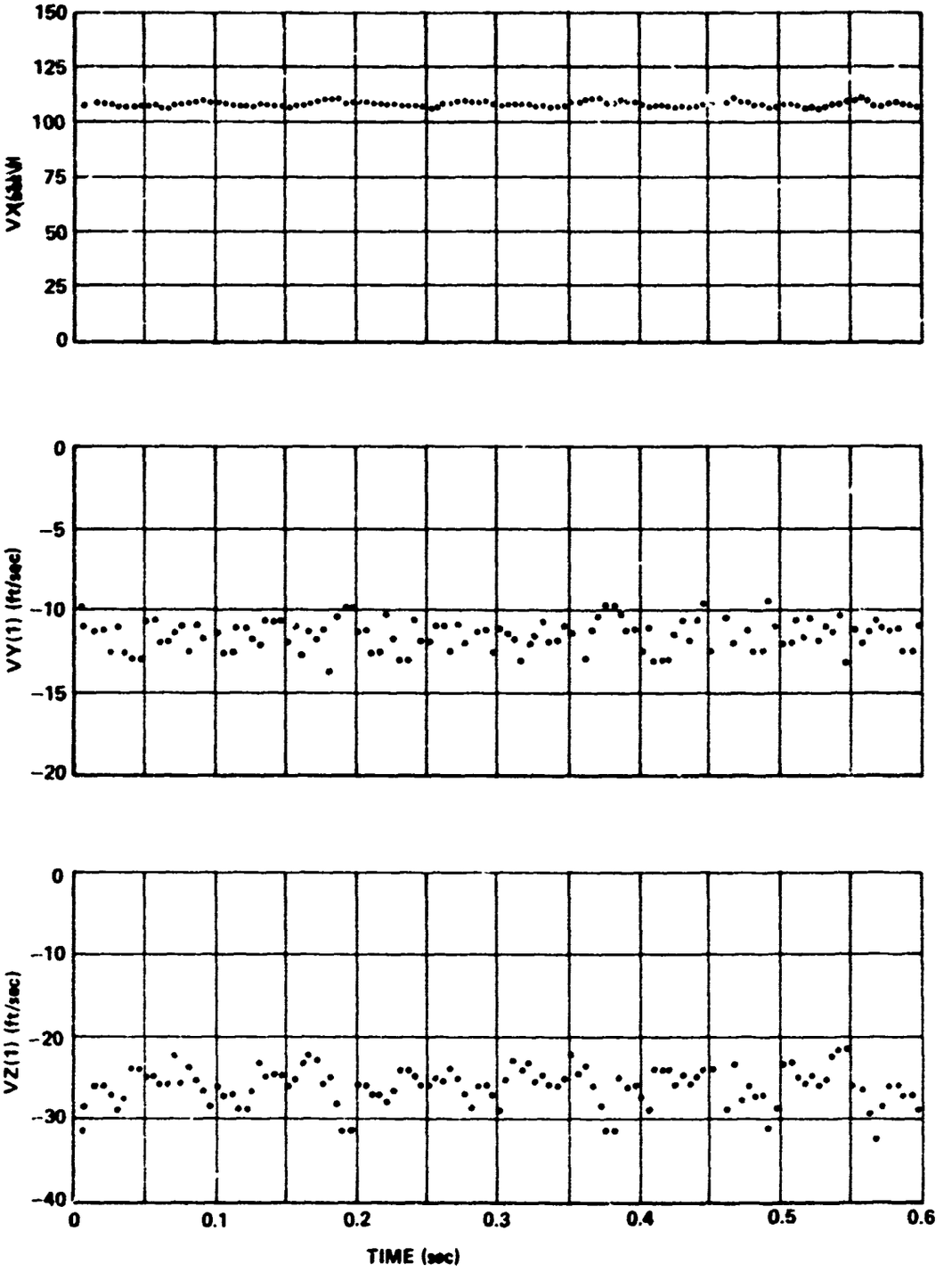

Figure 13. UH-1M helicopter flow field velocity components - flight record 5 and sensor No. 1.

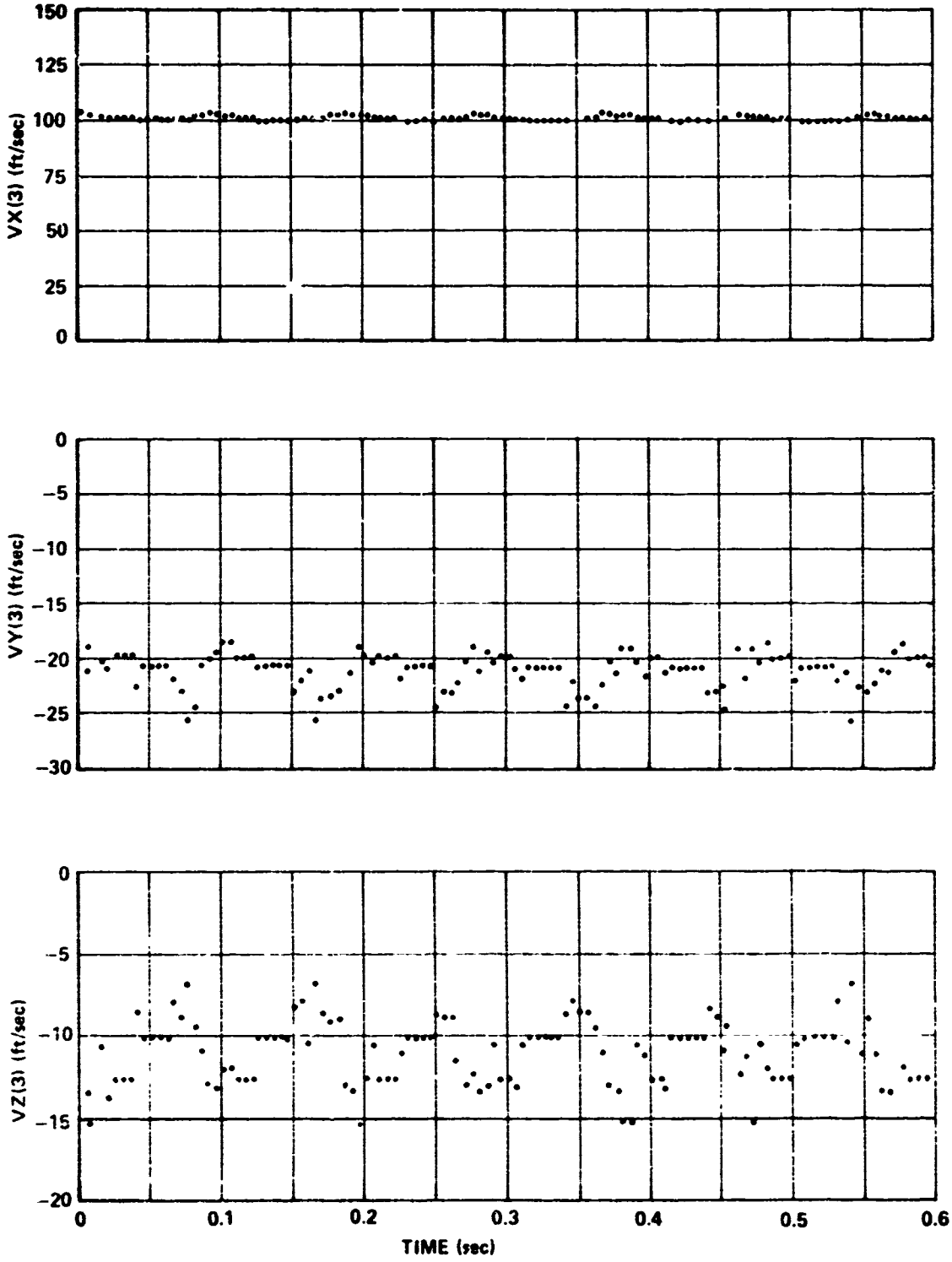

Figure 14. UH-1M helicopter flow field velocity components - flight record 5 and sensor No. 3.

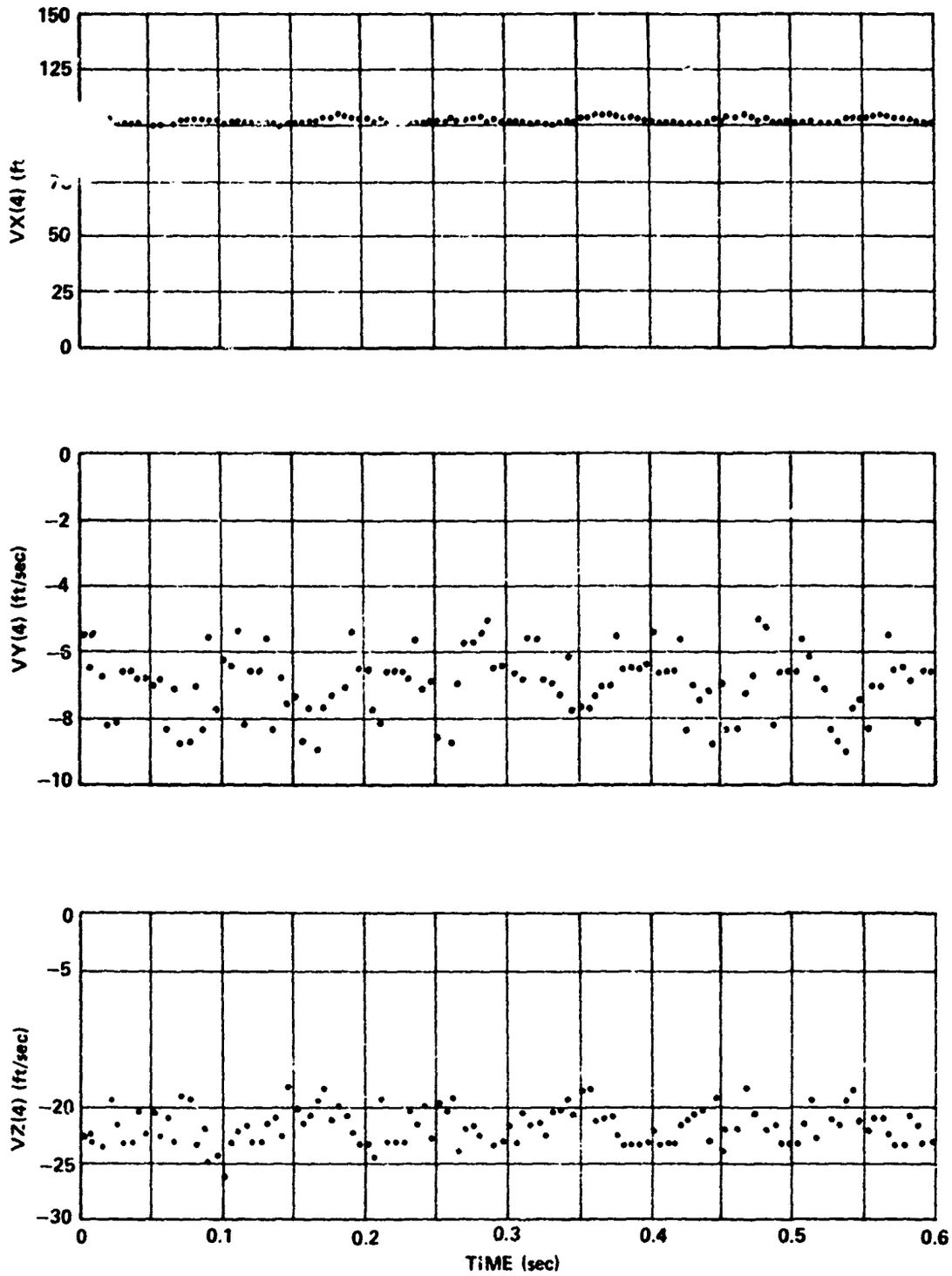

Figure 15. UH-1M helicopter flow field velocity components - flight record 5 and sensor No. 4.

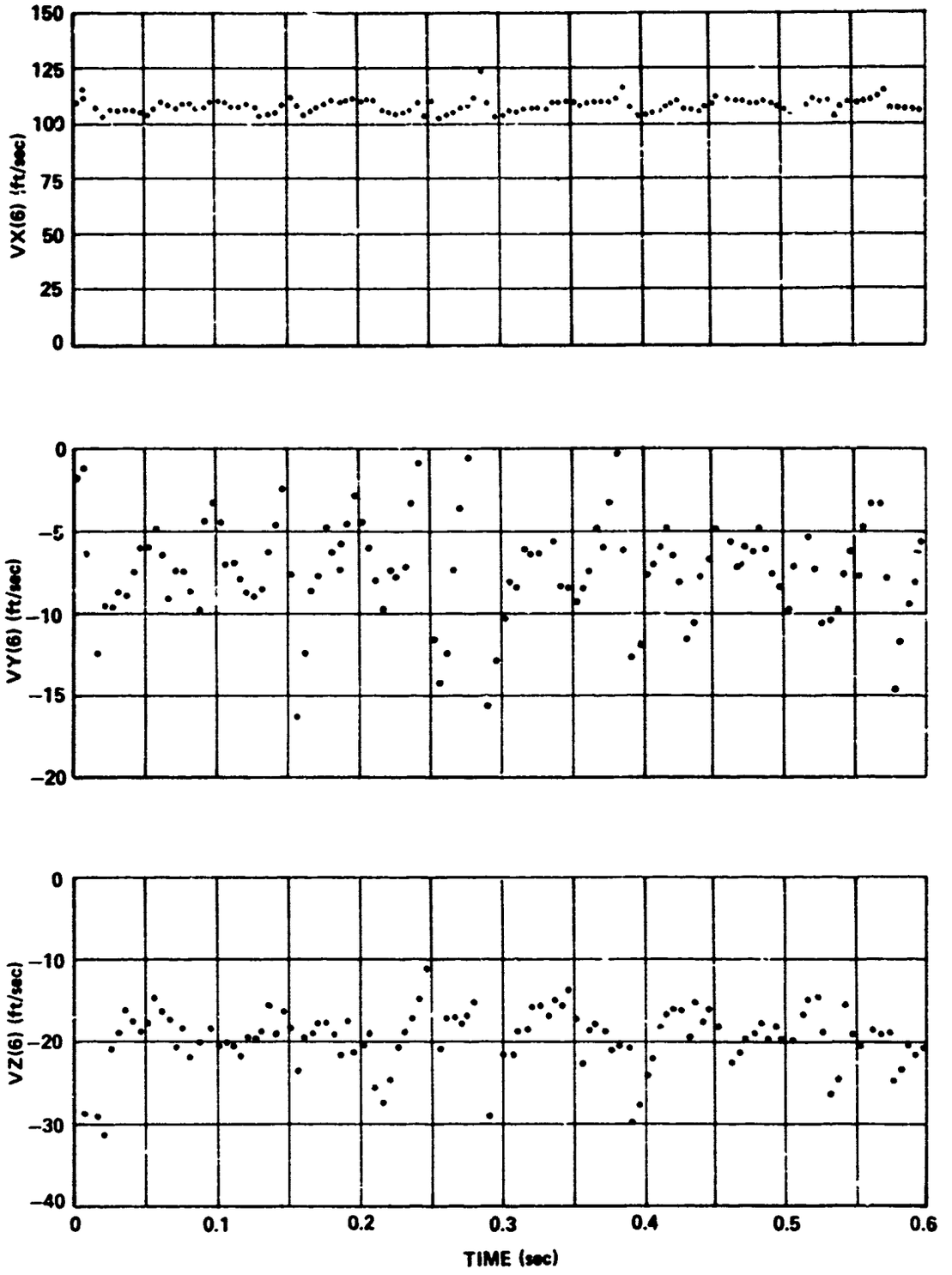

Figure 16. UH-1M helicopter flow field velocity components - flight record 5 and sensor No 6.

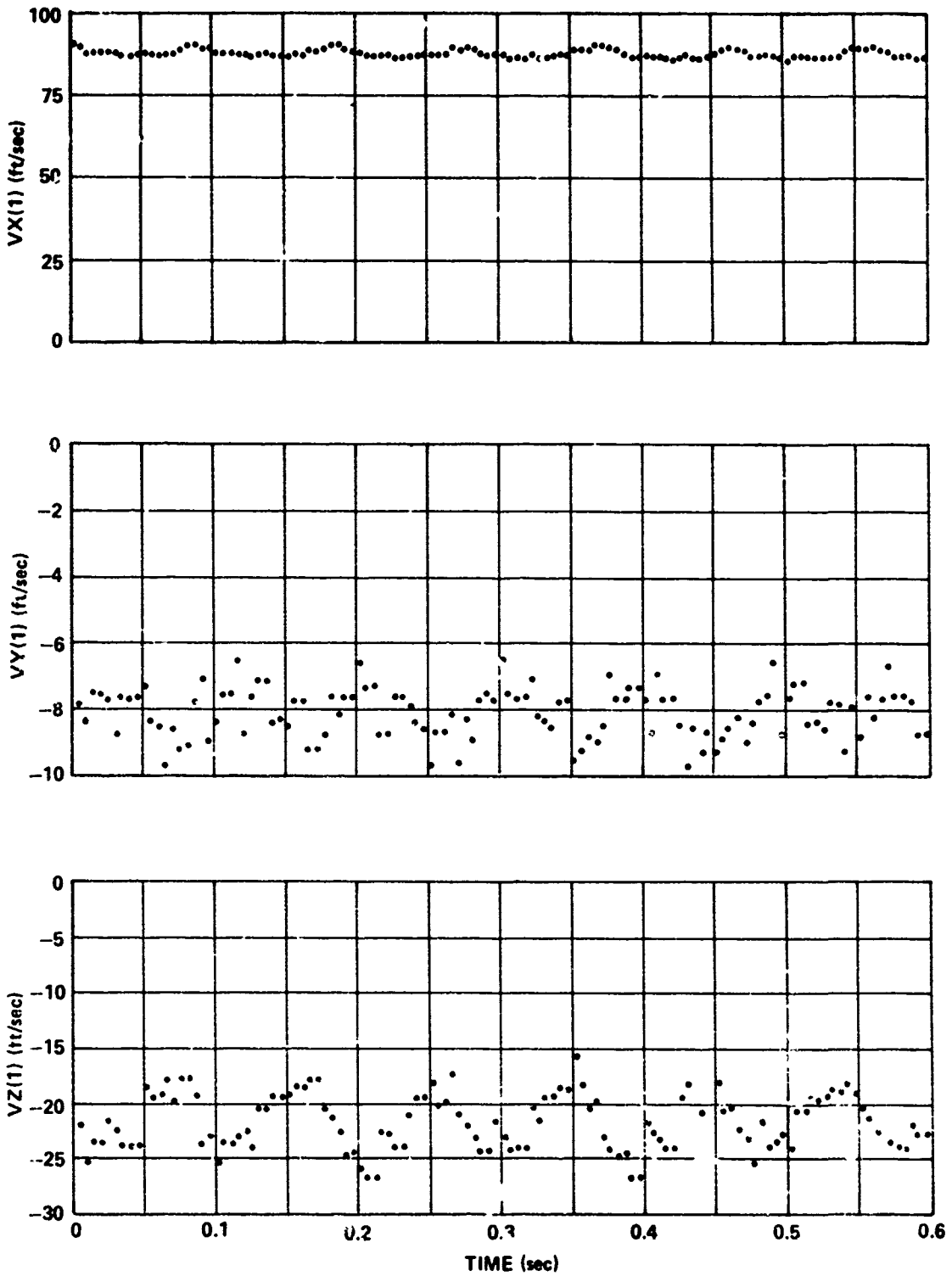

Figure 17. UH-1M helicopter flow field velocity components - flight record 7 and sensor No. 1.

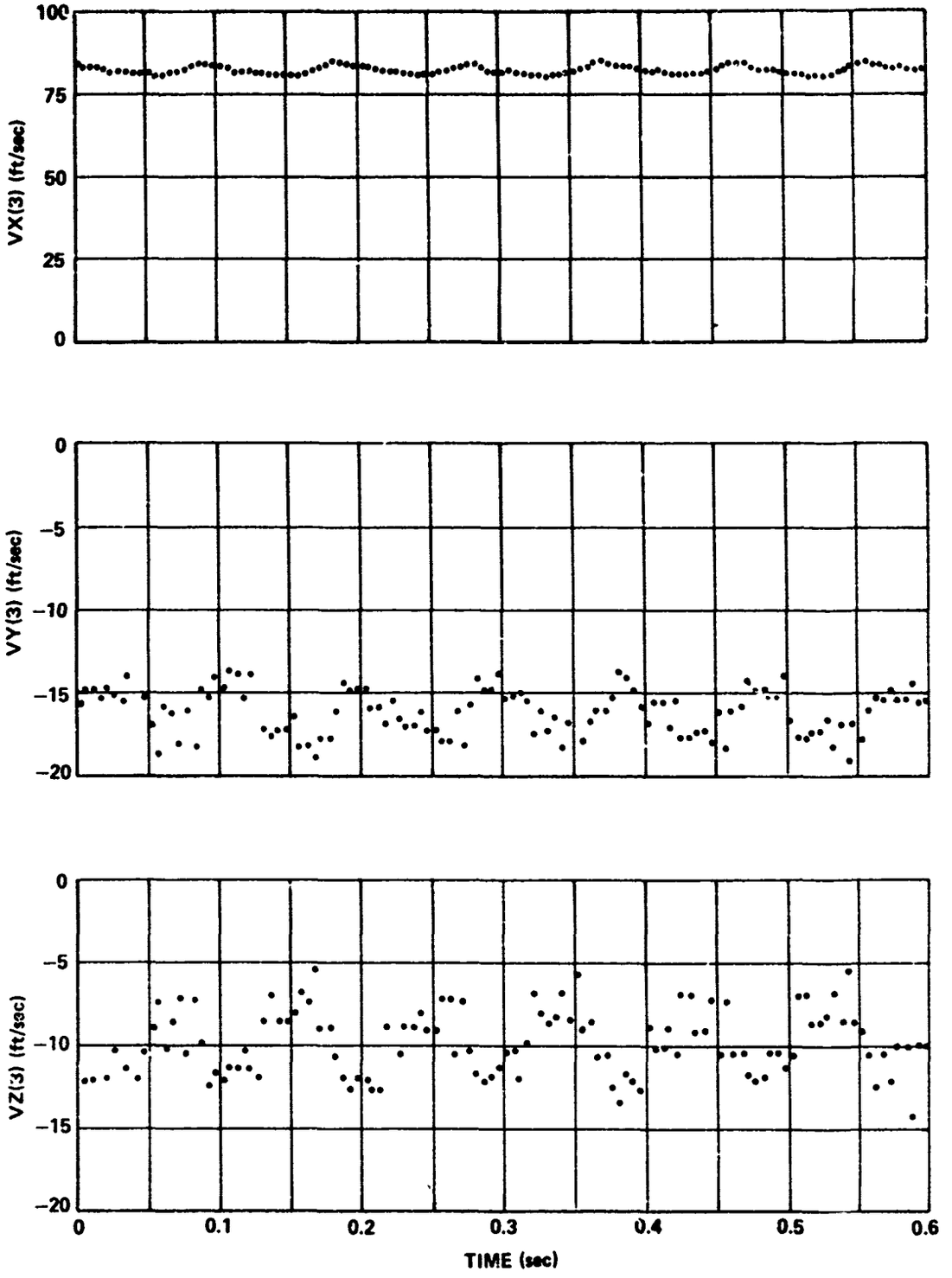

Figure 18. UH-1M helicopter flow field velocity components - flight record 7 and sensor No. 3.

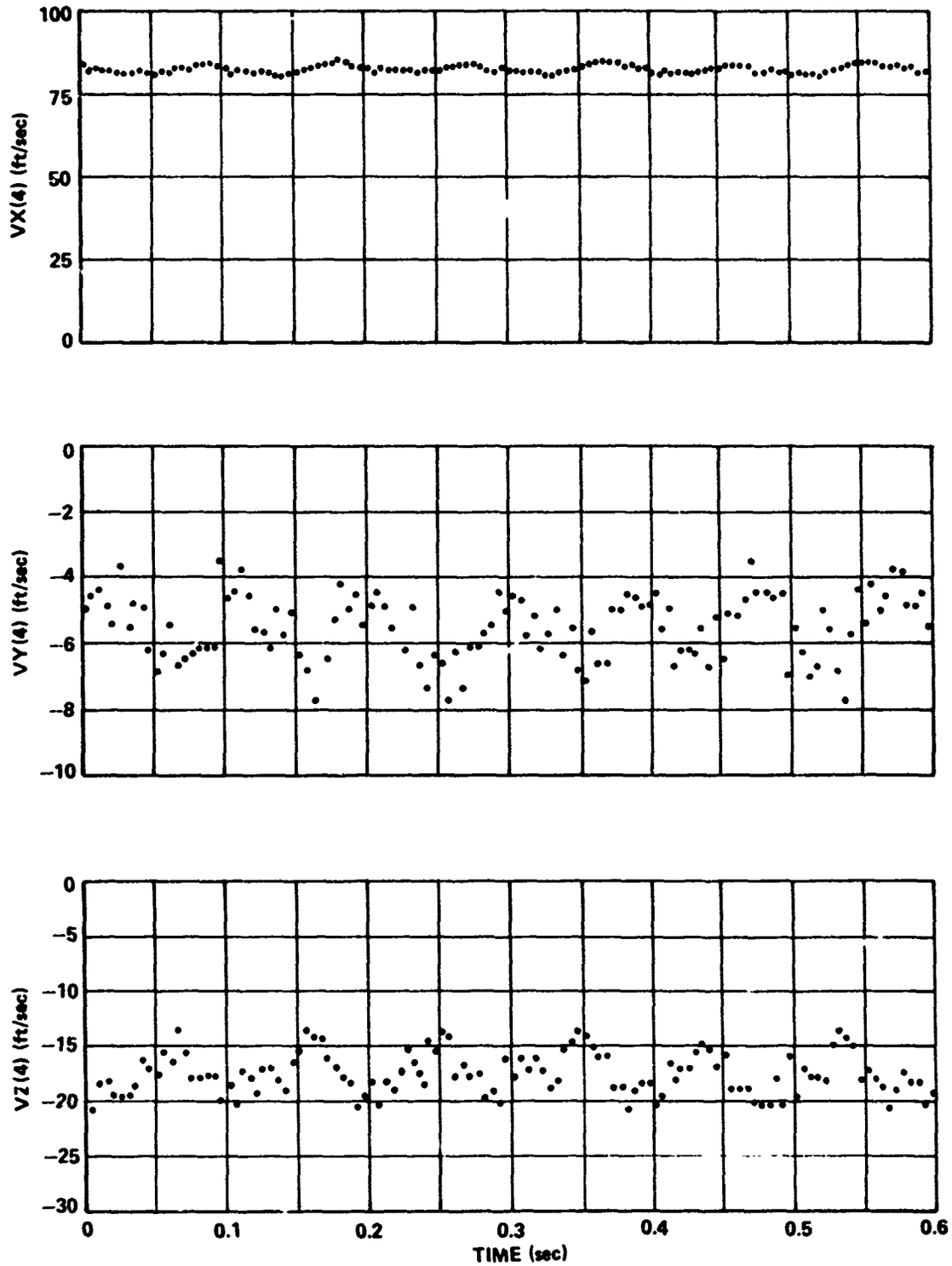

Figure 19. UH-1M helicopter flow field velocity components - flight record 7 and sensor No. 4.

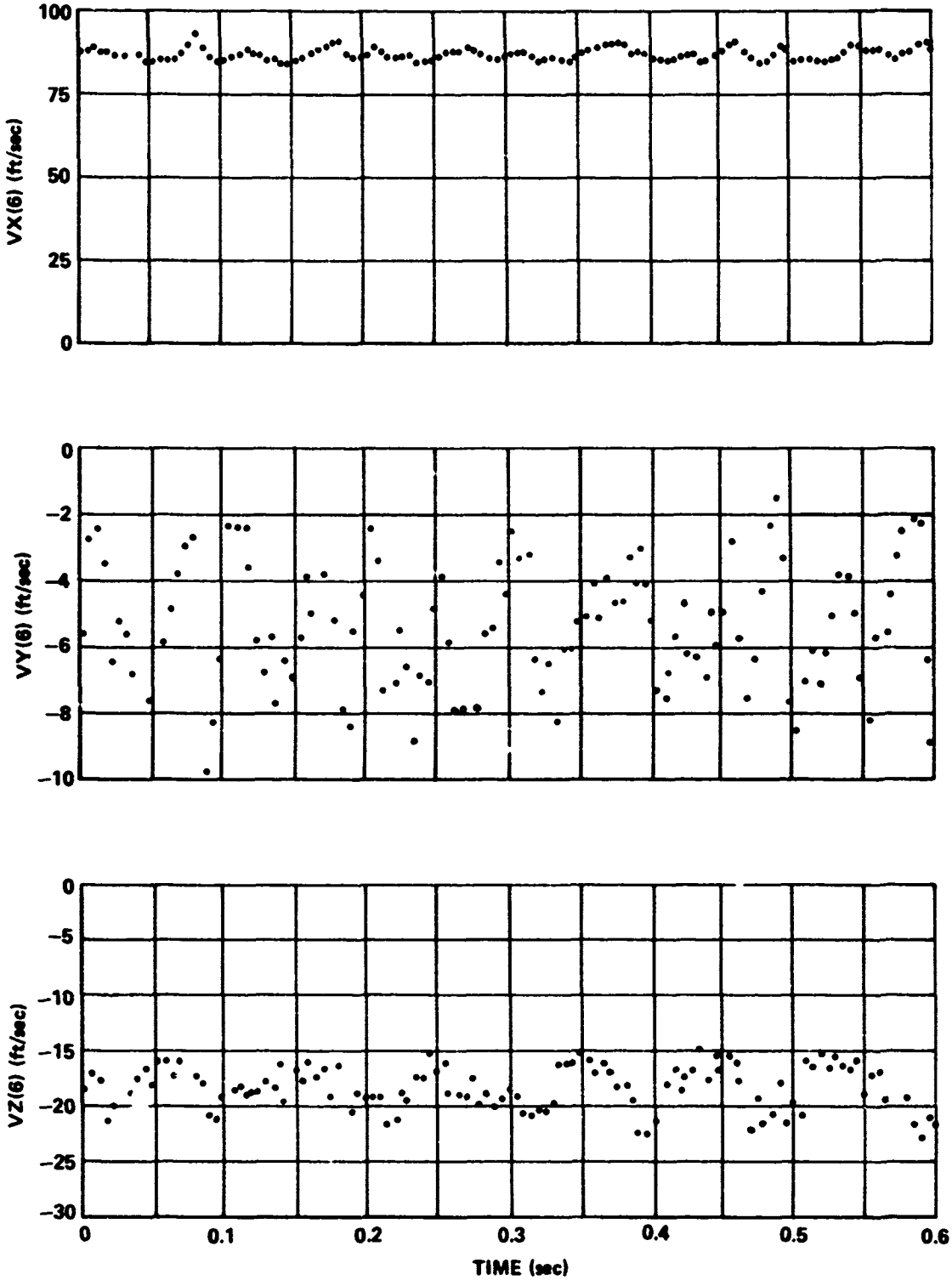

Figure 20. UH-1M helicopter flow field velocity components - flight record 7 and sensor No. 6.

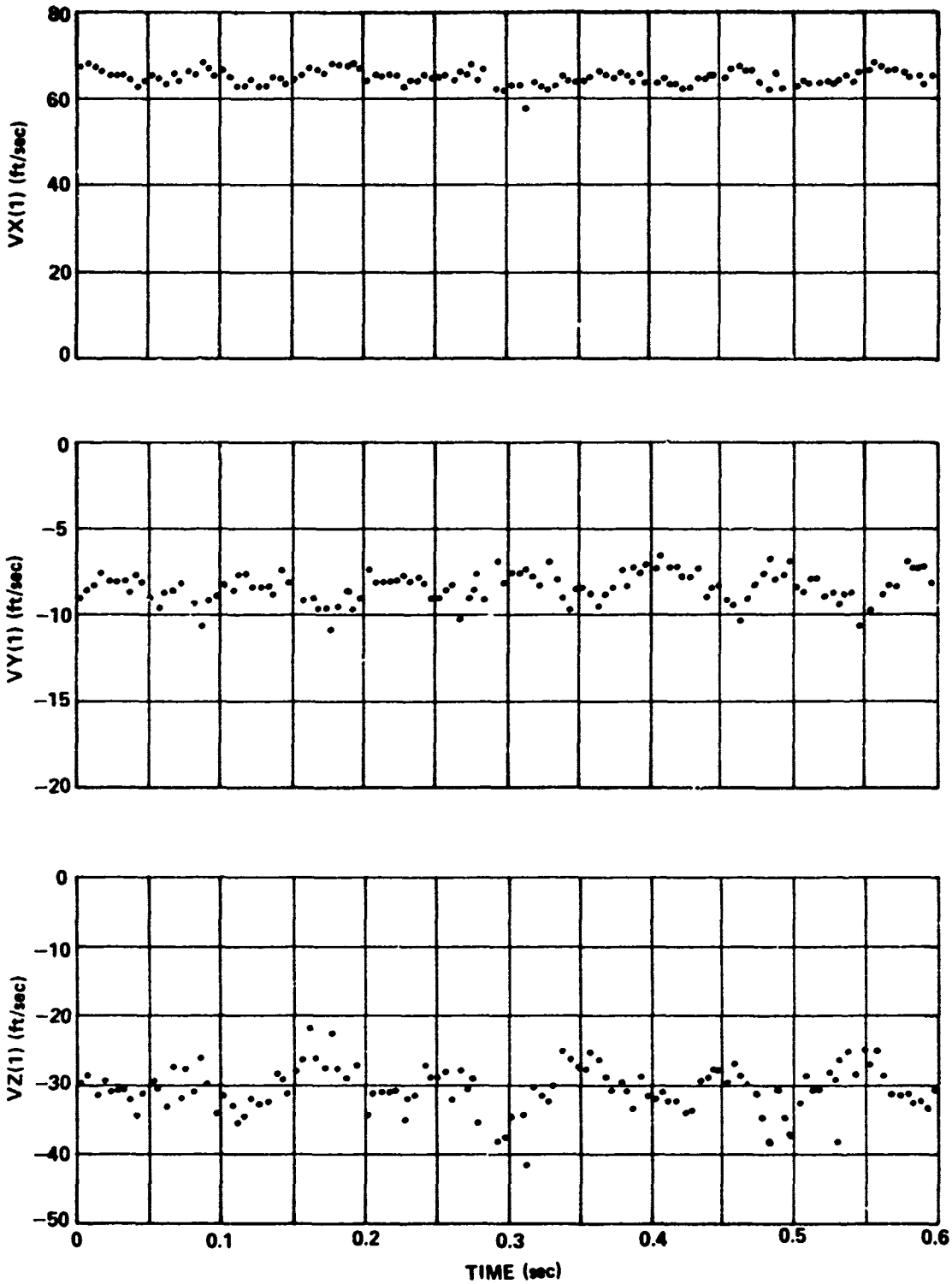

Figure 21. UH-1M helicopter flow field velocity components - flight record 9 and sensor No. 1.

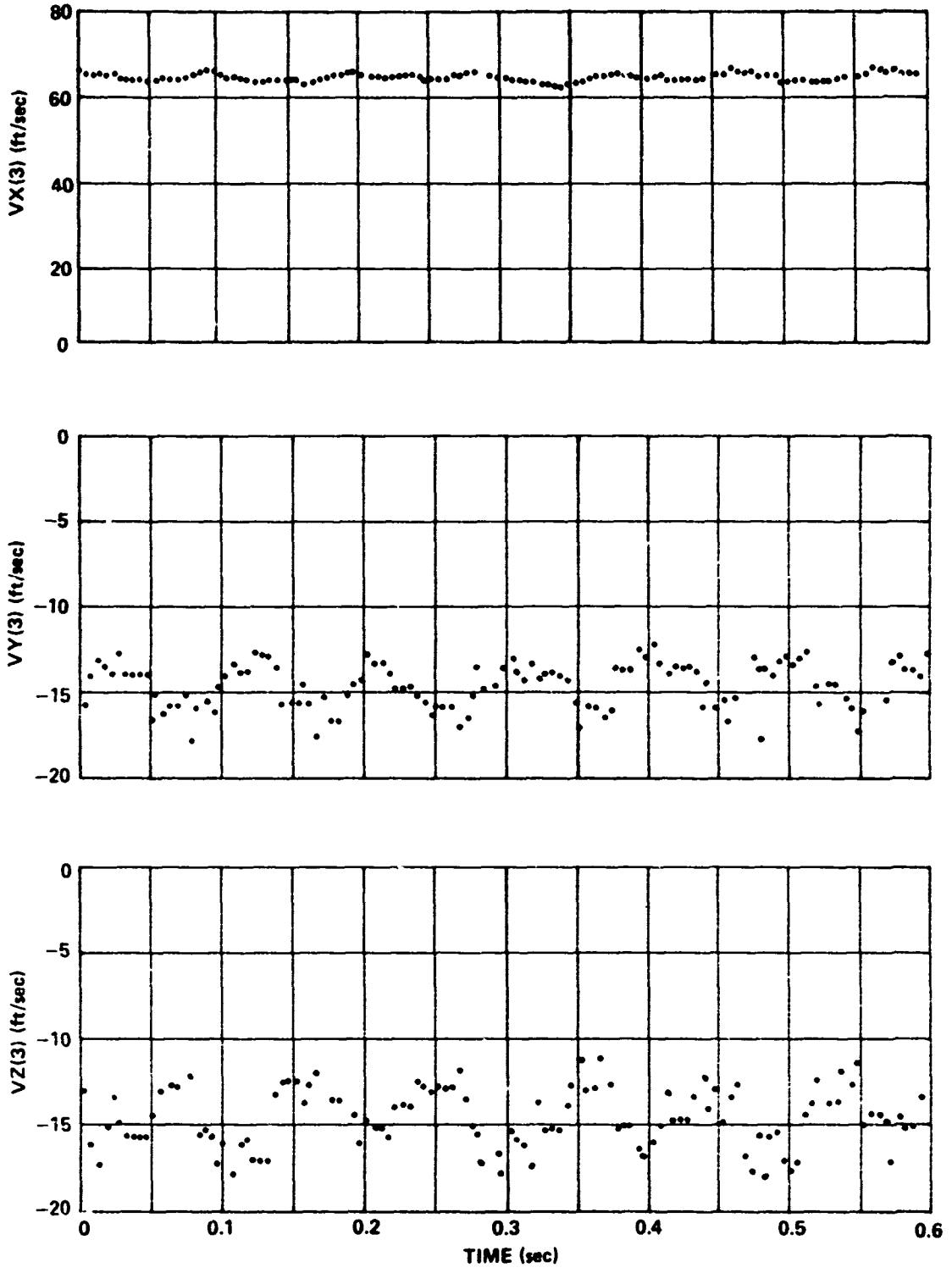

Figure 22. UH-1M helicopter flow field velocity components - flight record 9 and sensor No. 3.

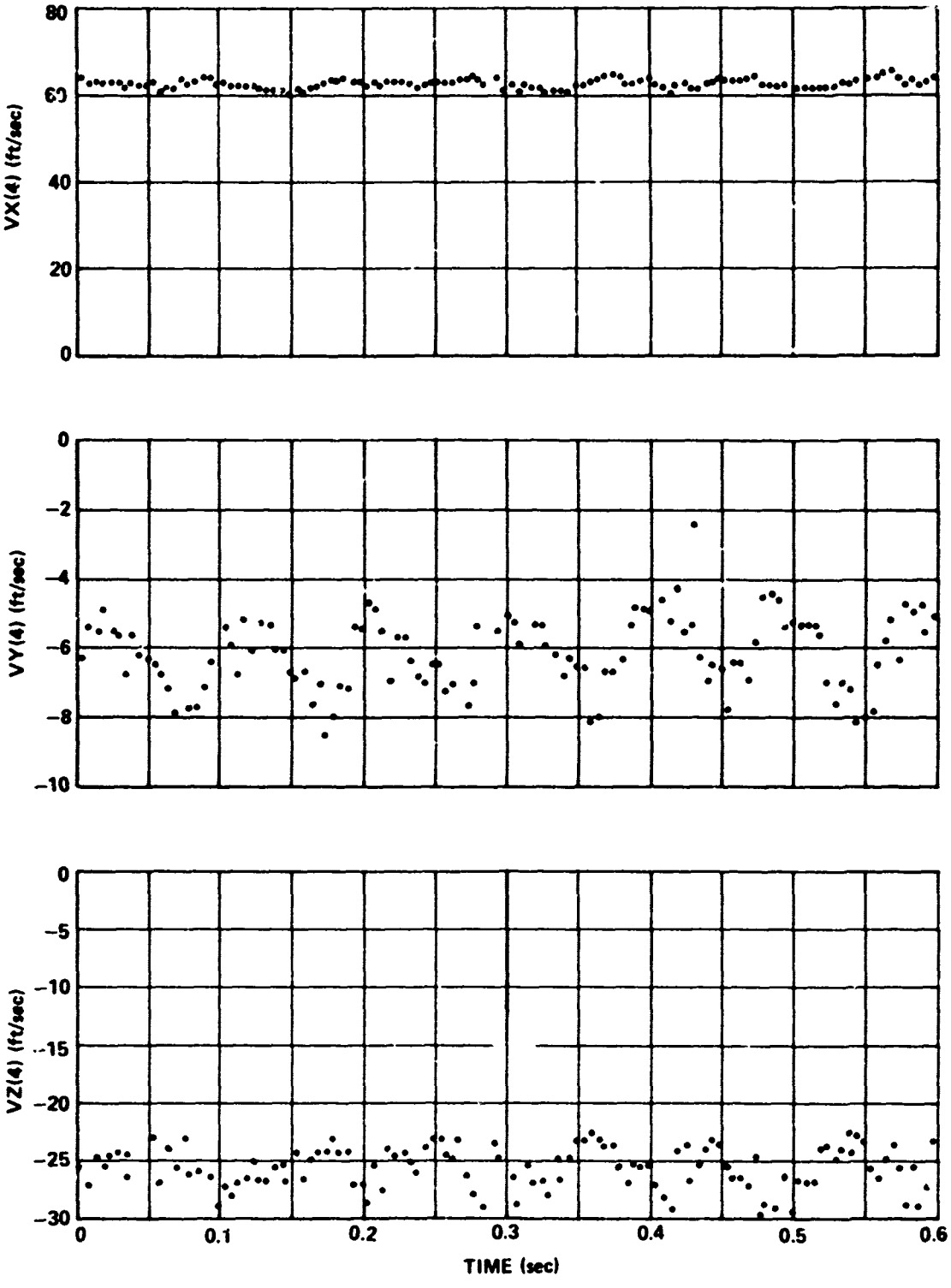

Figure 23. UH-1M helicopter flow field velocity components - flight record 9 and sensor No. 4.

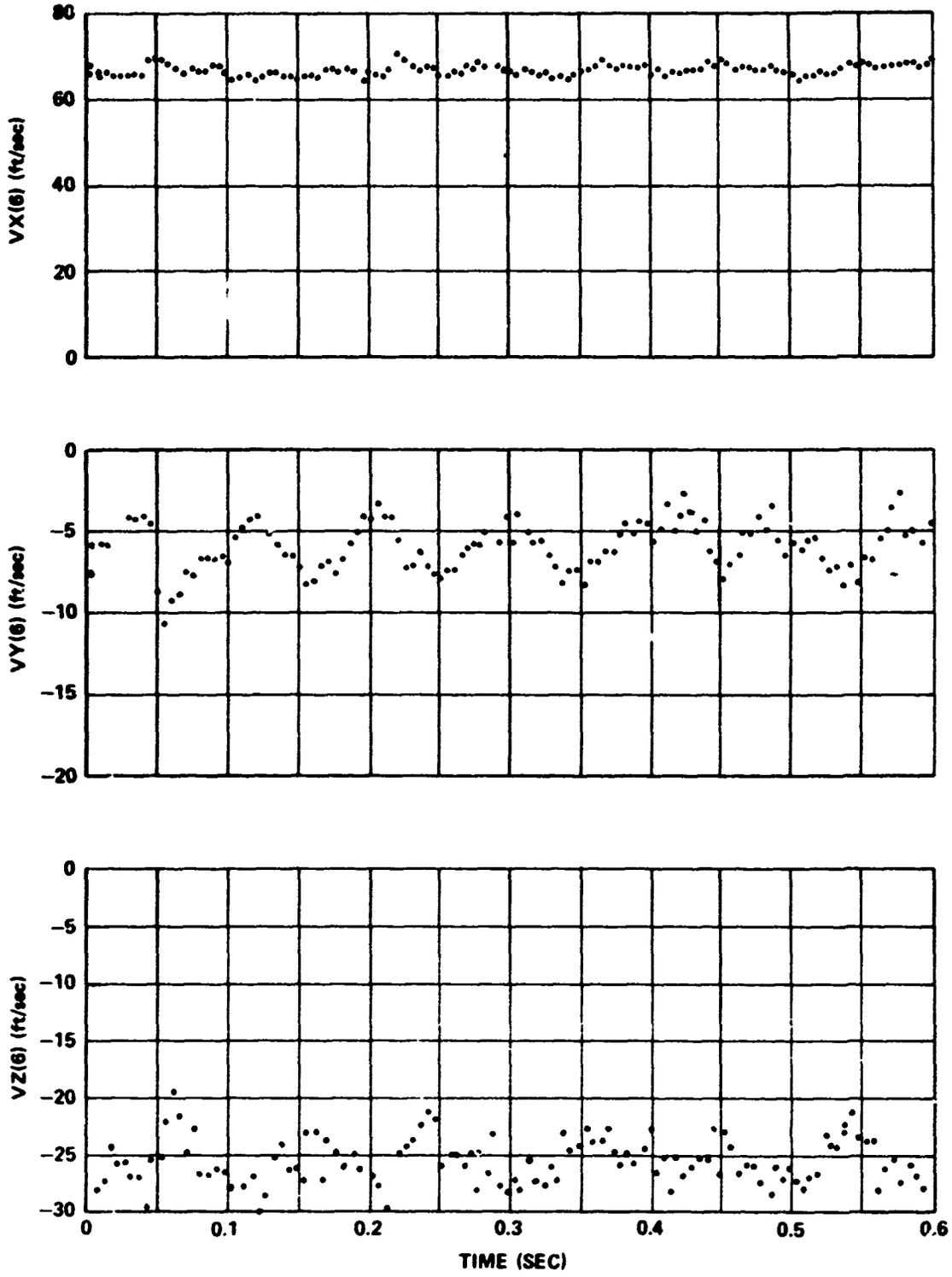

Figure 24. UH-1M helicopter flow field velocity components - flight record 9 and sensor No. 6.

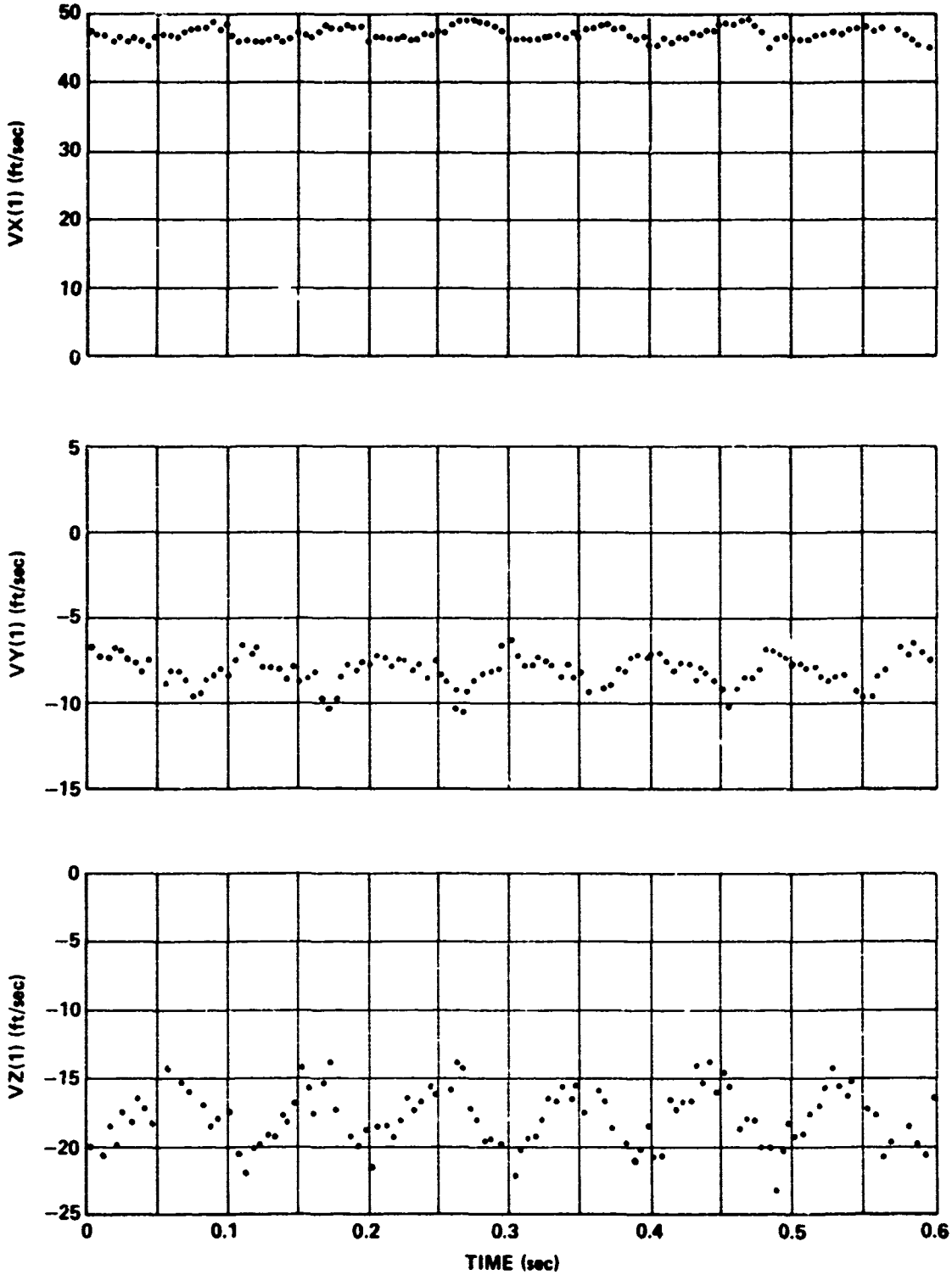

Figure 25. UH-1M helicopter flow field velocity components - flight record 11 and sensor No. 1.

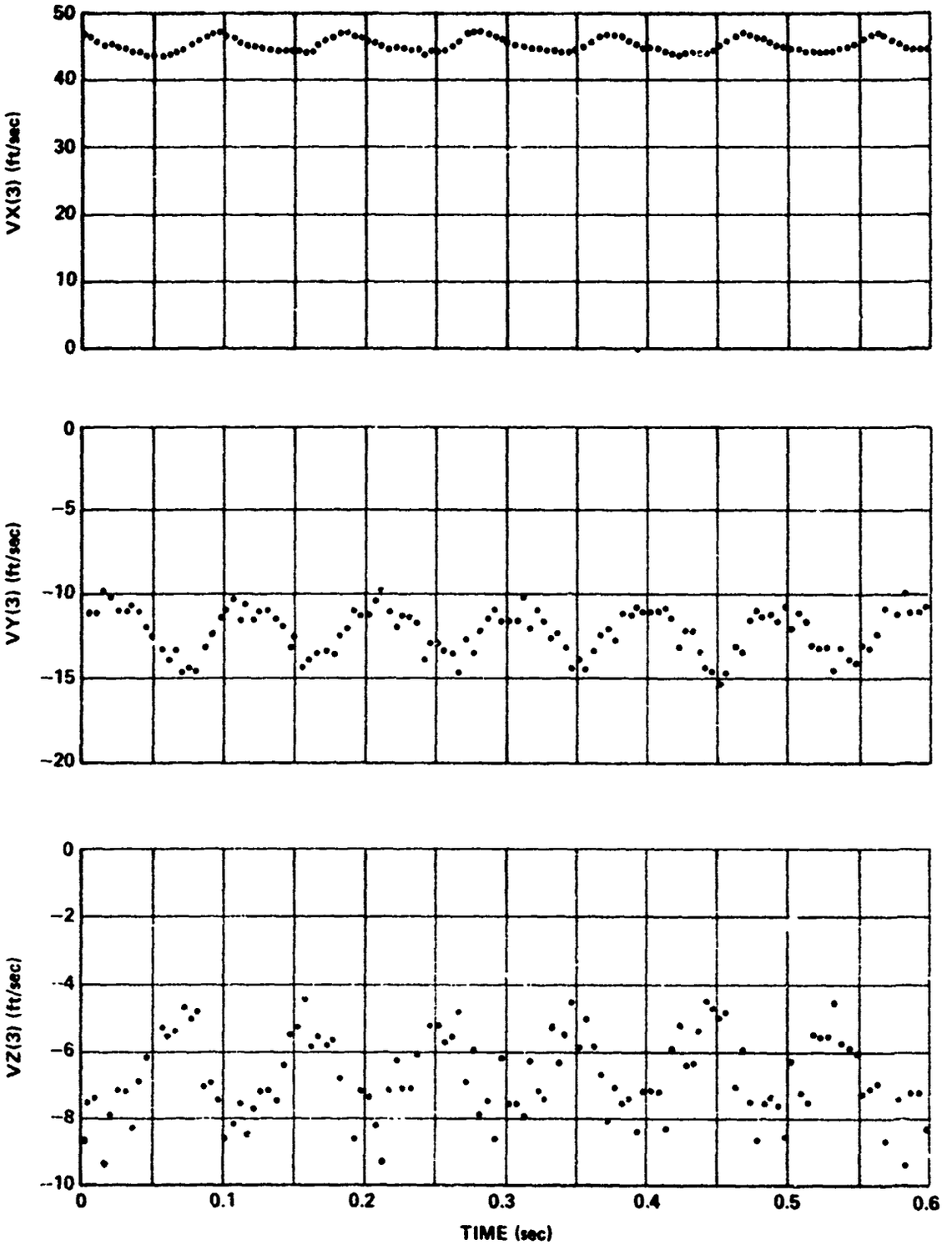

Figure 26. UH-1M helicopter flow field velocity components - flight record 11 and sensor No. 3.

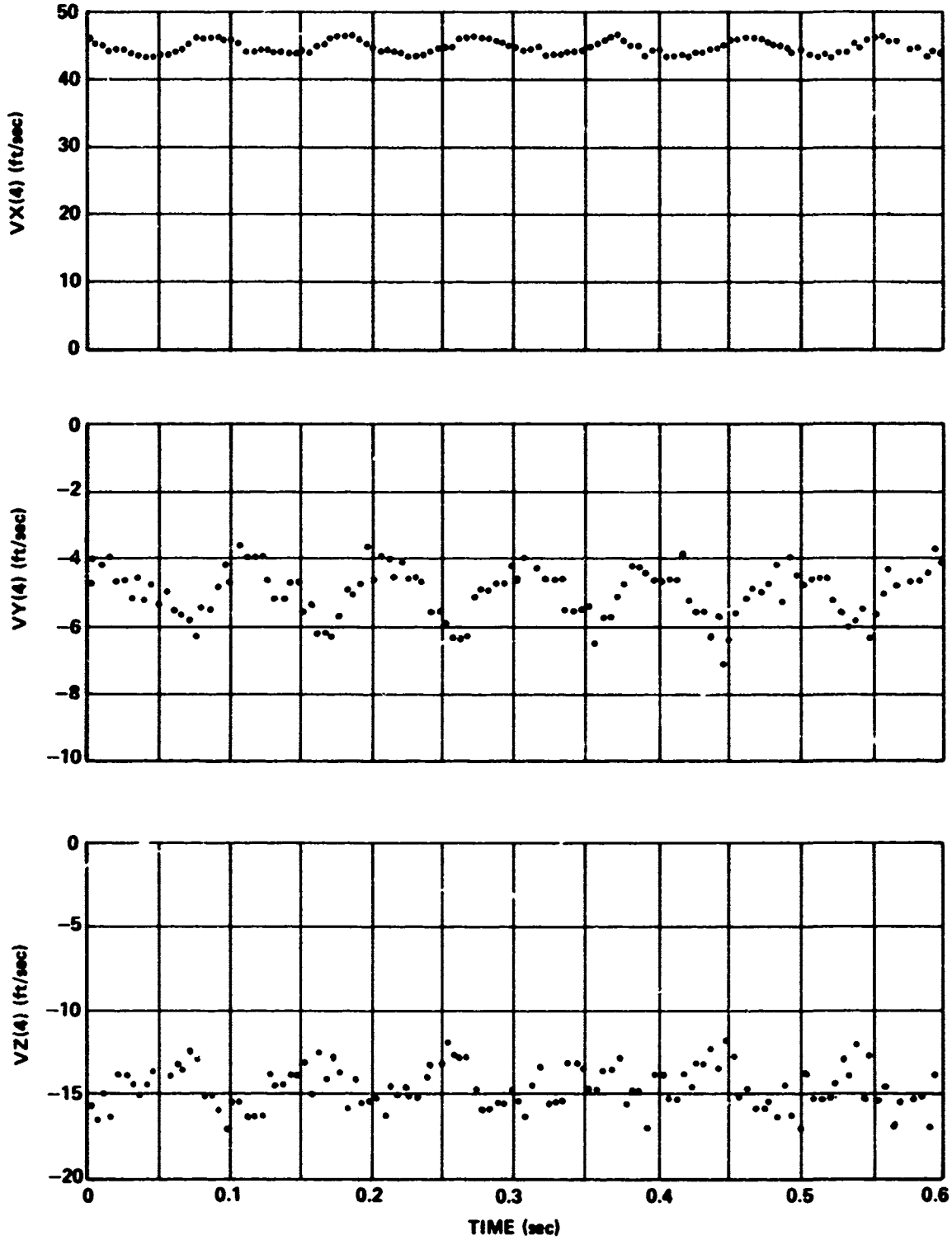

Figure 27. UH-1M helicopter flow field velocity components - flight record 11 and sensor No. 4.

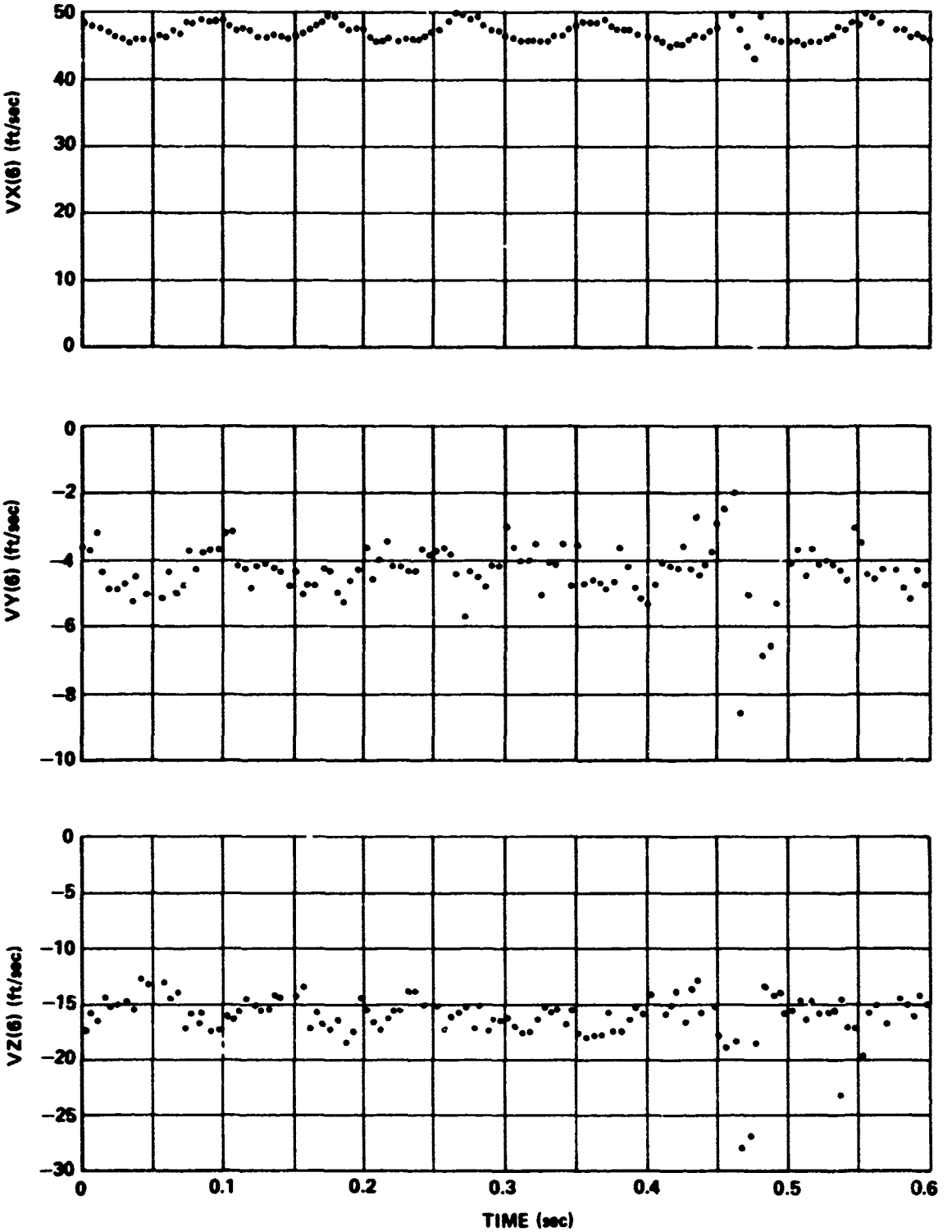

Figure 28. UH-1M helicopter flow field velocity components - flight record 11 and sensor No. 6.

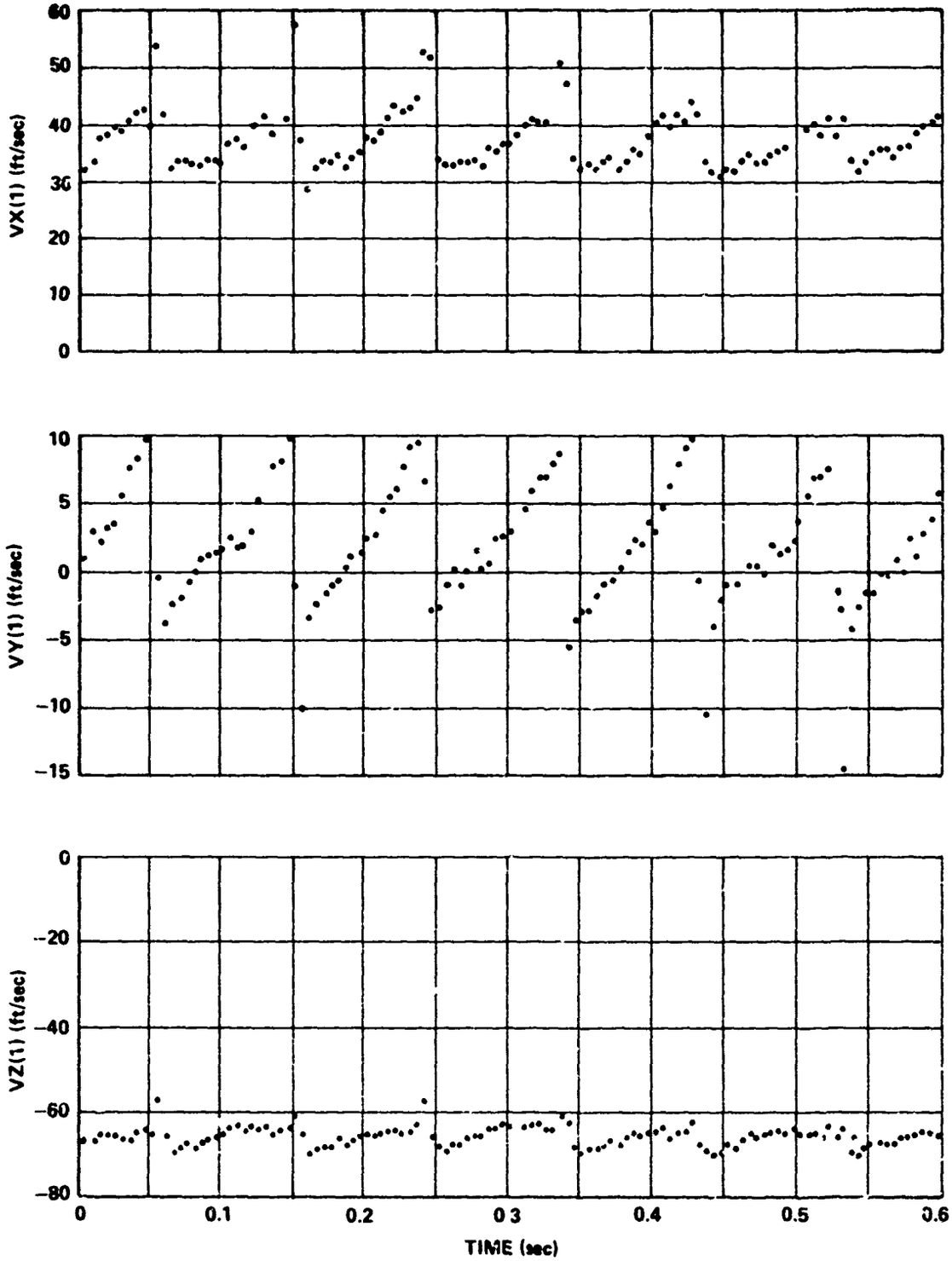

Figure 29. UH-1M helicopter flow field velocity components - flight record 13 and sensor No. 1.

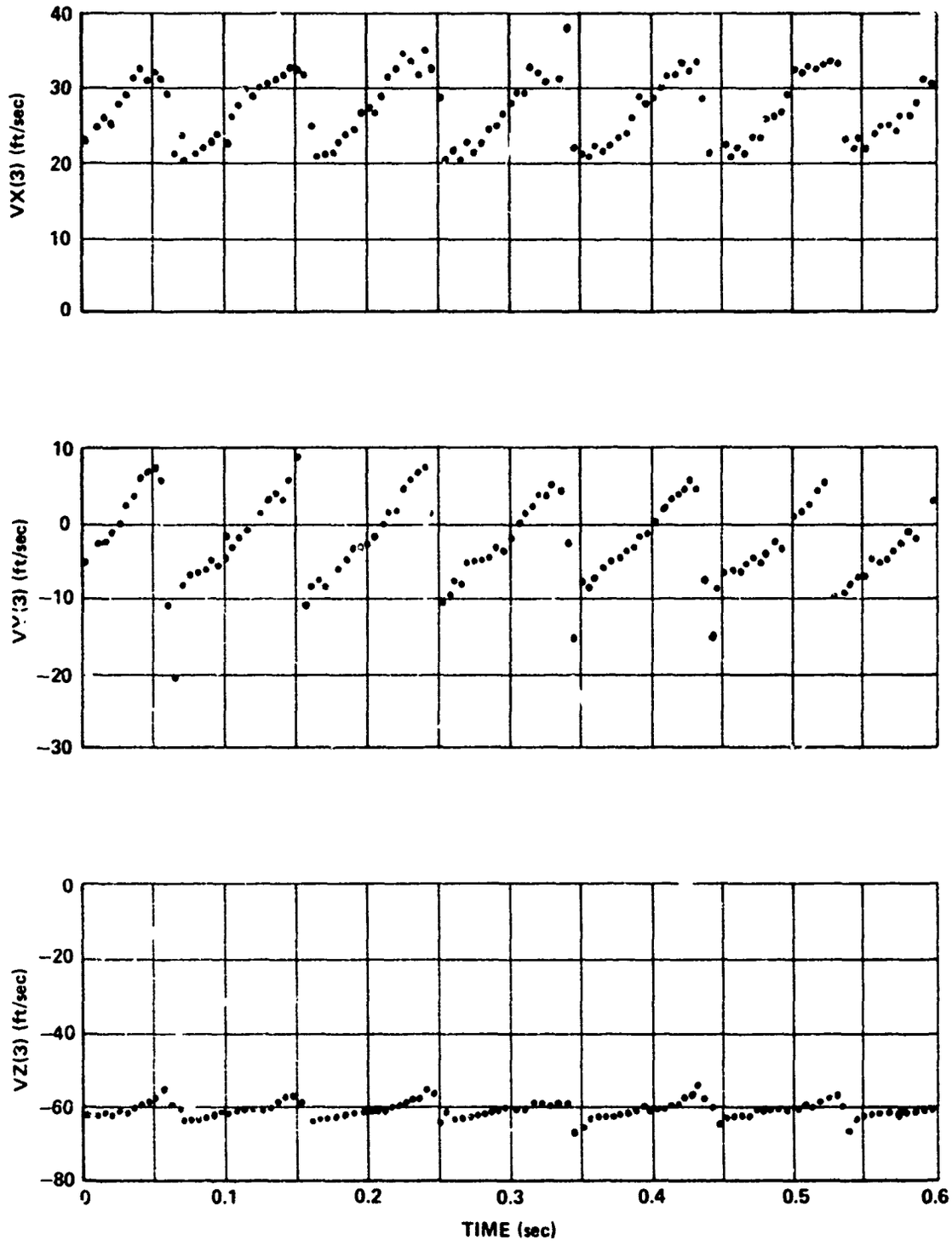

Figure 30. UH-1M helicopter flow field velocity components - flight record 13 and sensor No. 3.

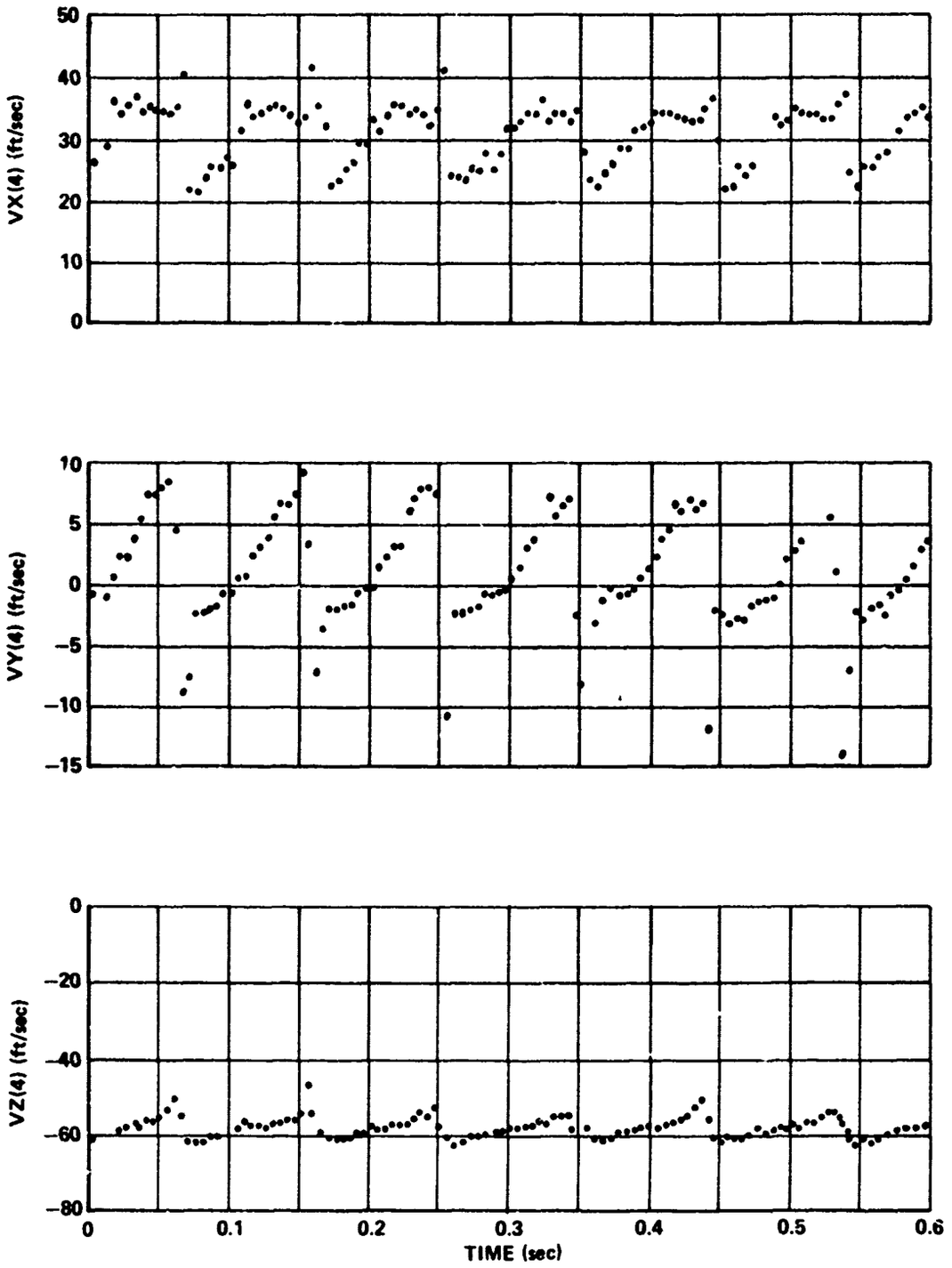

Figure 31. UH-1M helicopter flow field velocity components - flight record 13 and sensor No. 4.

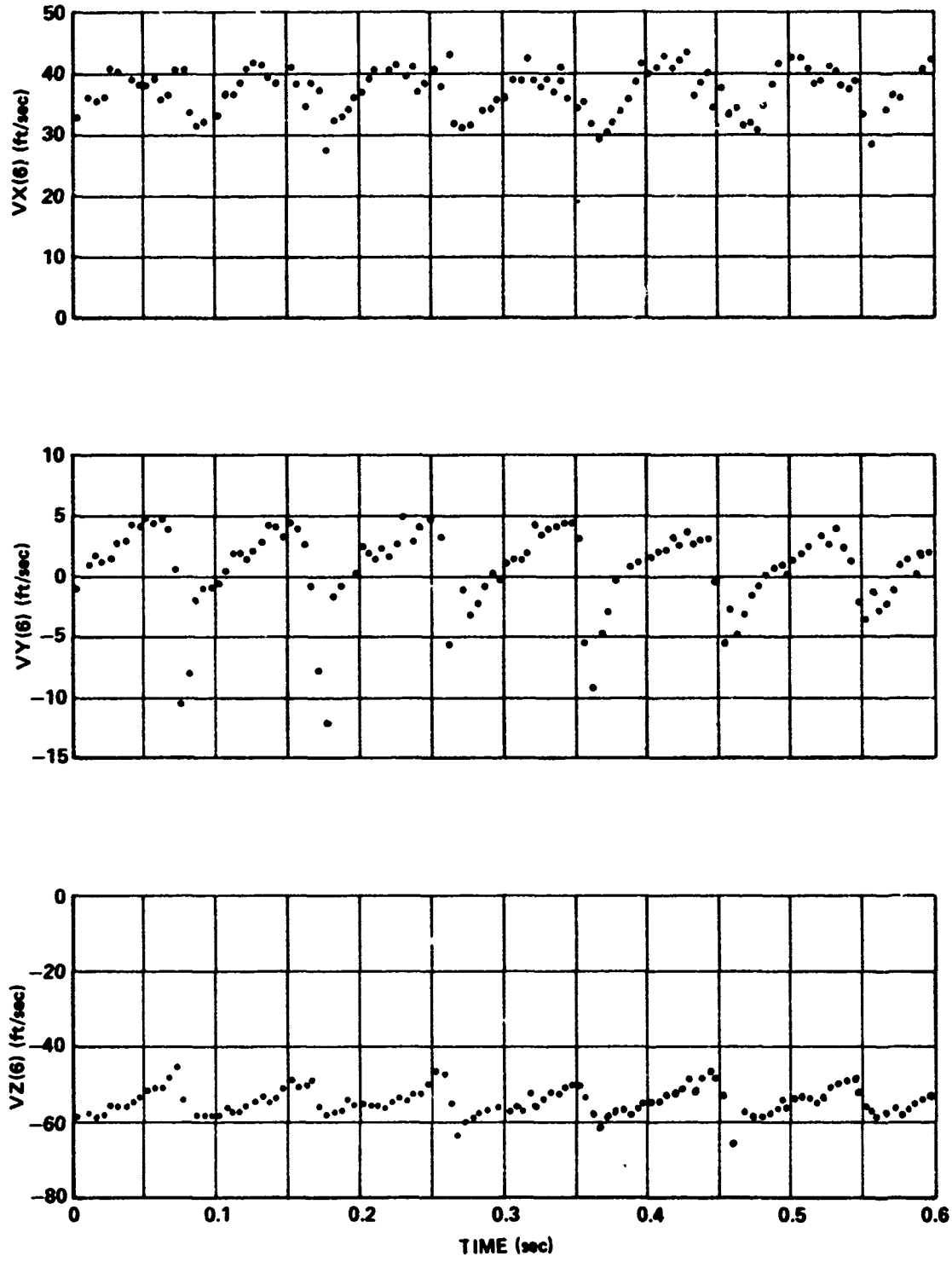

Figure 32. UH-1M helicopter flow field velocity components - flight record 13 and sensor No. 6.

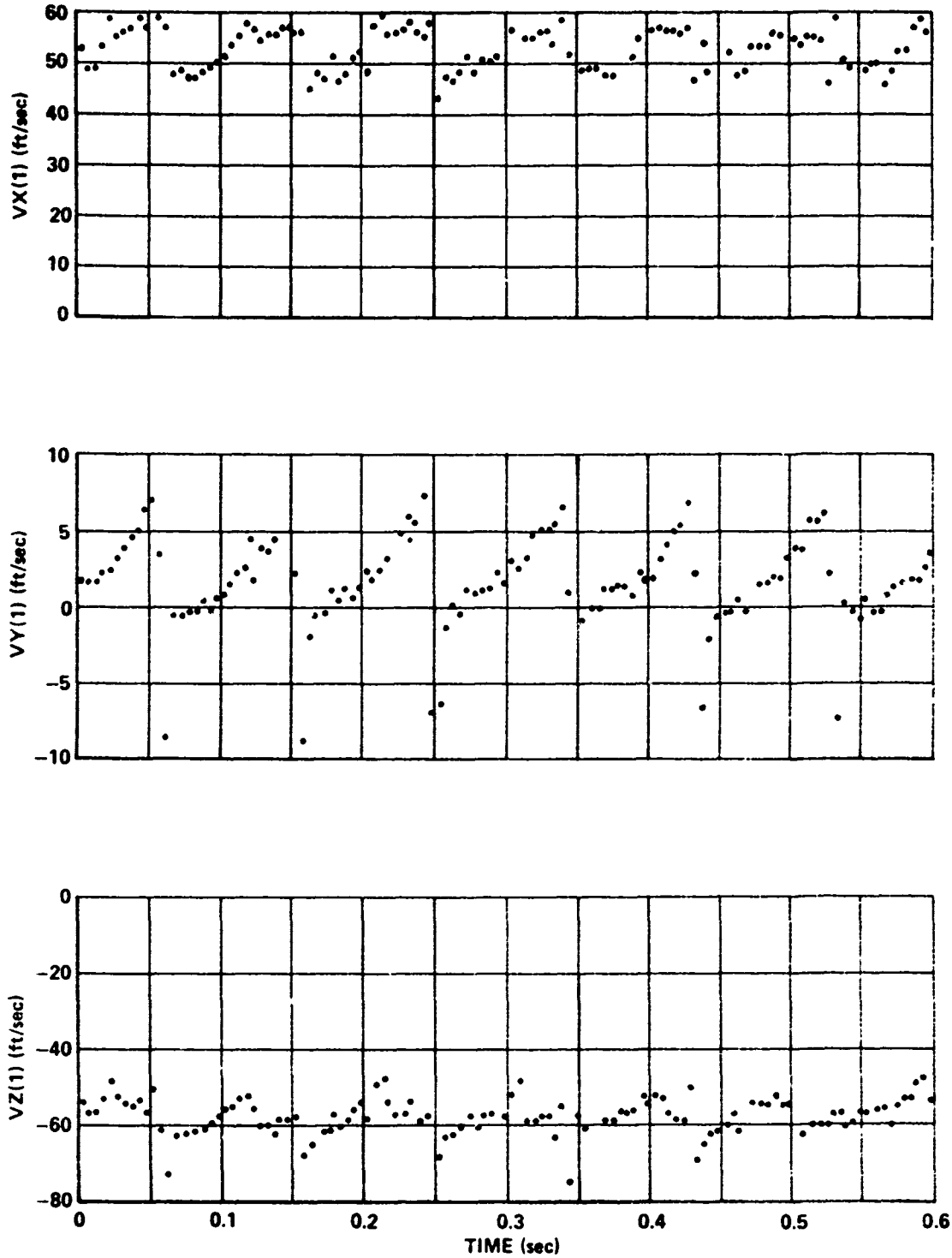

Figure 33. UH-1M helicopter flow field velocity components - flight record 15 and sensor No. 1.

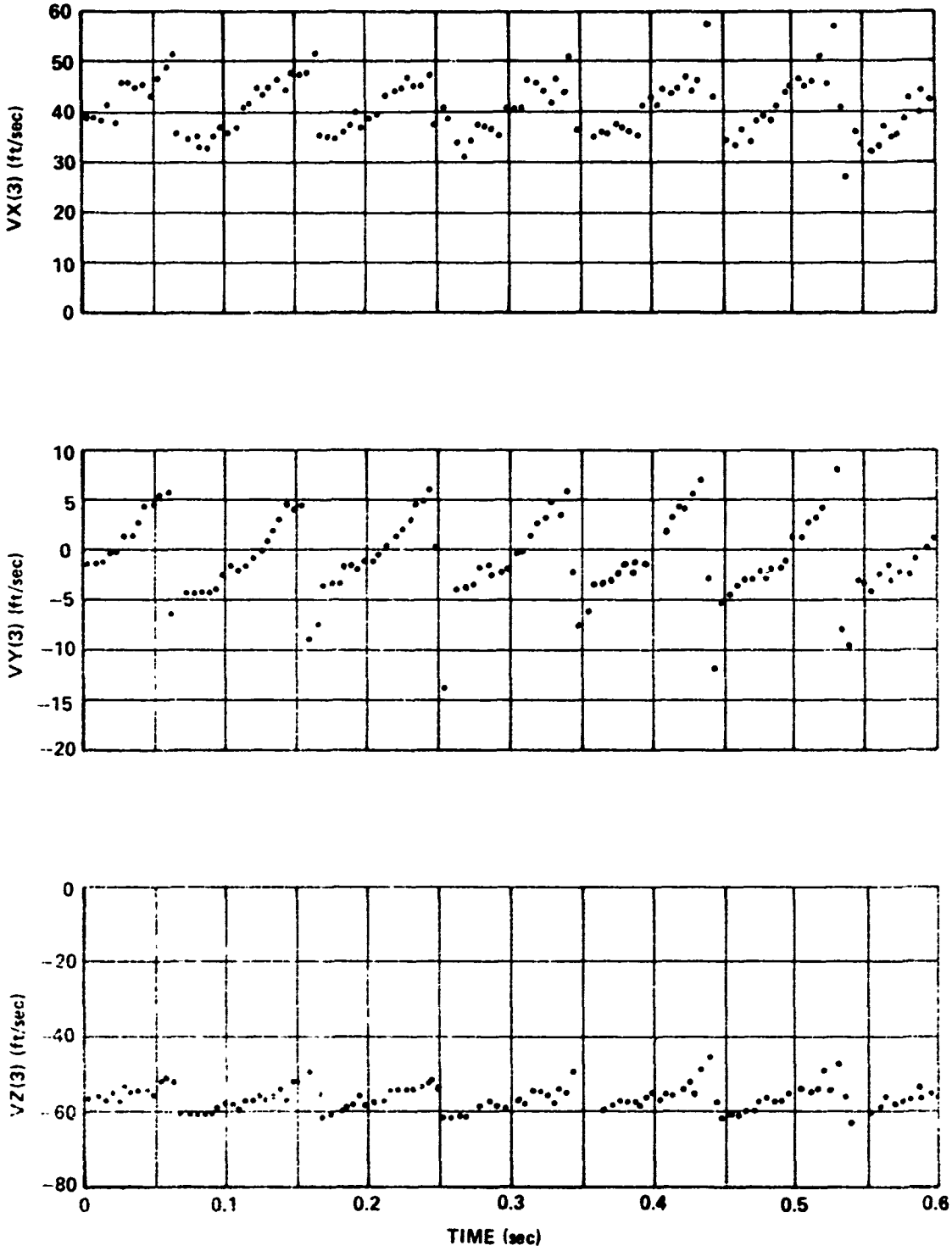

Figure 34. UH-1N helicopter flow field velocity components - flight record 15 and sensor No. 3.

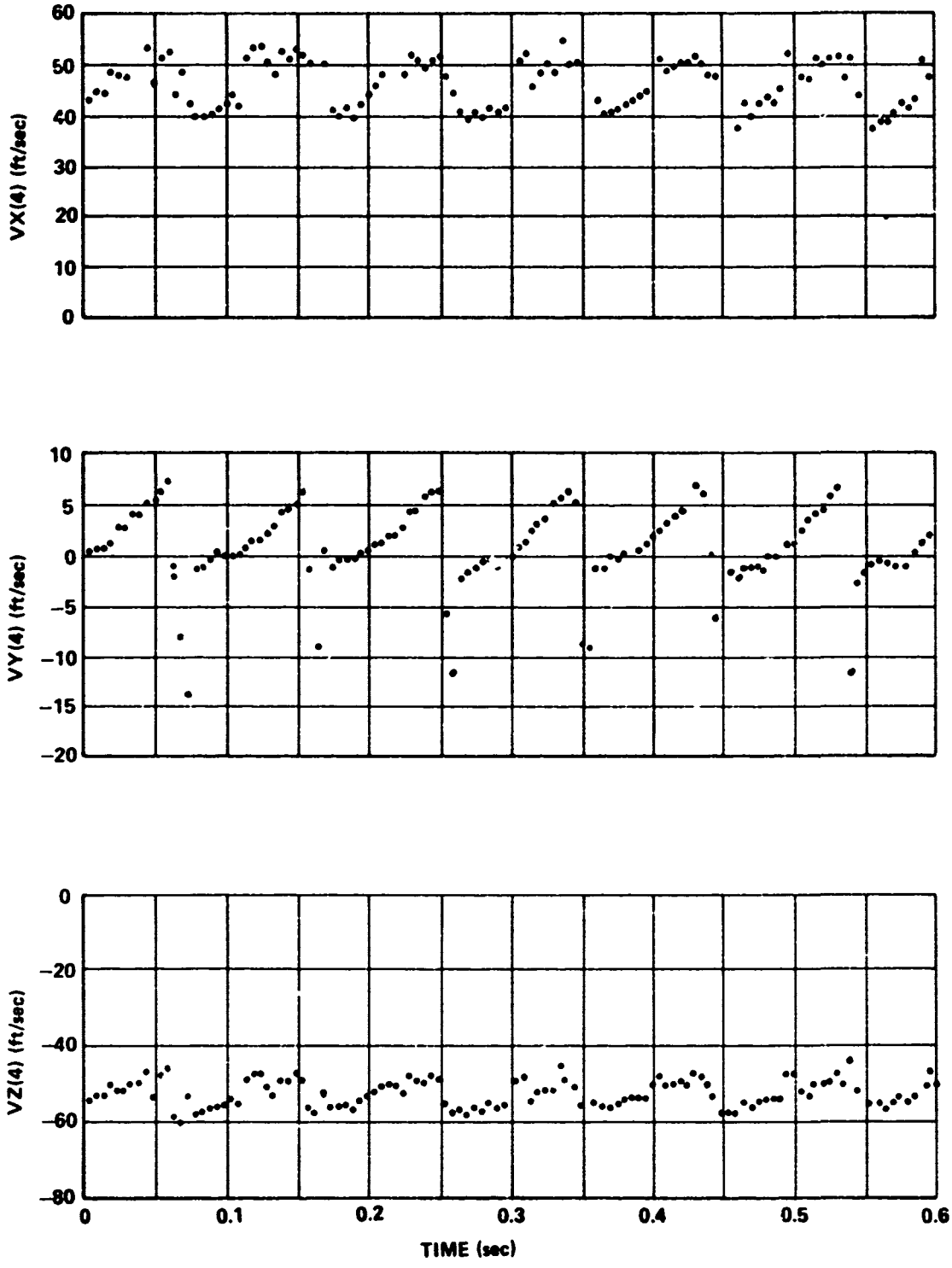

Figure 35. UH-1M helicopter flow field velocity components - flight record 15 and sensor No. 4.

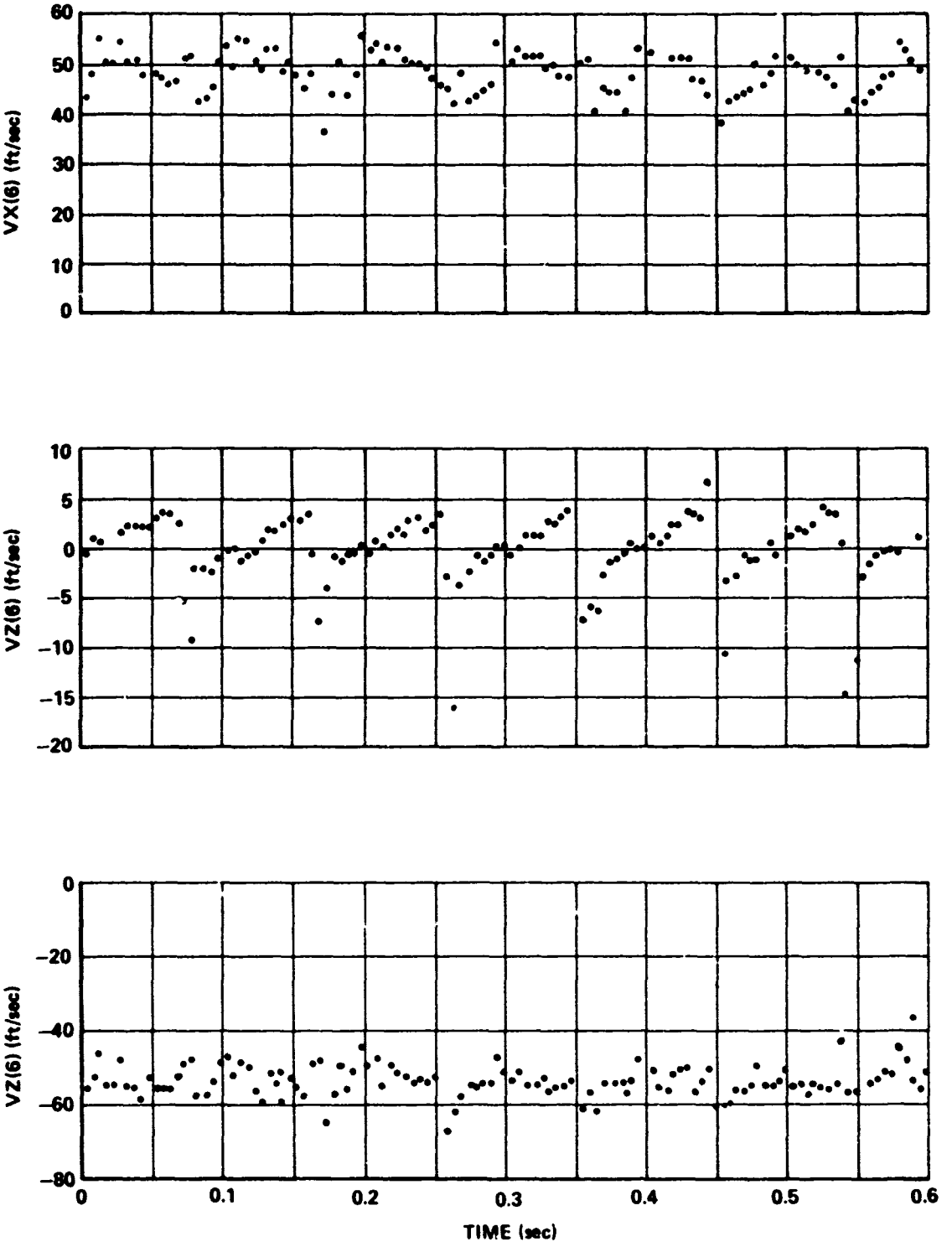

Figure 36. UH-1H helicopter flow field velocity components - flight record 15 and sensor No. 6.

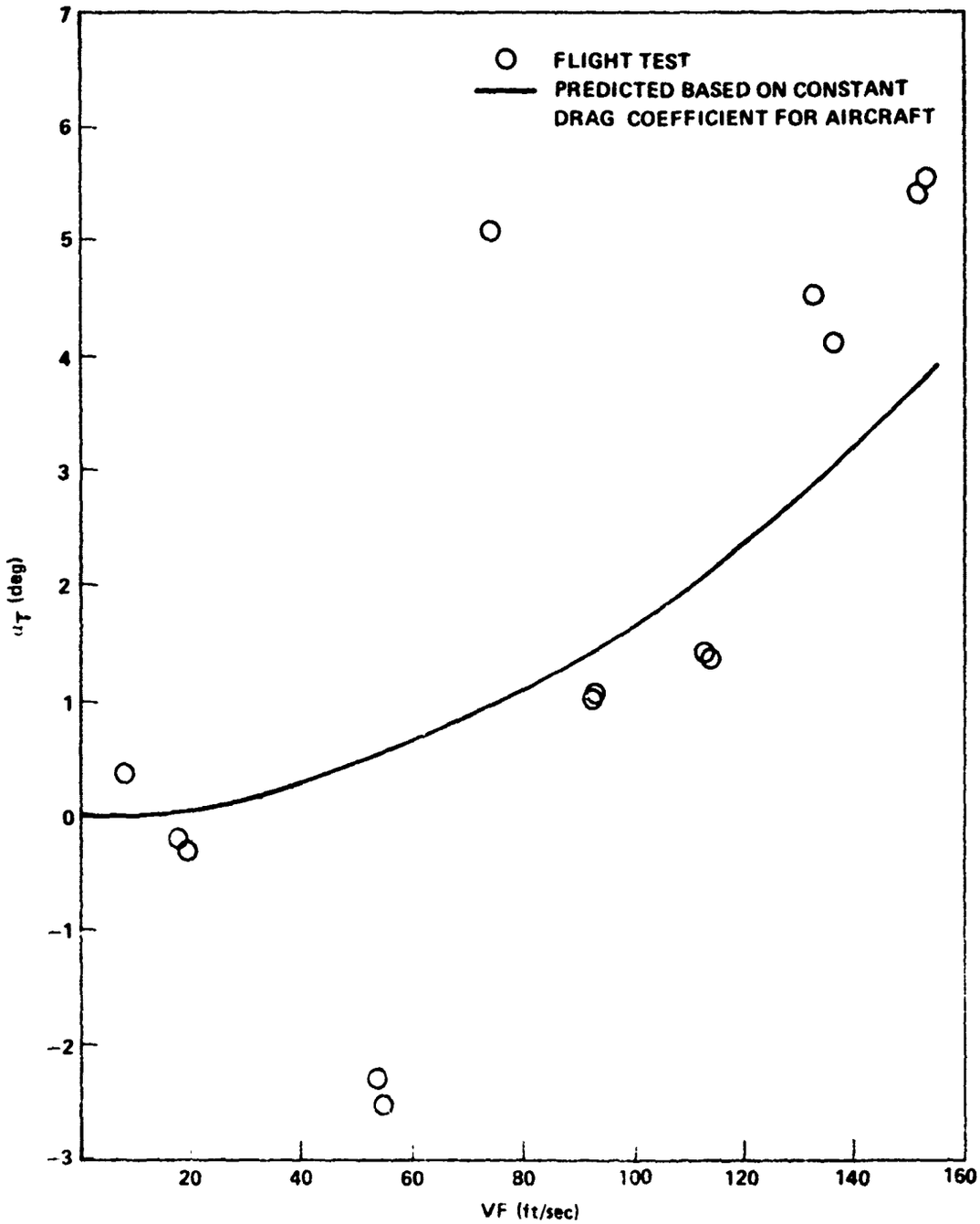

Figure 37. Variation of inclination of tip path plane of helicopter to freestream with helicopter airspeed.

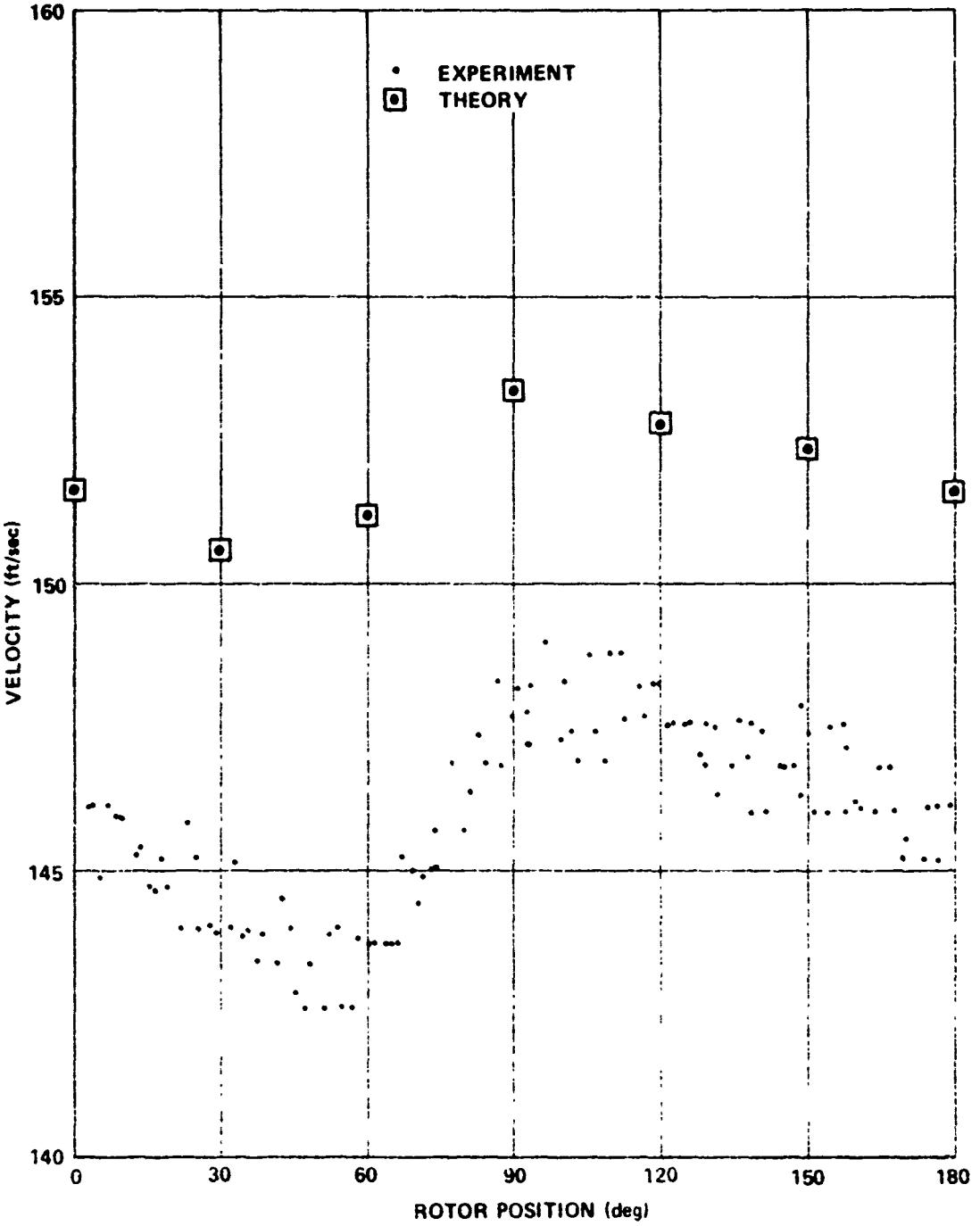

Figure 38. Folded comparison - flight record 1, sensor No. 1, and trial period 0.093500.

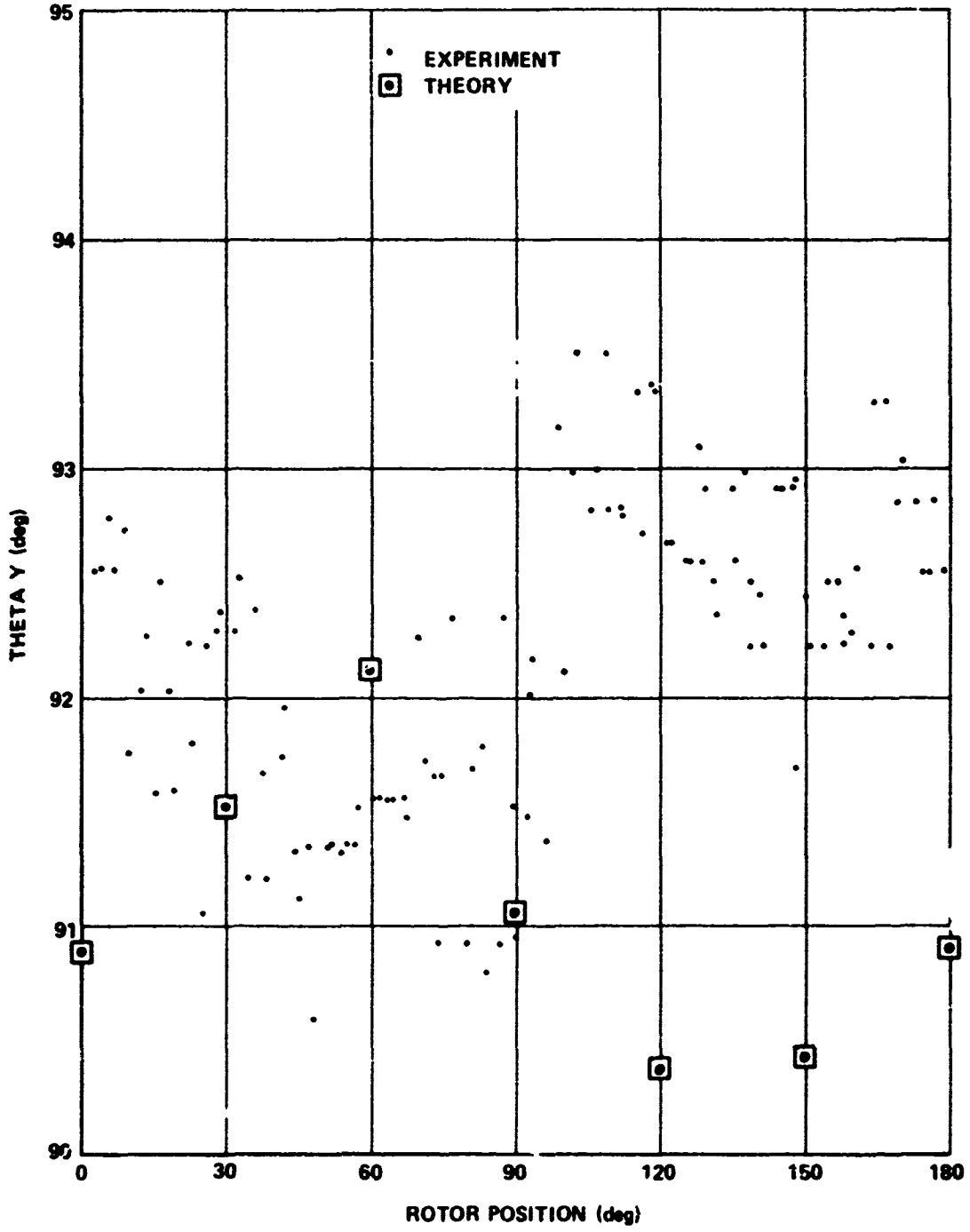

Figure 39. Folded comparison - flight record 1, sensor No. 1, and trial period 0.093500.

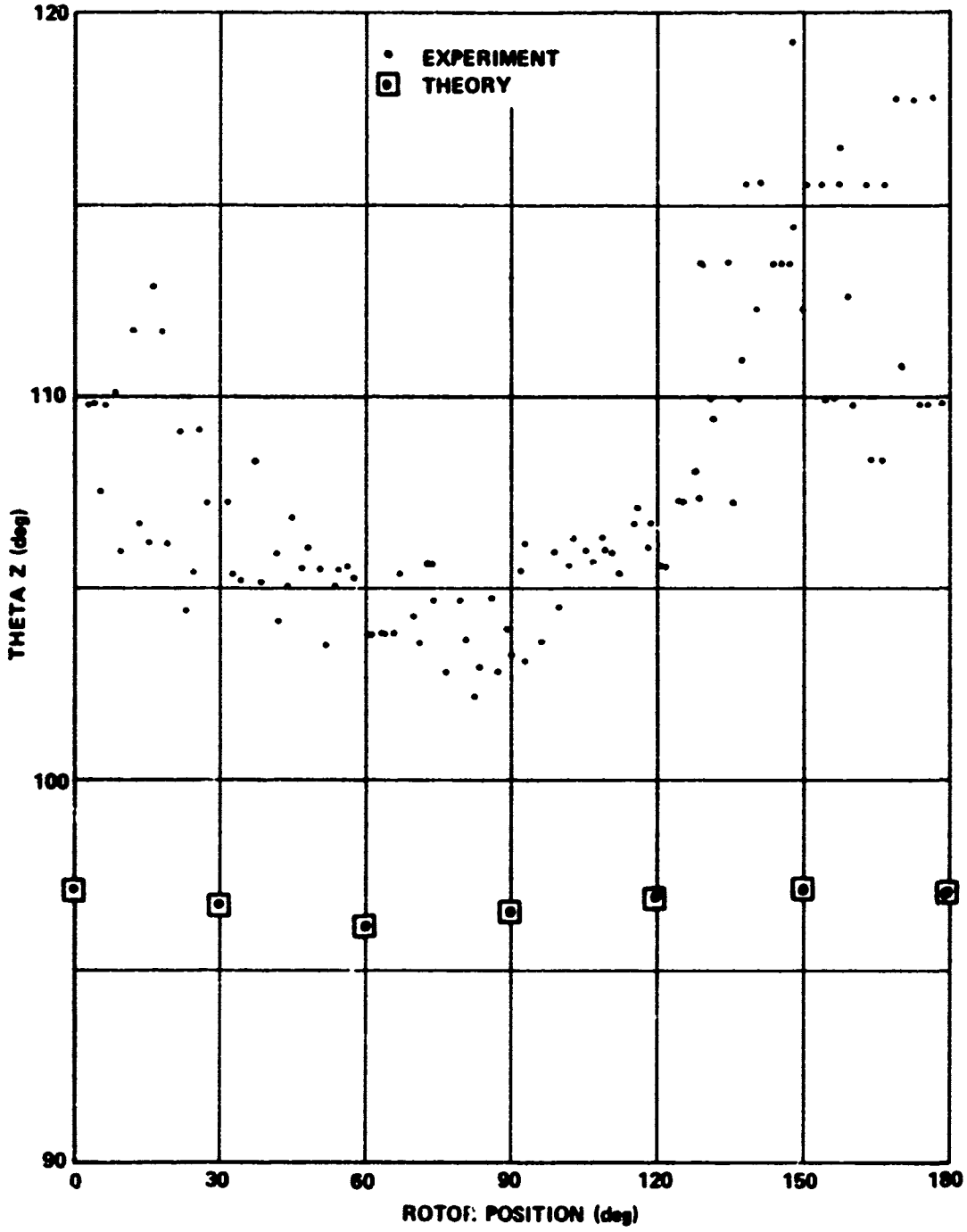

Figure 40. Folded comparison - flight record 1, sensor No. 1, and trial period 0.093500.

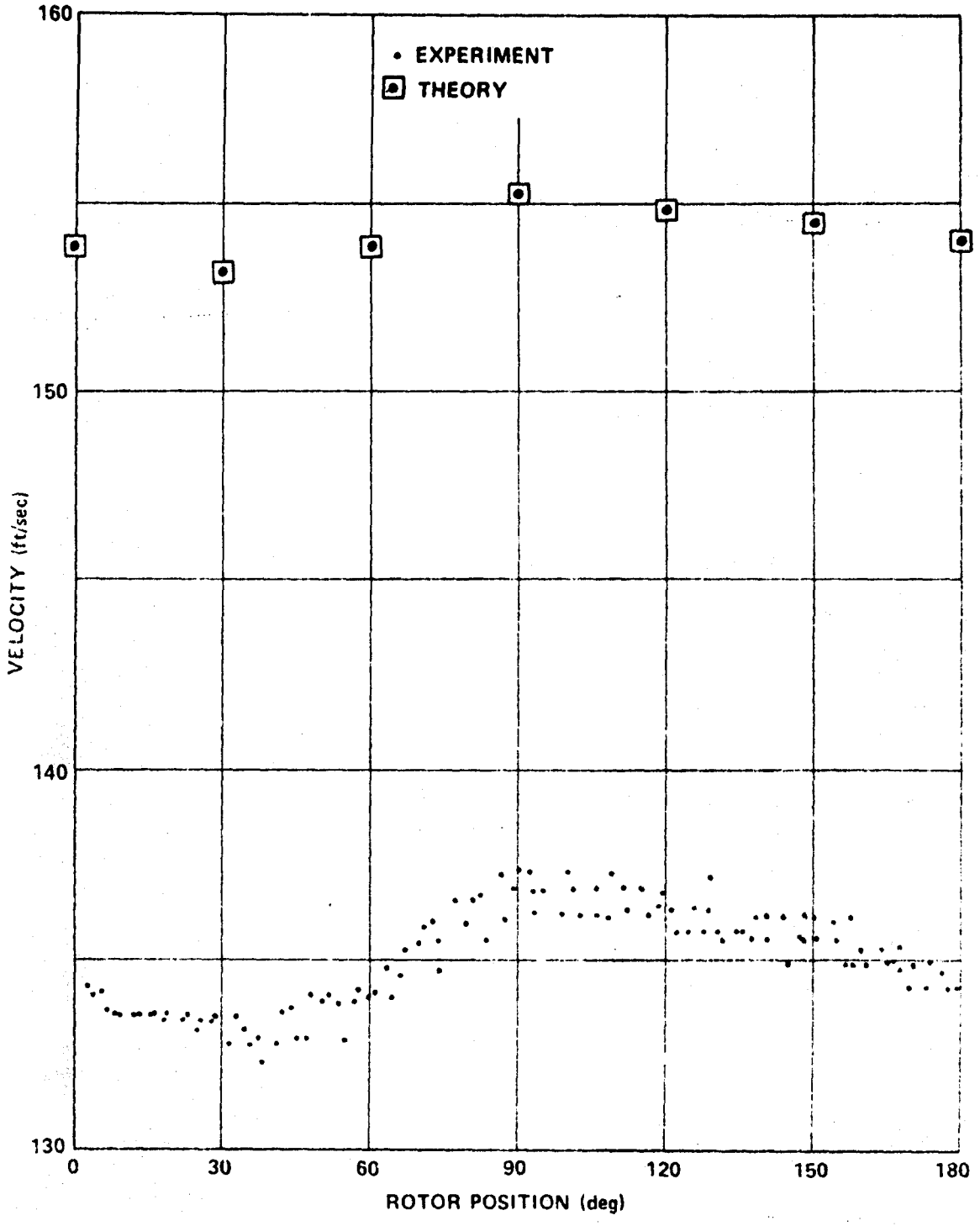

Figure 41. Folded comparison - Flight record 1, sensor No. 3, and trial period 0.093500.

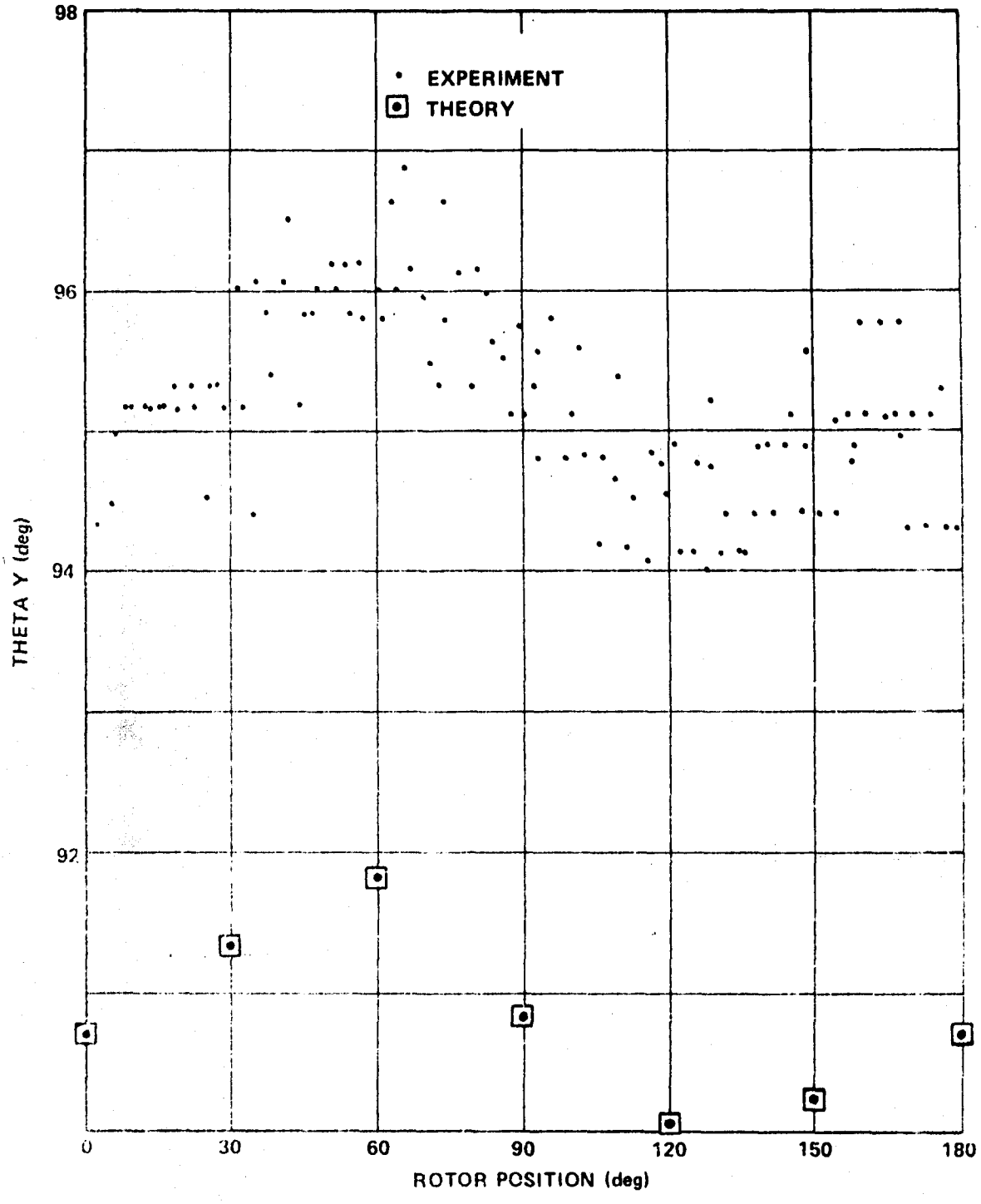

Figure 42. Folded comparison - flight record 1, sensor No. 3, and trial period 0.093500.

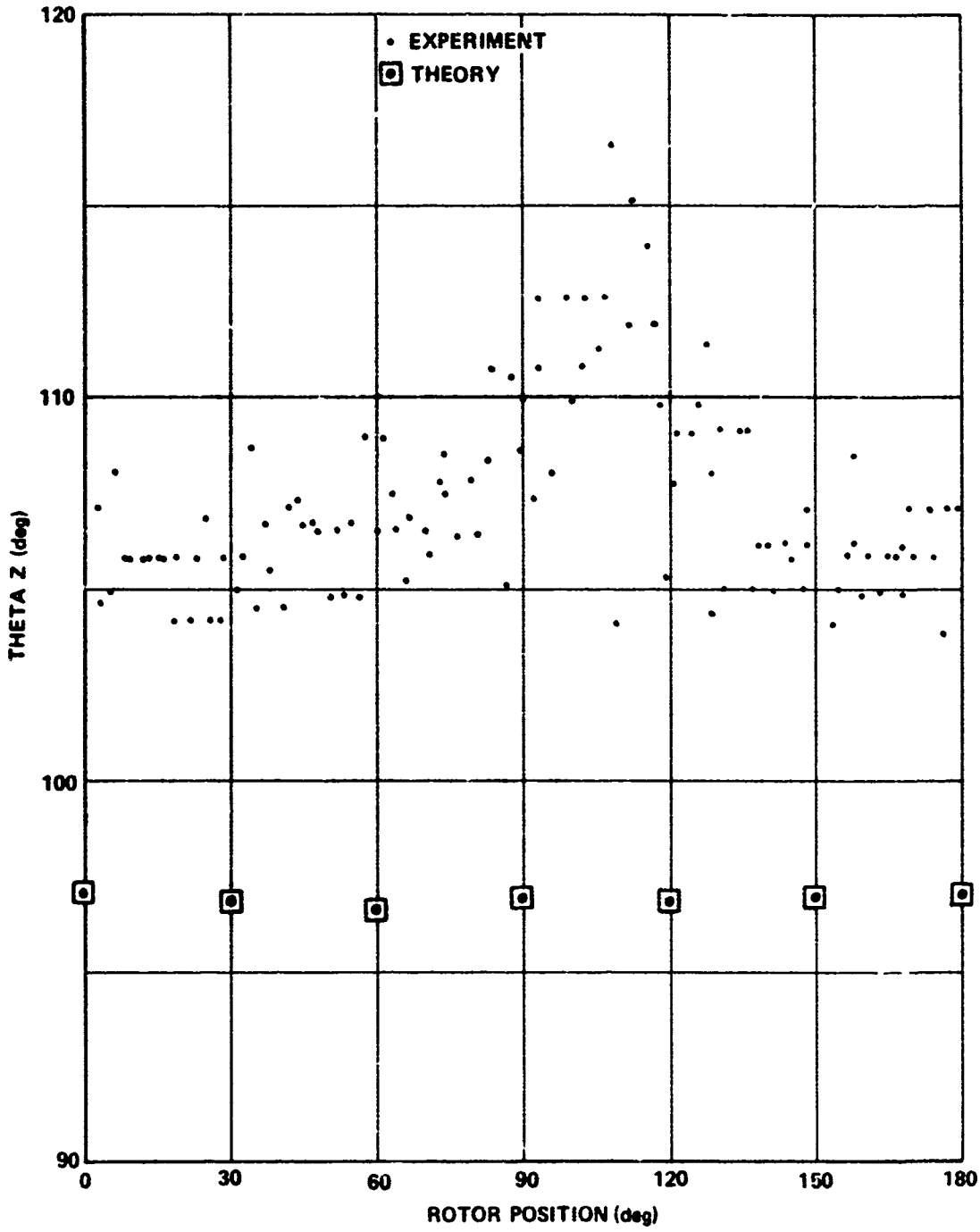

Figure 43. Folded comparison - flight record 1, sensor No. 3, and trial period 0.093500.

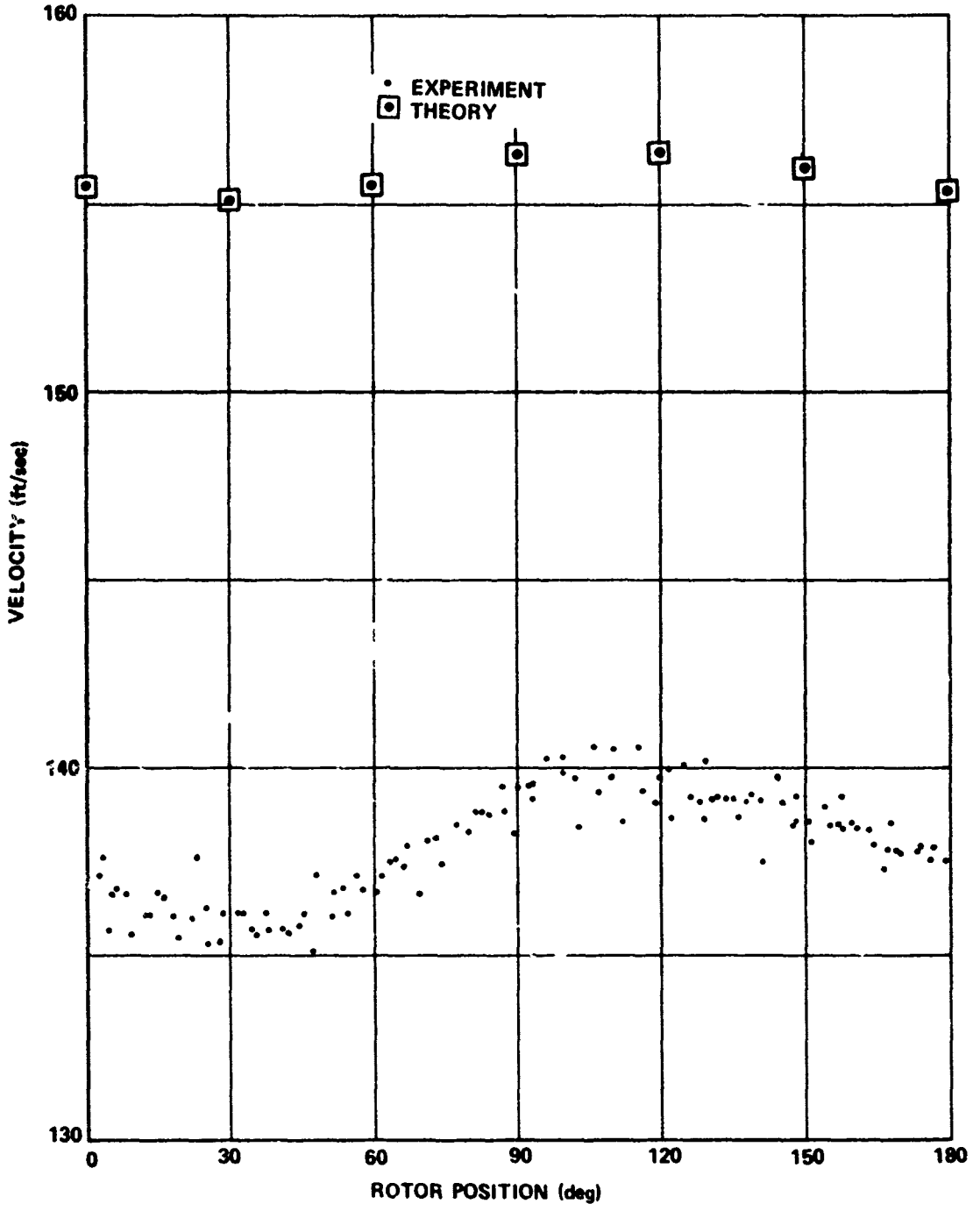

Figure 44. Folded comparison - flight record 1, sensor No. 4, and trial period 0.093500.

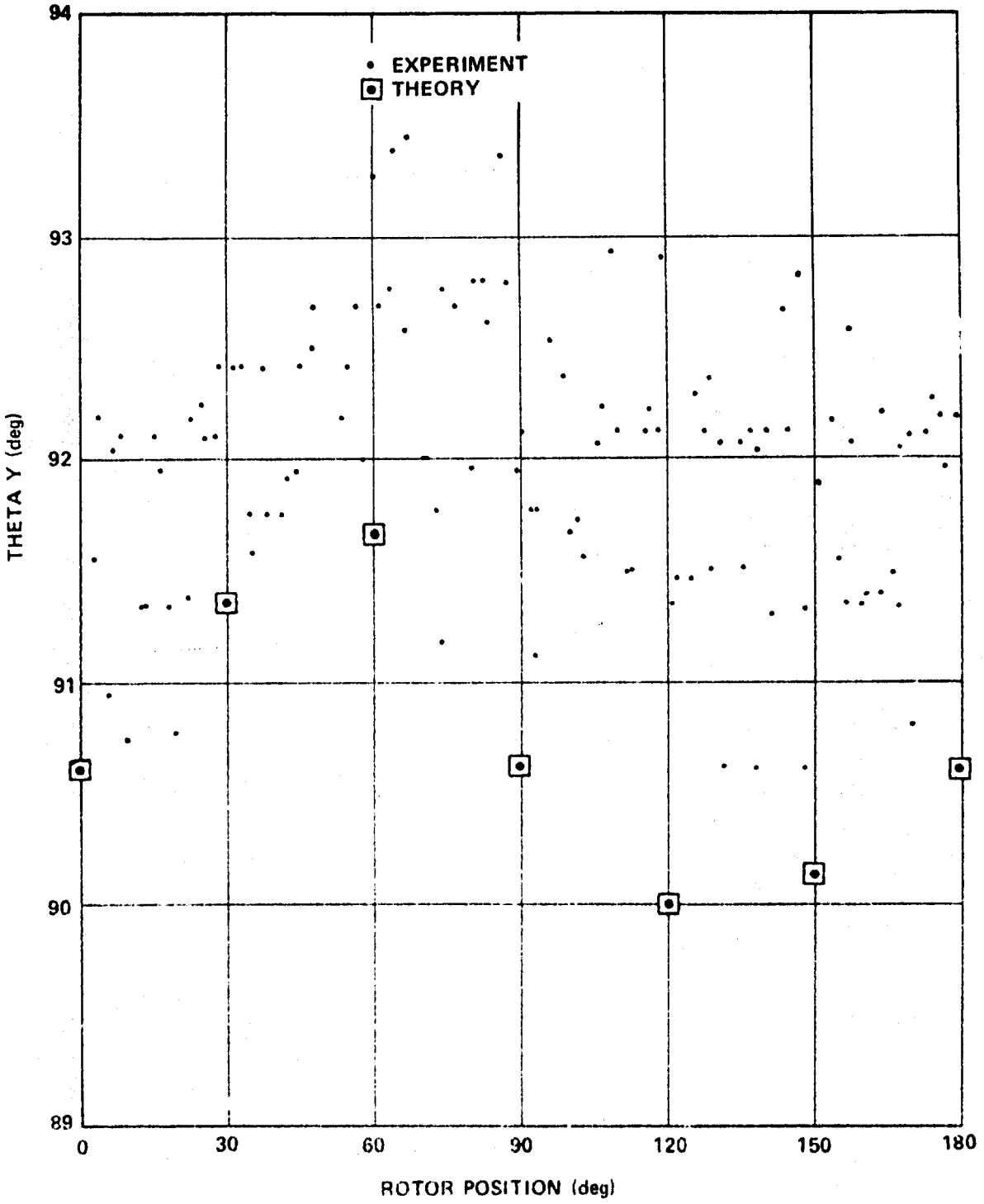

Figure 45. Folded comparison – flight record 1, sensor No. 4, trial period 0.093500.

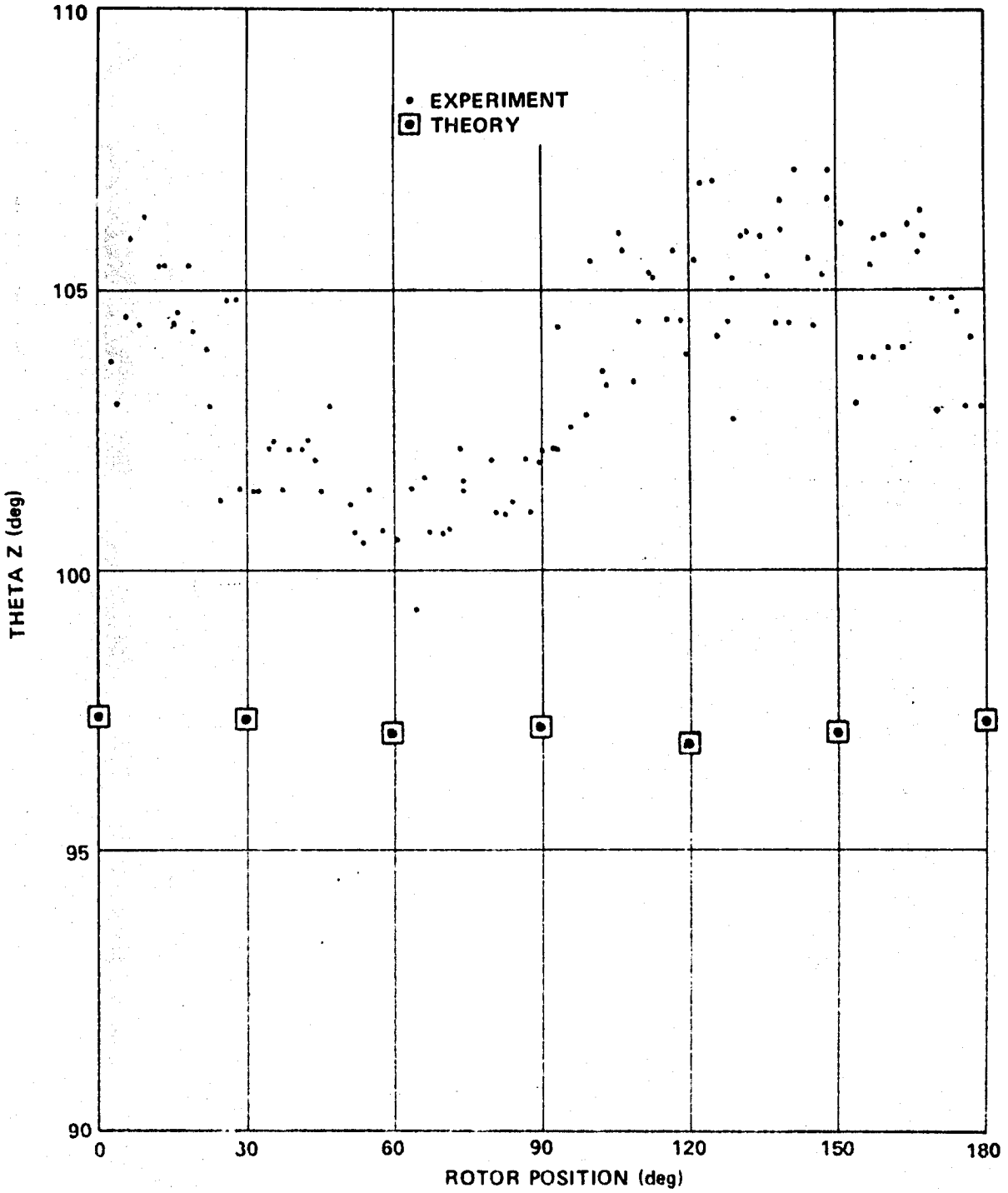

Figure 46. Folded comparison - flight record 1, sensor No. 4, and trial period 0.093500.

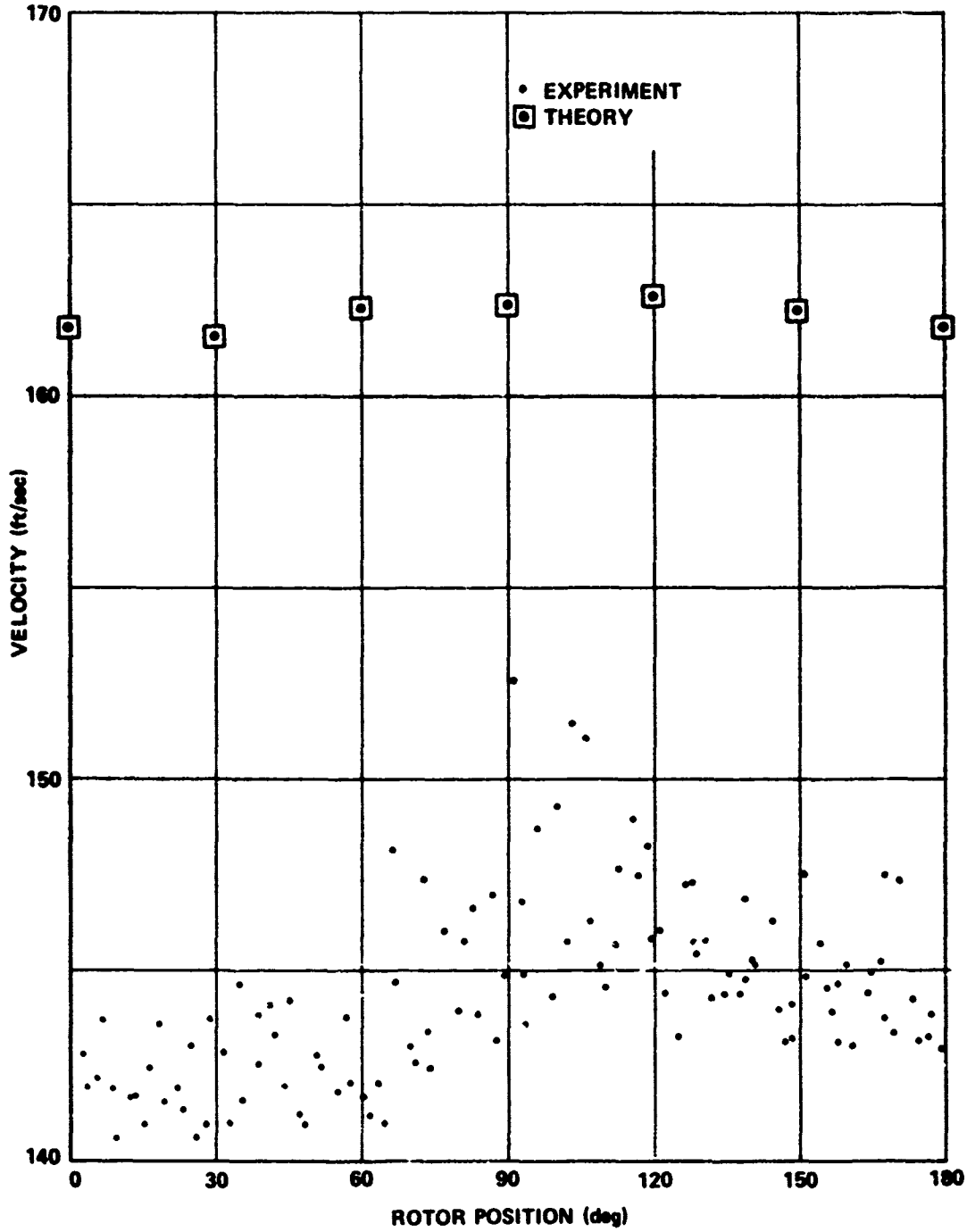

Figure 47. Folded comparison - flight record 1, sensor No. 6, and trial period 0.093500.

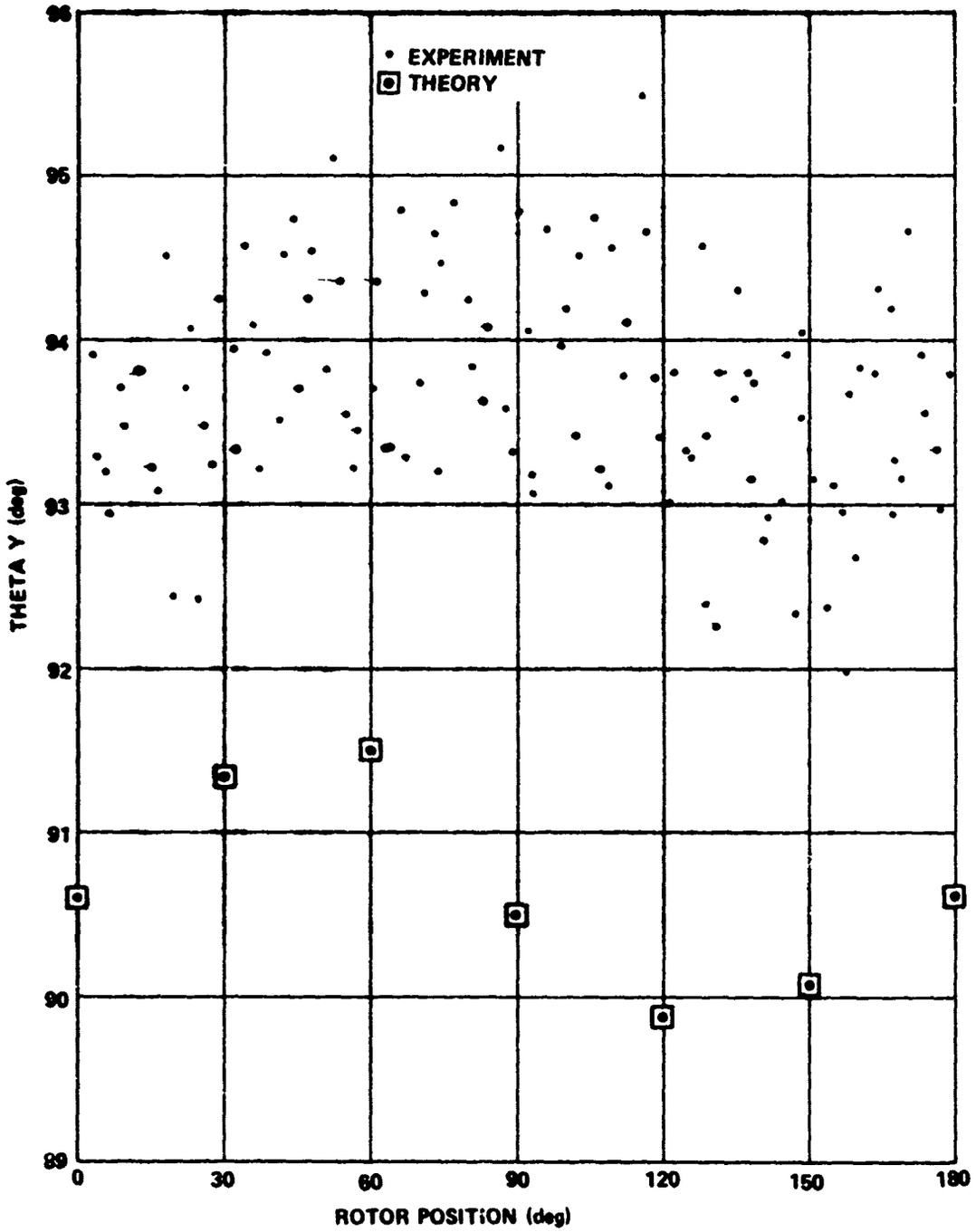

Figure 48. Folded comparison - flight record 1, sensor No. 6, and trial period 0.093500.

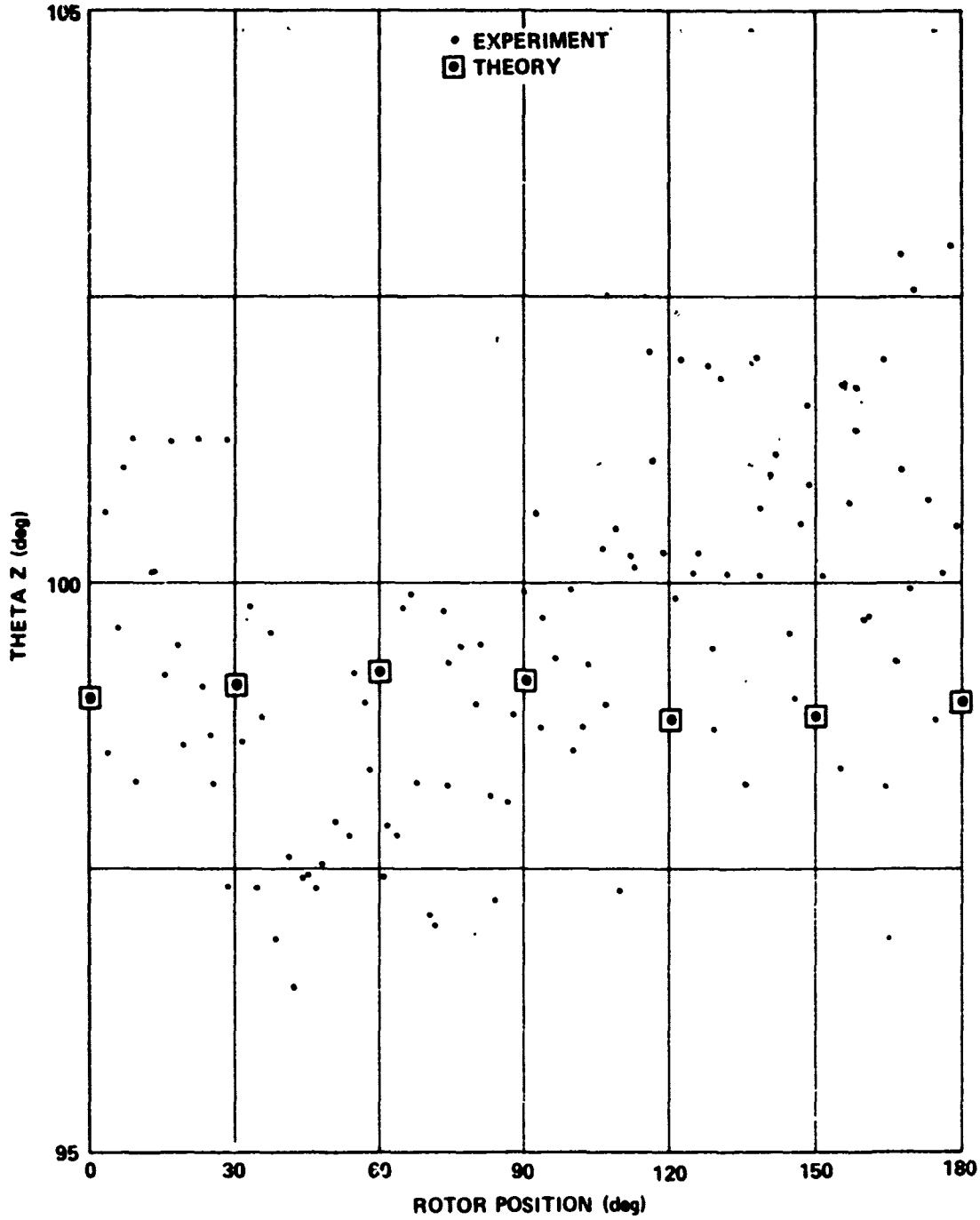

Figure 49. Folded comparison - flight record 1, sensor No. 6, and trial period 0.093500.

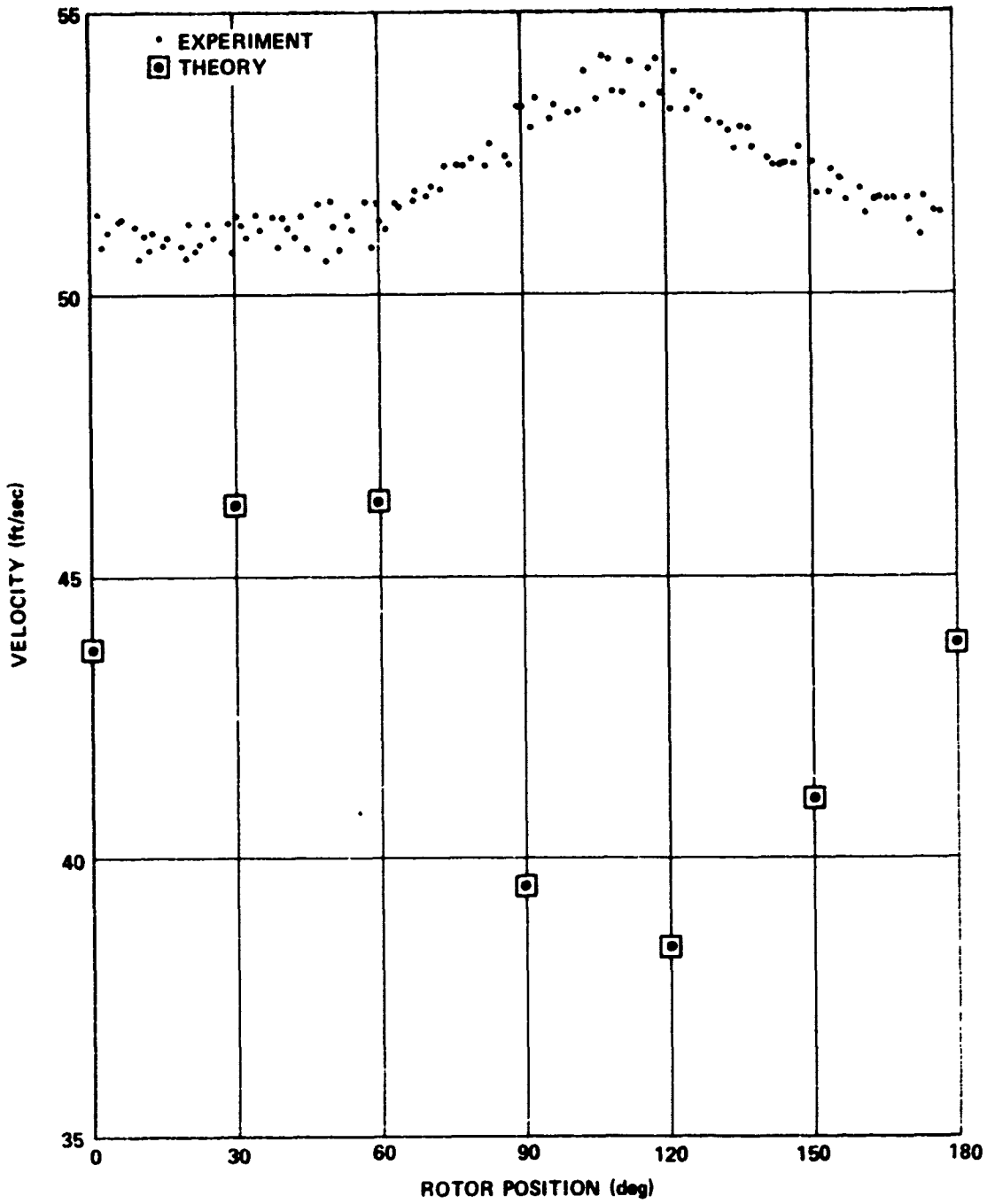

Figure 30. Folded comparison - flight record 10, sensor No. 1, and trial period 0.093500.

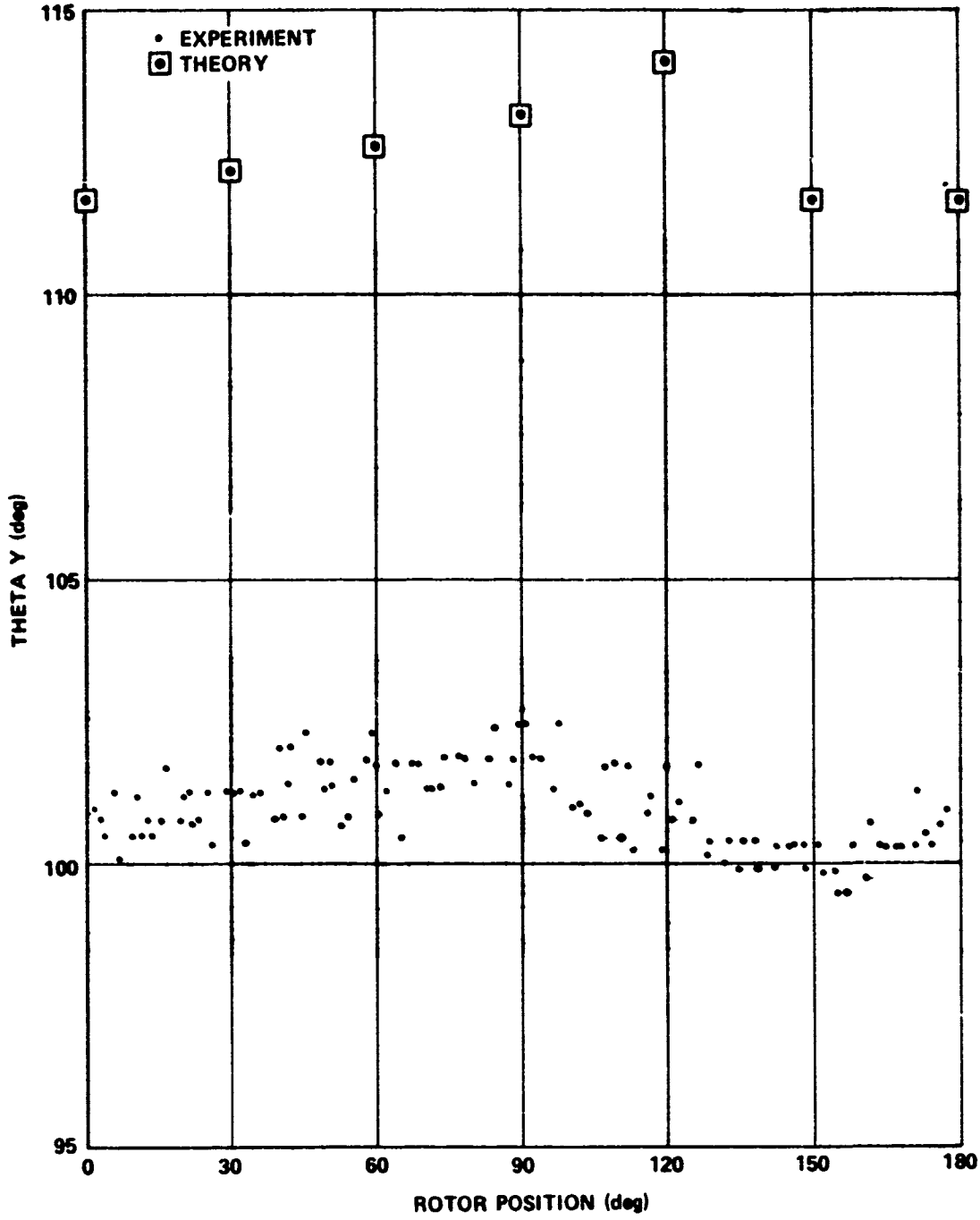

Figure 51. Folded comparison - flight record 10, sensor No. 1, and trial period 0.093500.

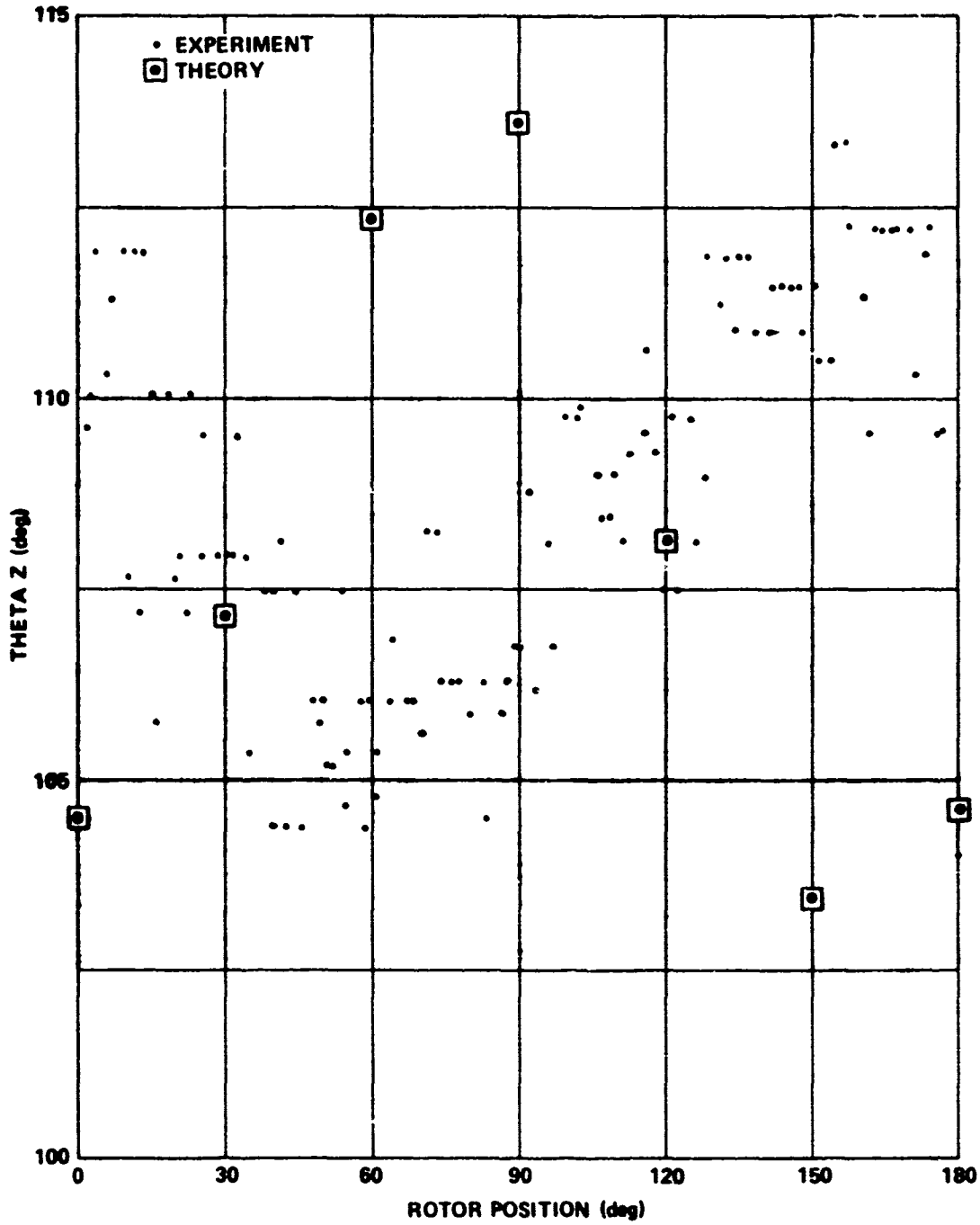

Figure 52. Folded comparison - flight record 10, sensor No. 1, and trial period 0.093500.

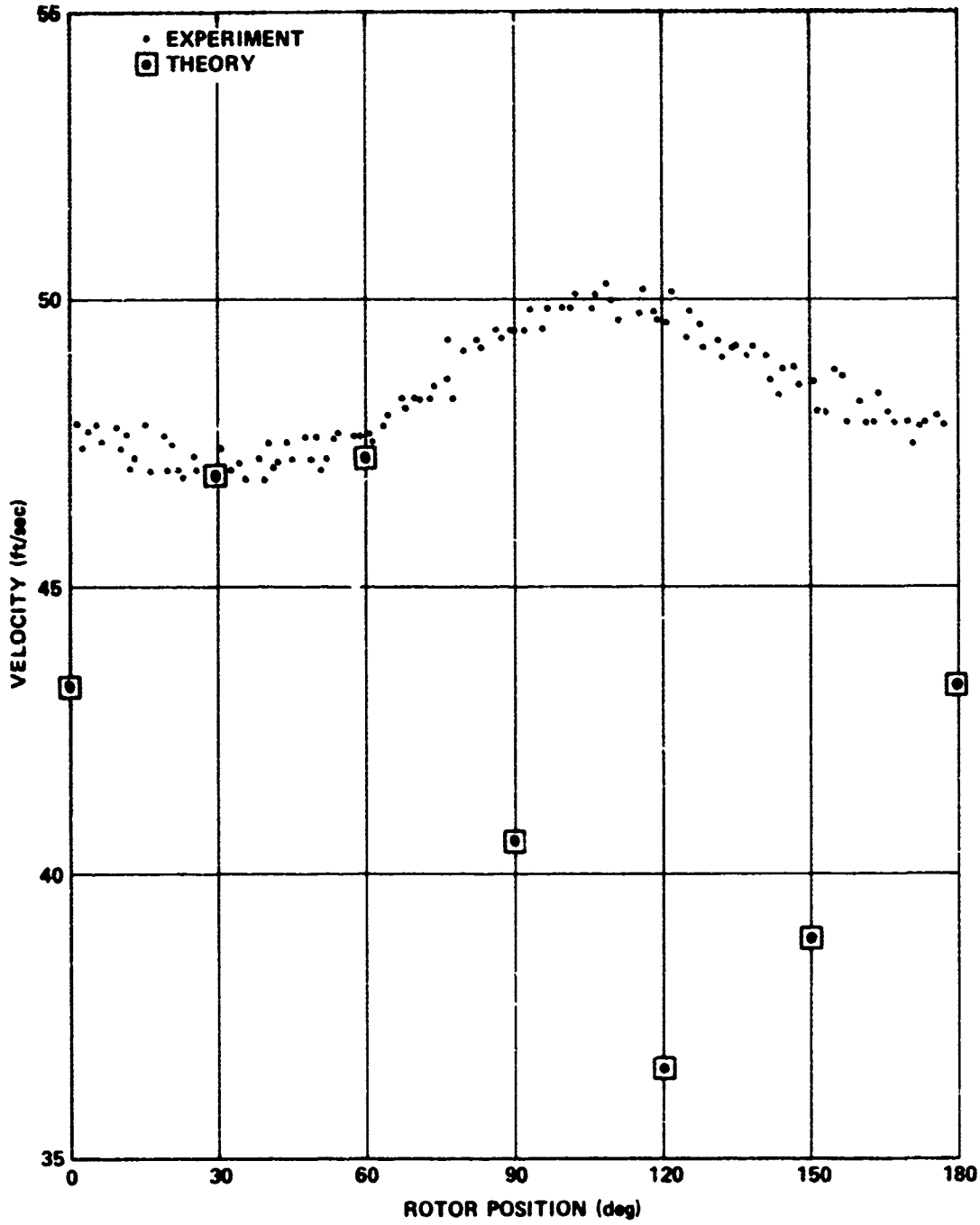

Figure 53. Folded comparison - flight record 10, sensor No. 3, and trial period 0.093500.

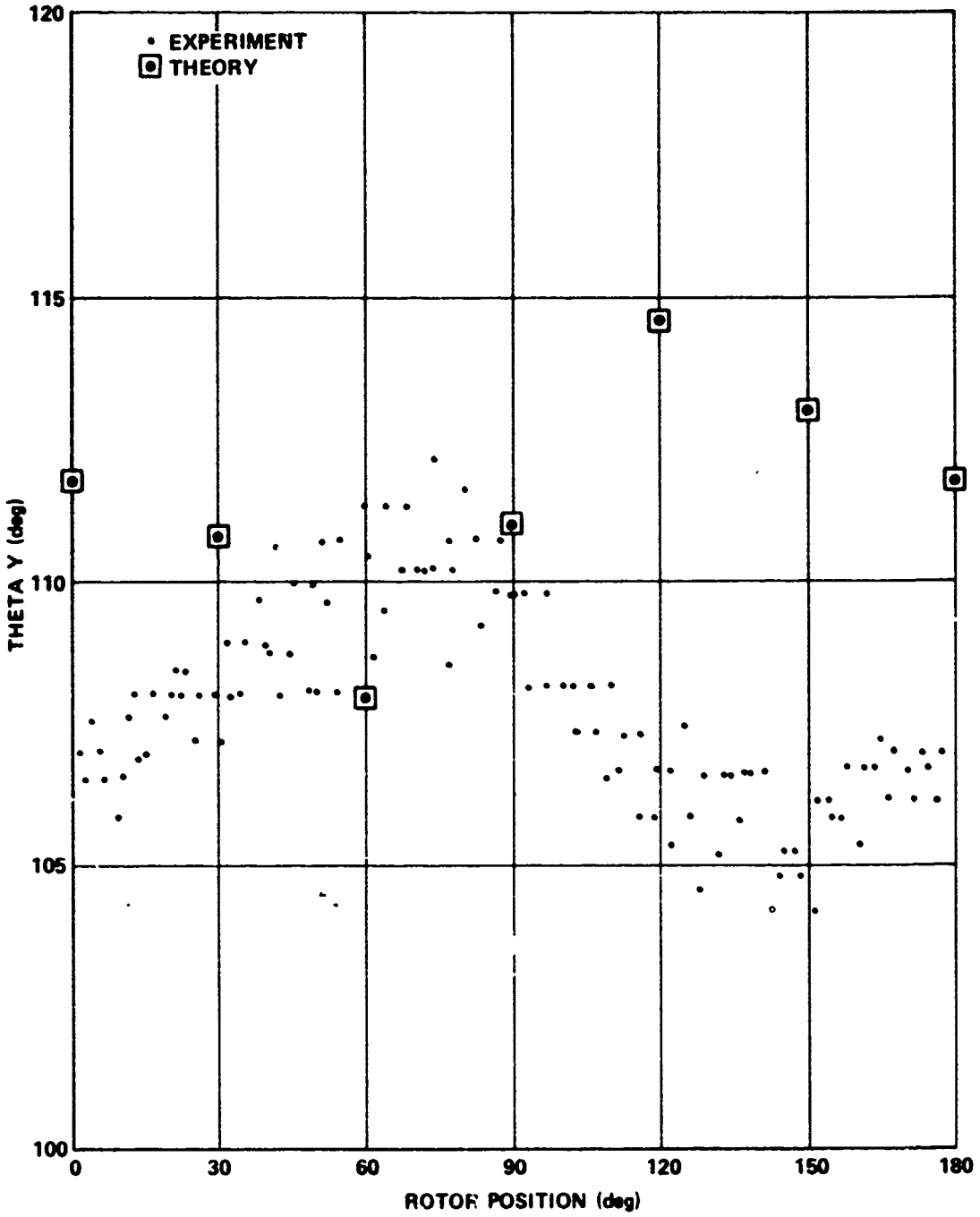

Figure 54. Folded comparison - flight record 10, sensor No. 3, and trial period 0.093500.

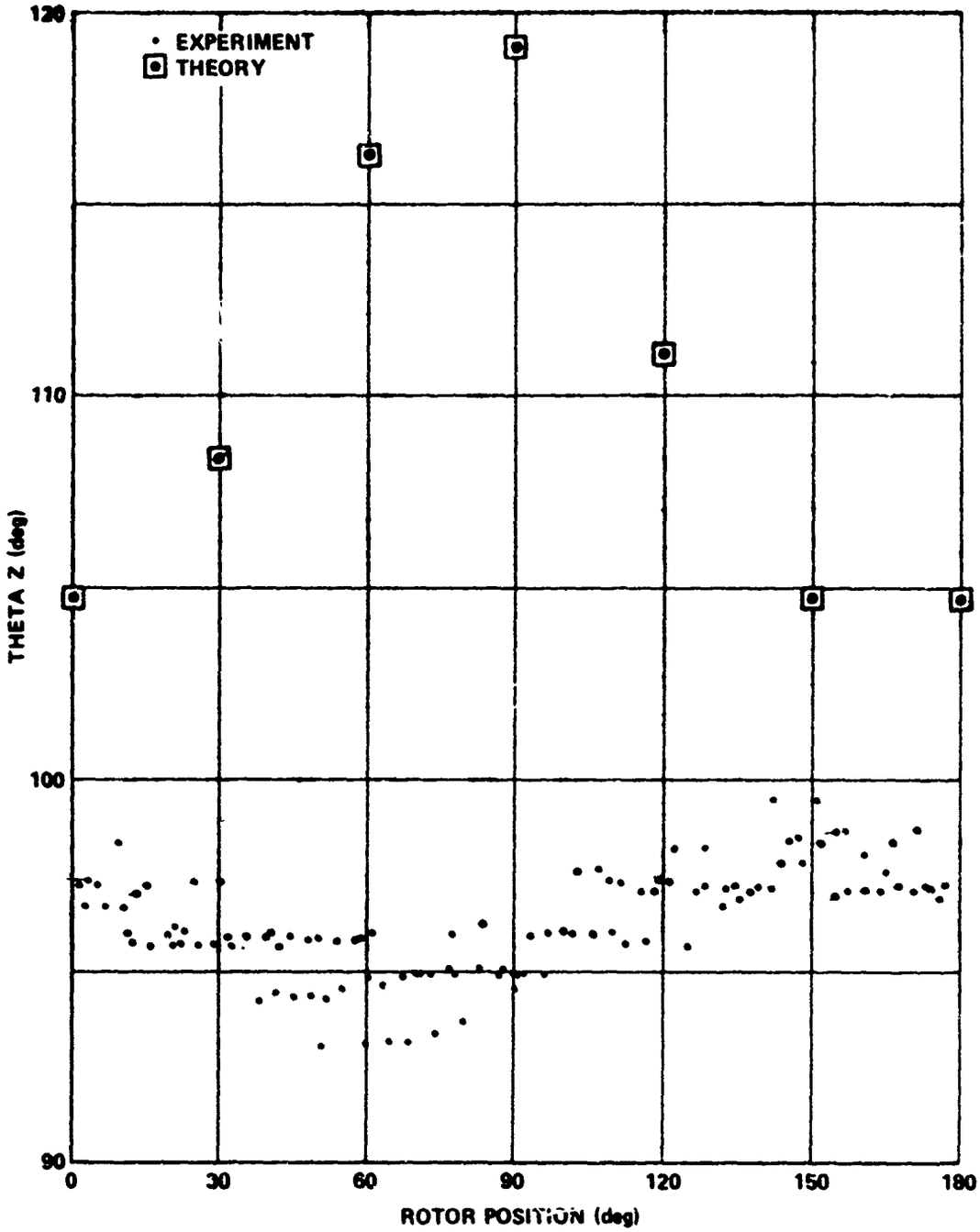

Figure 55. Folded comparison - flight record 10, sensor No. 3, and trial period 0.093500.

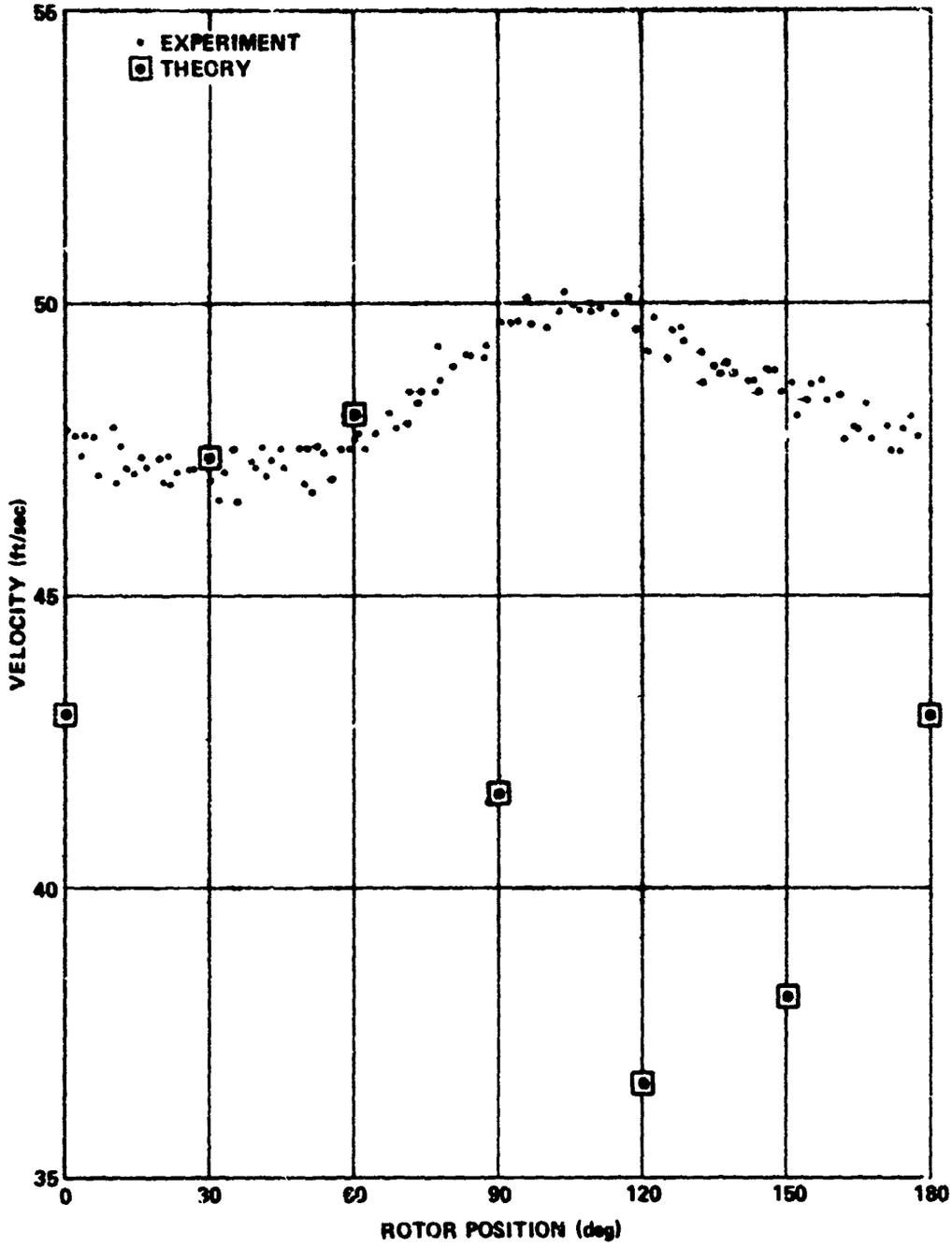

Figure 56. Folded comparison - flight record 10, sensor No. 4, and trial period 0.093500.

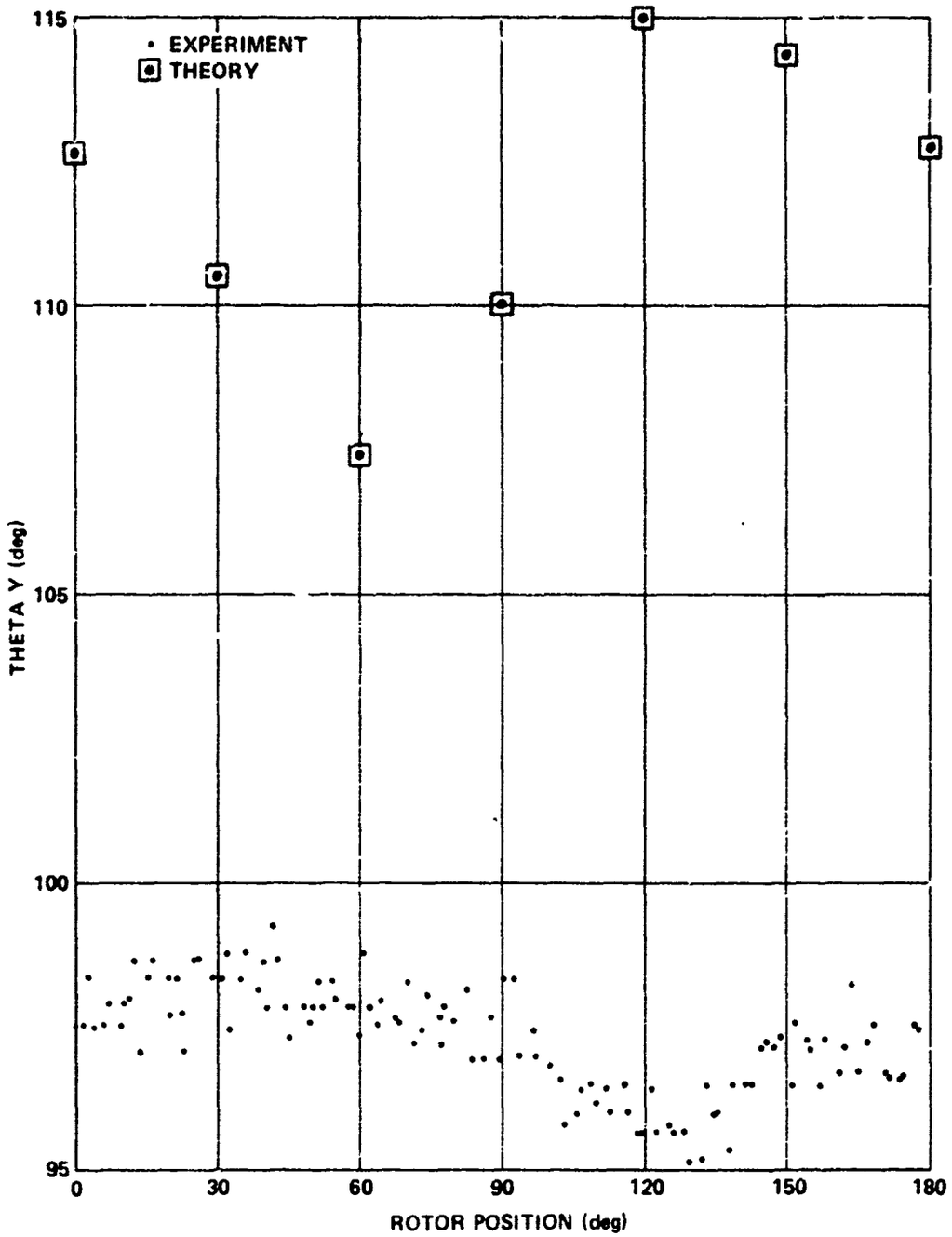

Figure 57. Folded comparison - flight record 10, sensor No. 4, and trial period 0.093500.

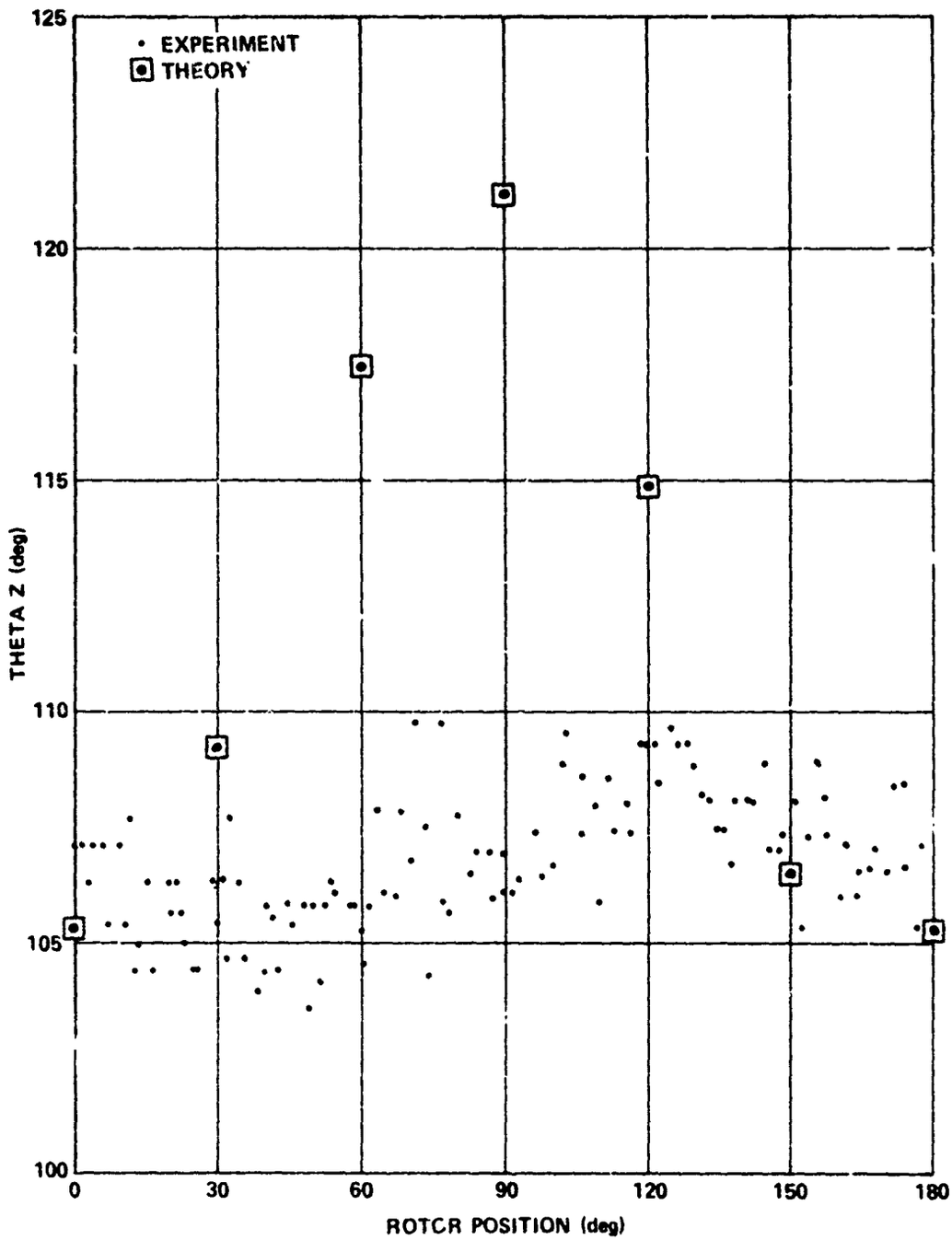

Figure 58. Folded comparison - flight record 10, sensor No. 4, and trial period 0.093500.

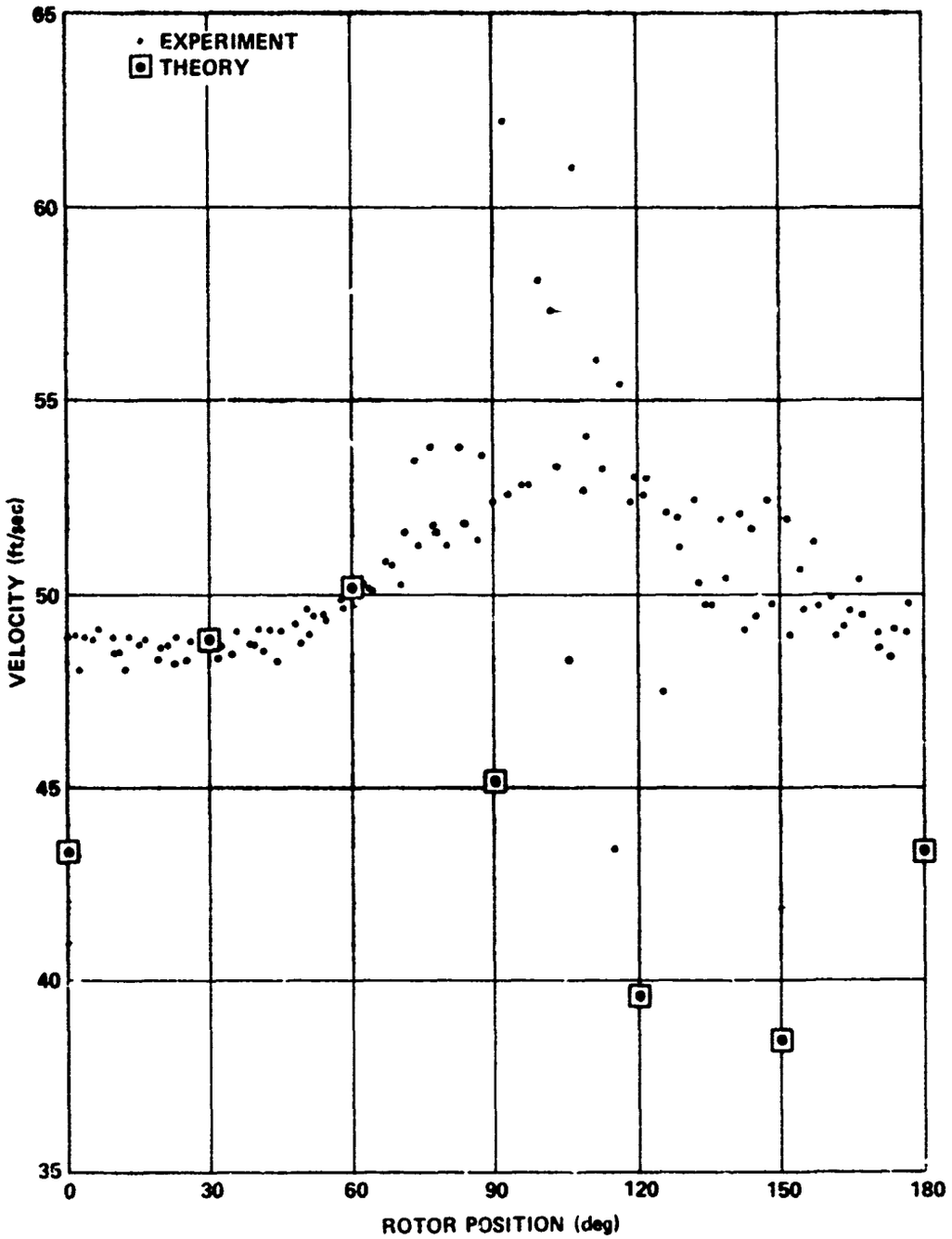

Figure 59. Folded comparison - flight record 10, sensor No. 6, and trial period 0.093500.

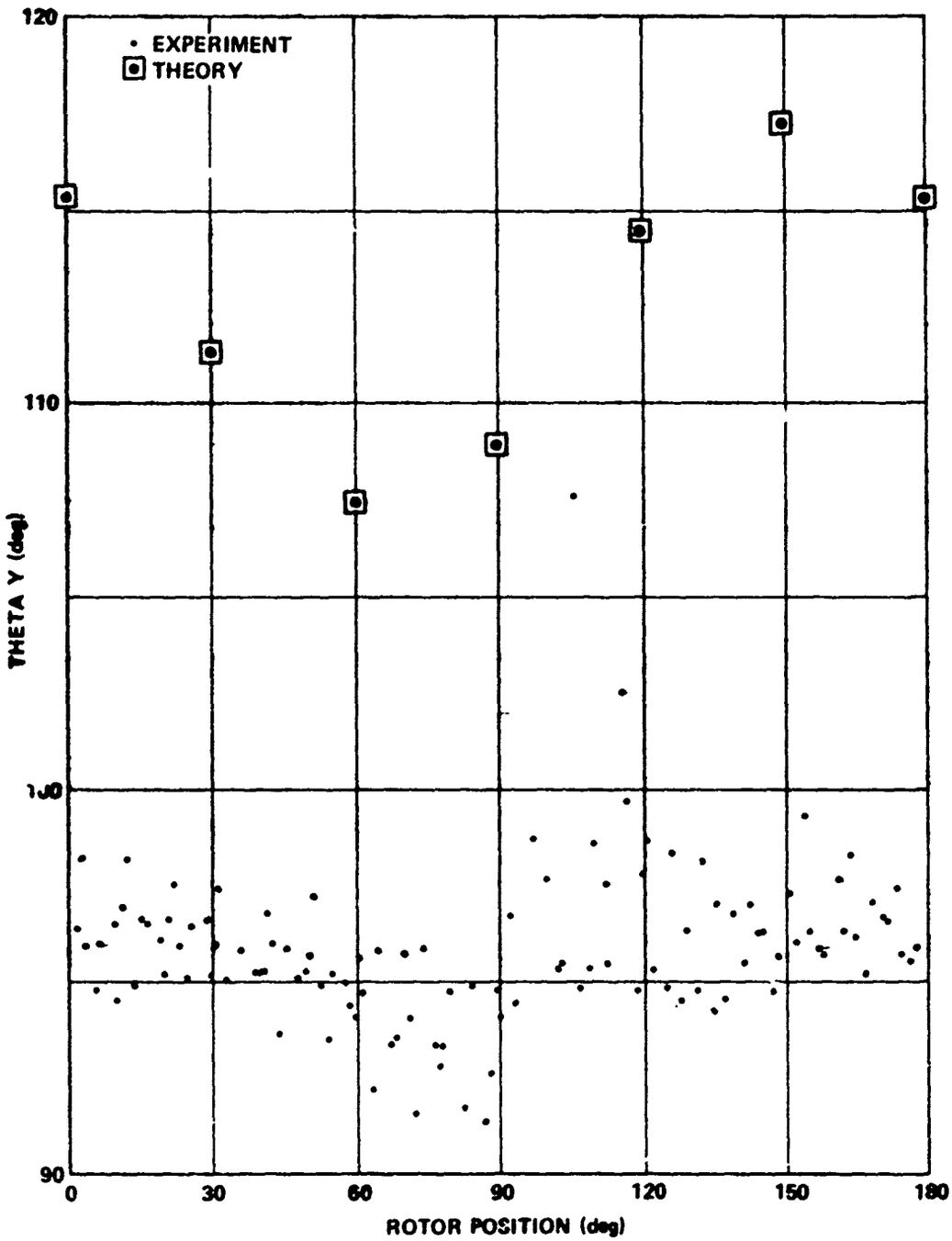

Figure 60. Folded comparison - flight record 10, sensor No. 6, and trial period 0.093500.

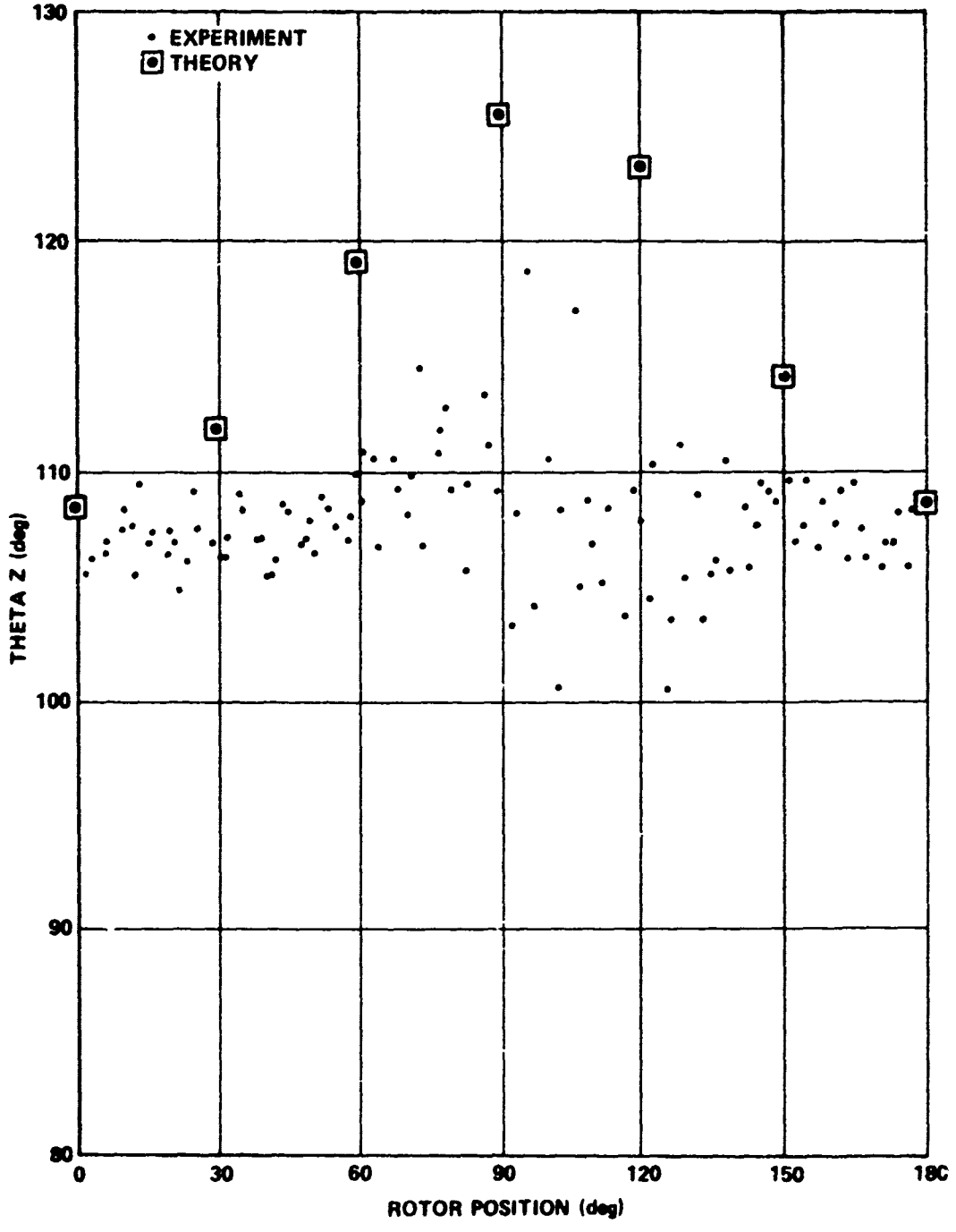

Figure 61. Folded comparison - flight record 10, sensor No. 6, and trial period 0.093500.

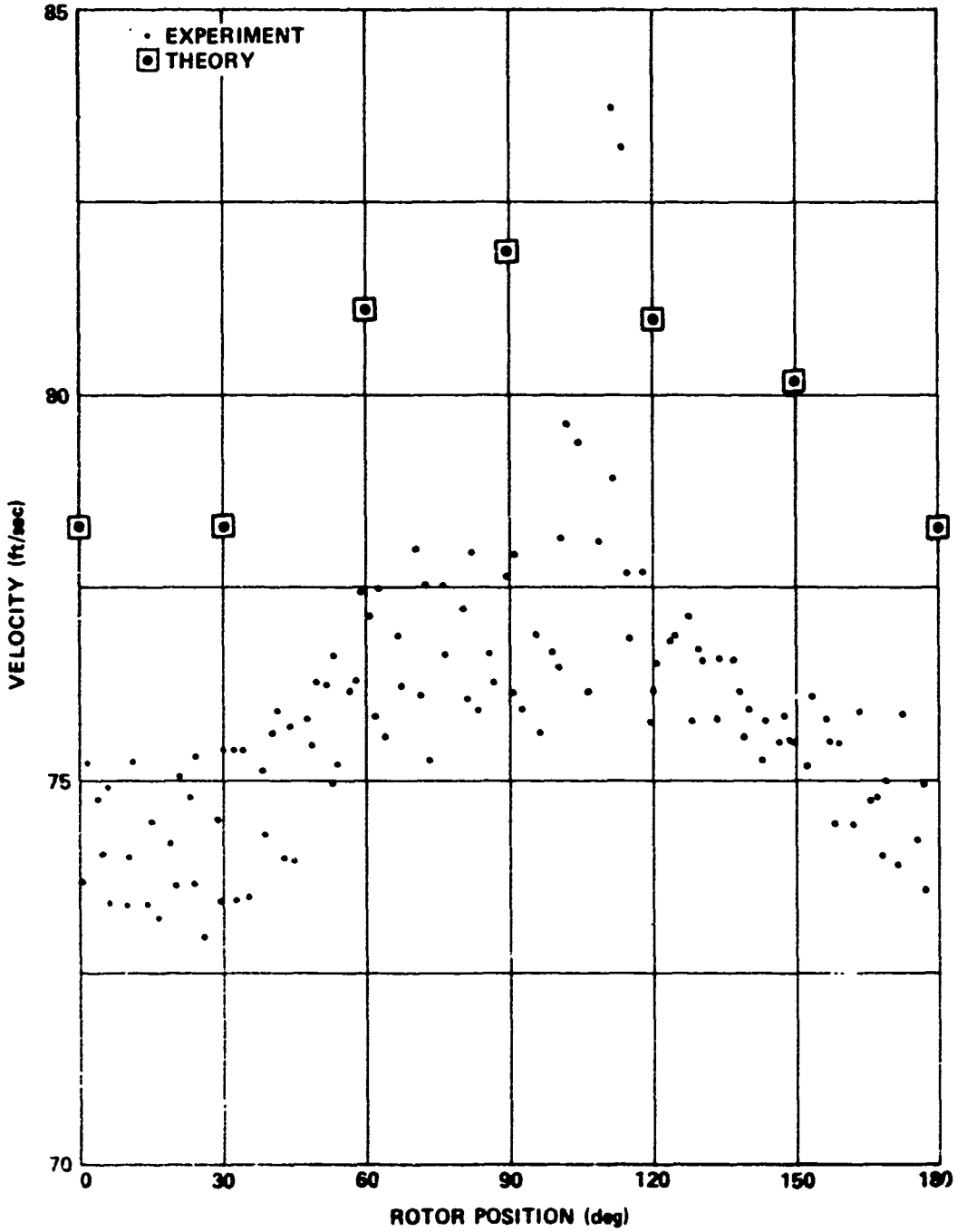

Figure 62. Folded comparison - flight record 13, sensor No. 1, and trial period 0.094500.

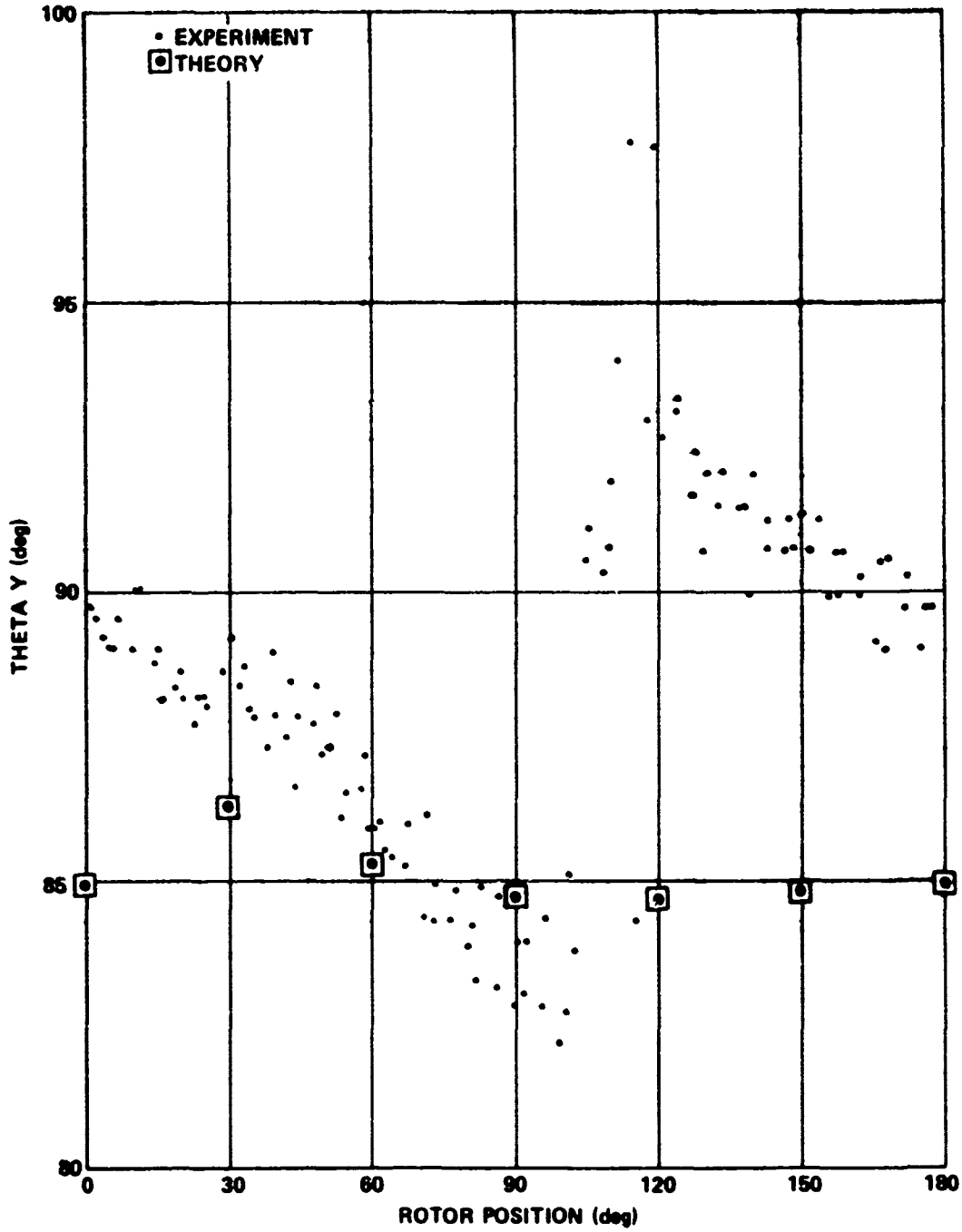

Figure 63. Folded comparison - flight record 13, sensor No. 1, and trial period 0.094500.

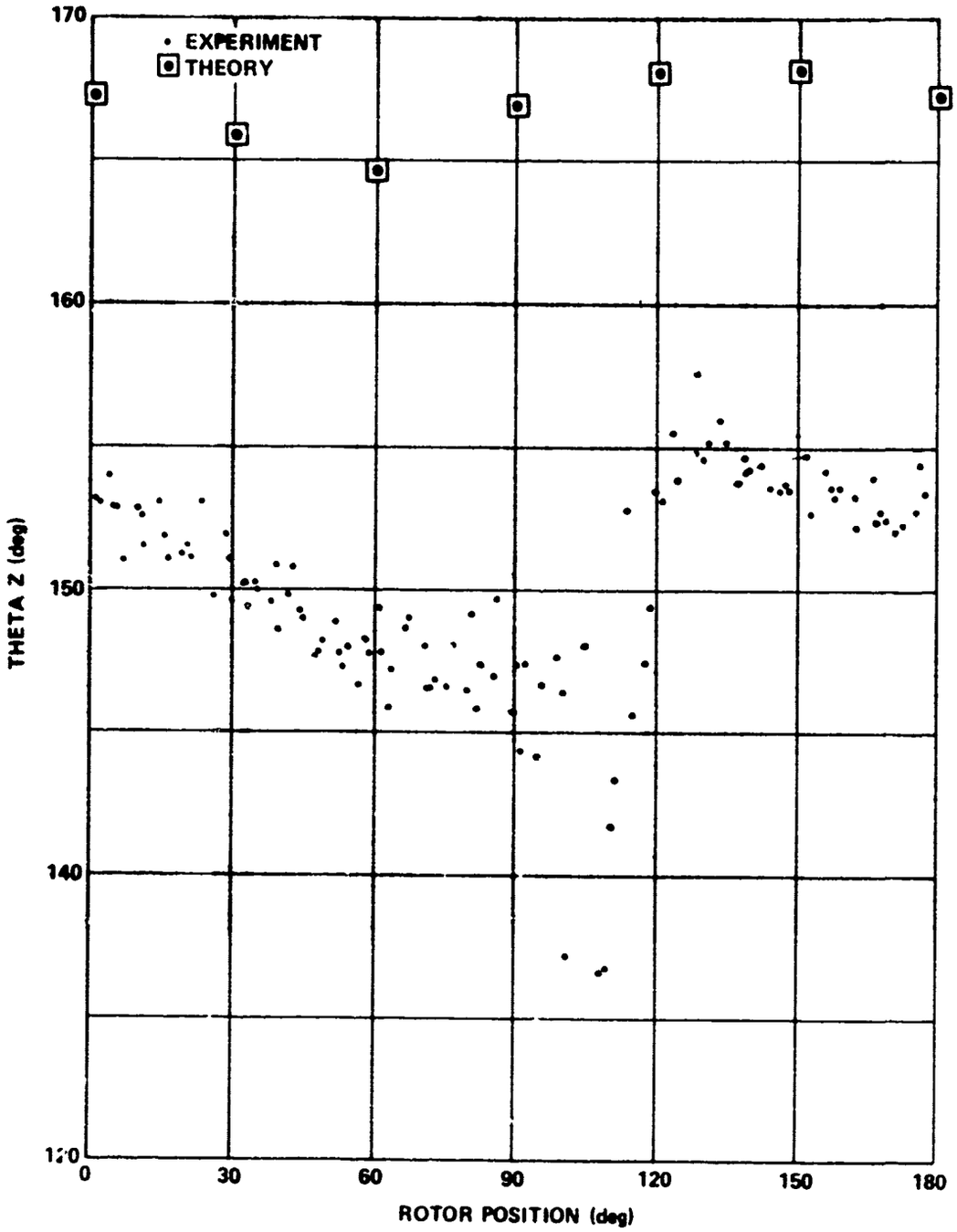

Figure 64. Folded comparison - flight record 13, sensor No. 1, and trial period 0.094500.

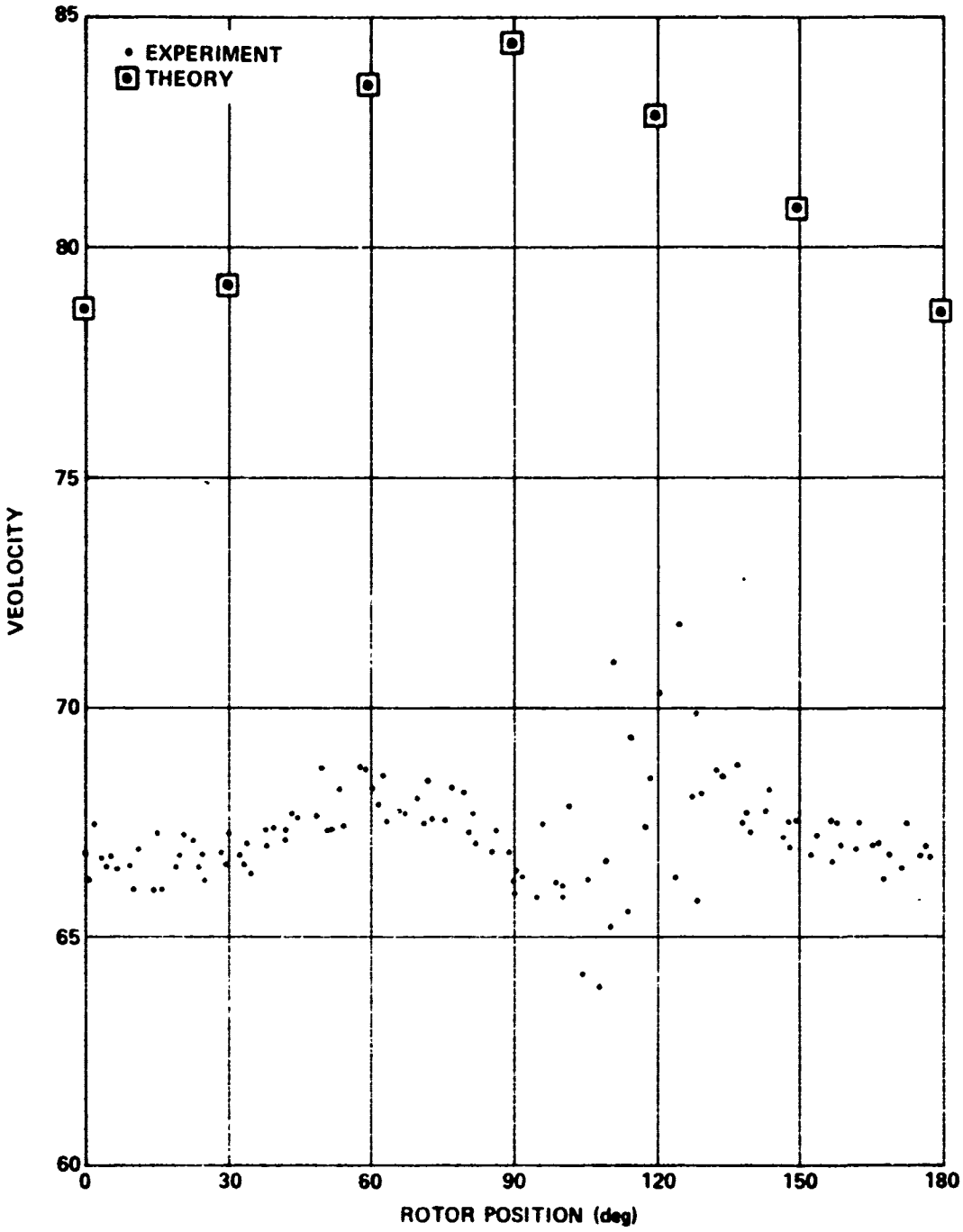

Figure 65. Folded comparison - flight record 13, sensor No. 3, and trial period 0.094500.

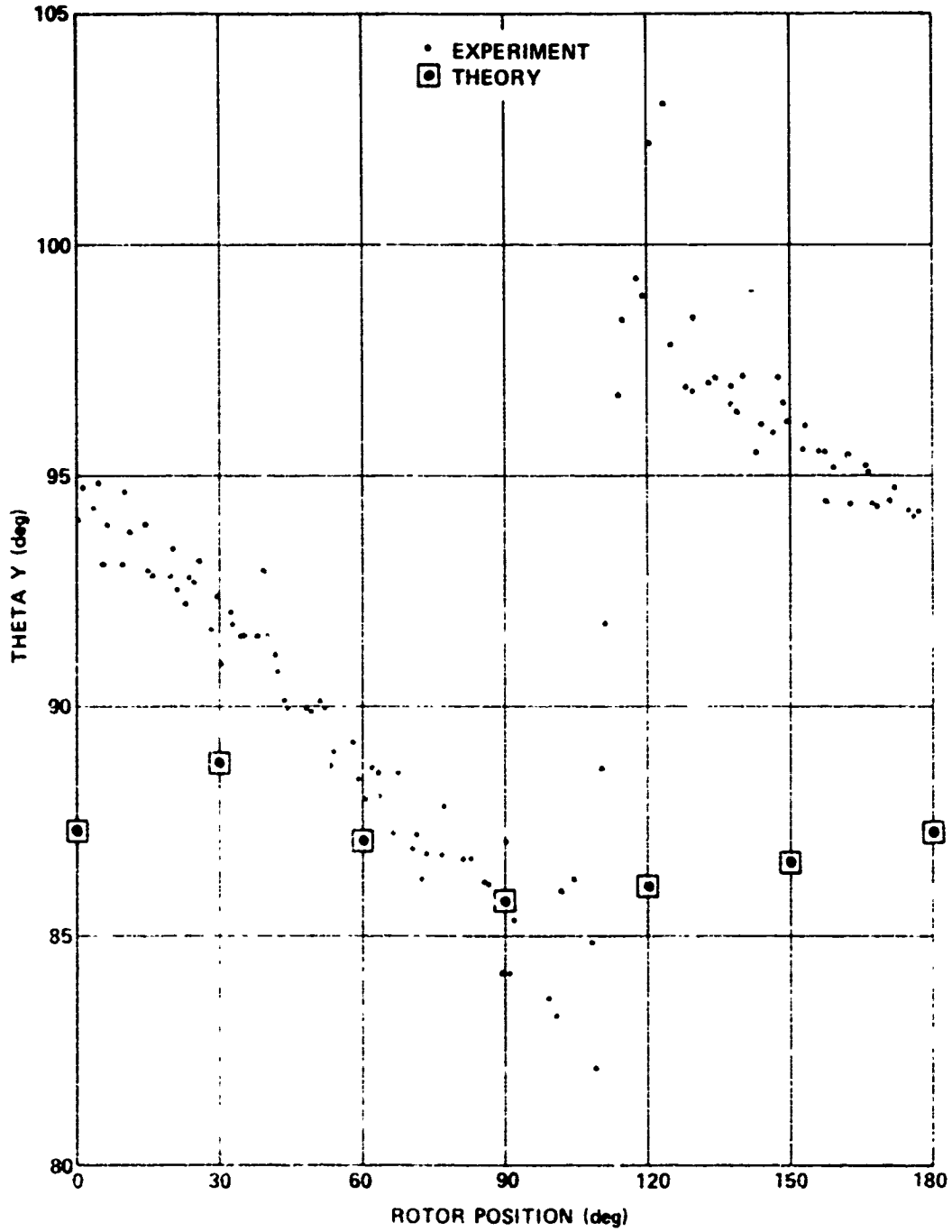

Figure [illegible]. Blade comparison - flight record 13, sensor No. 3, and trial period 0.09-.560.

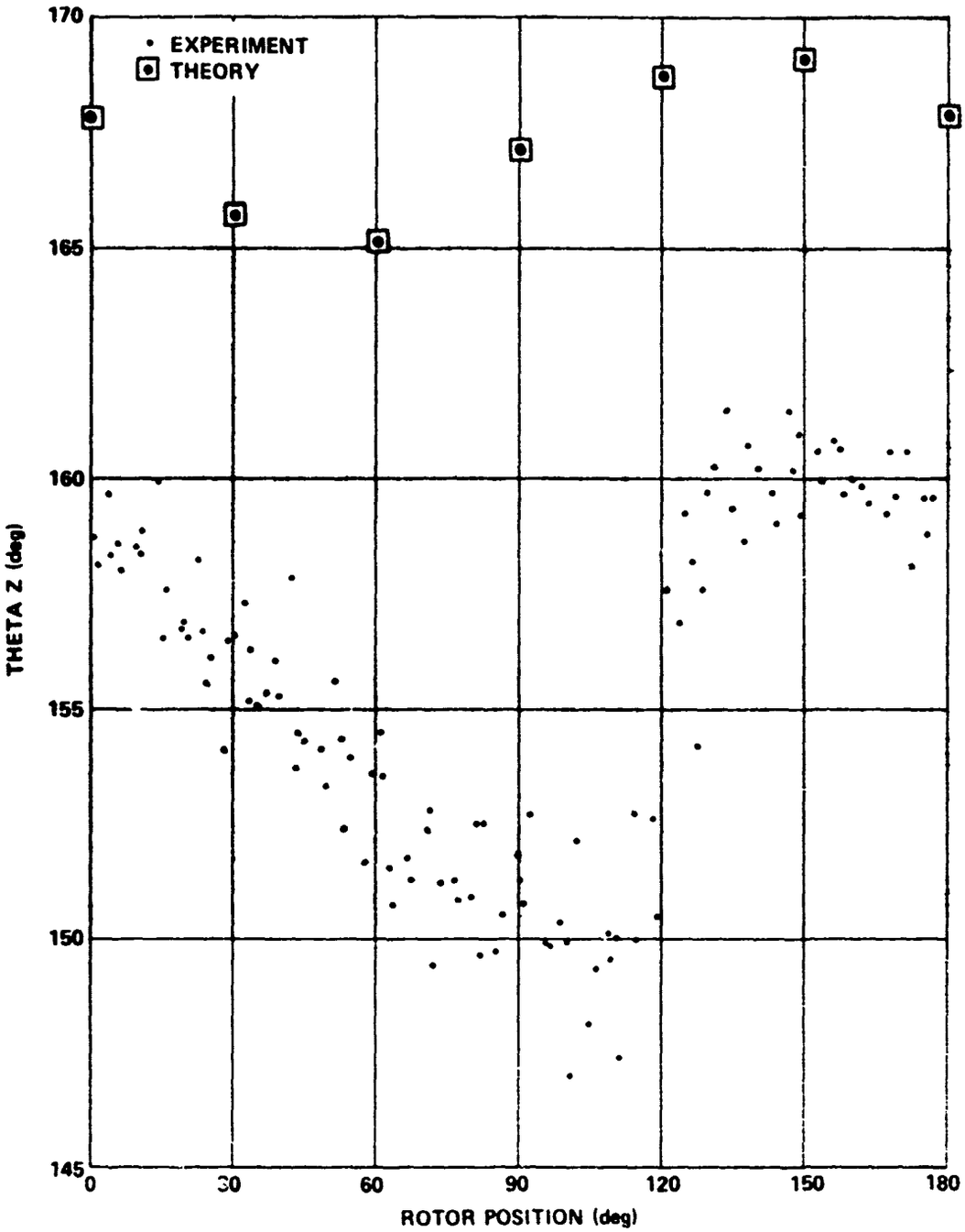

Figure 67. Folded comparison - flight record 13, sensor No. 3, and trial period 0.094500.

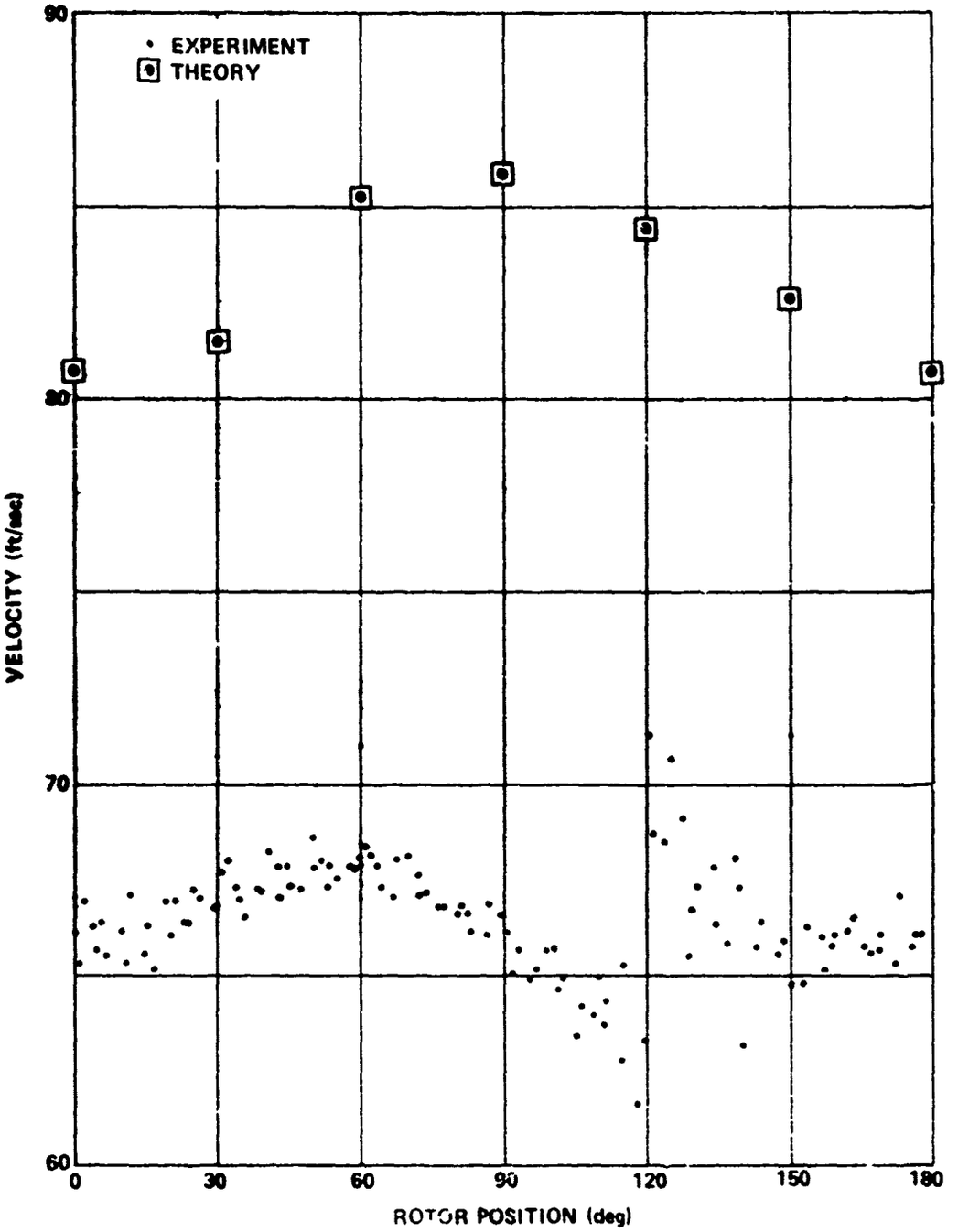

Figure 38. Folded comparison - flight record 1, sensor No. 4, and trial period 0.094500.

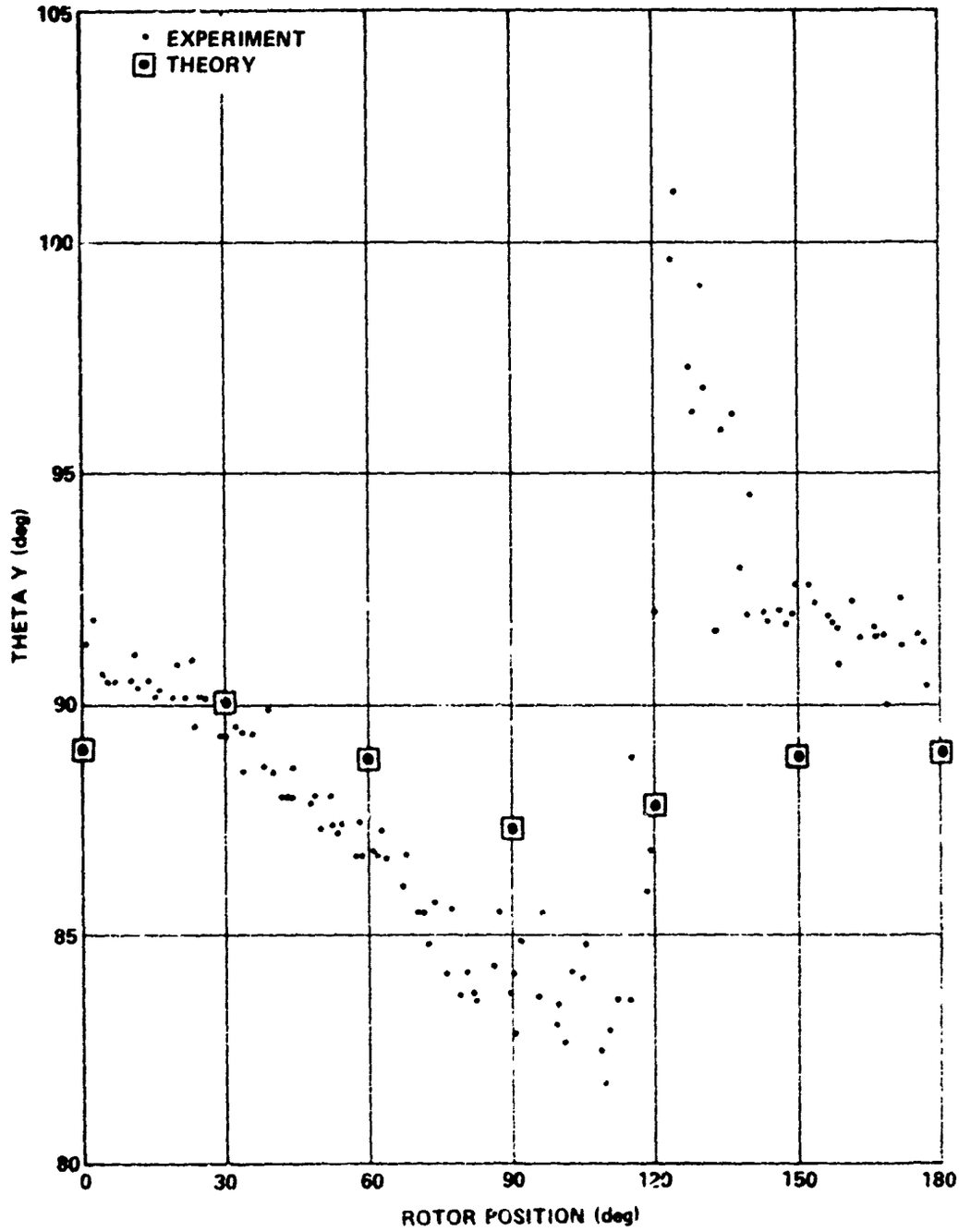

Figure 69. Folded comparison - flight record 18, sensor No. 4, and trial period 0.094500.

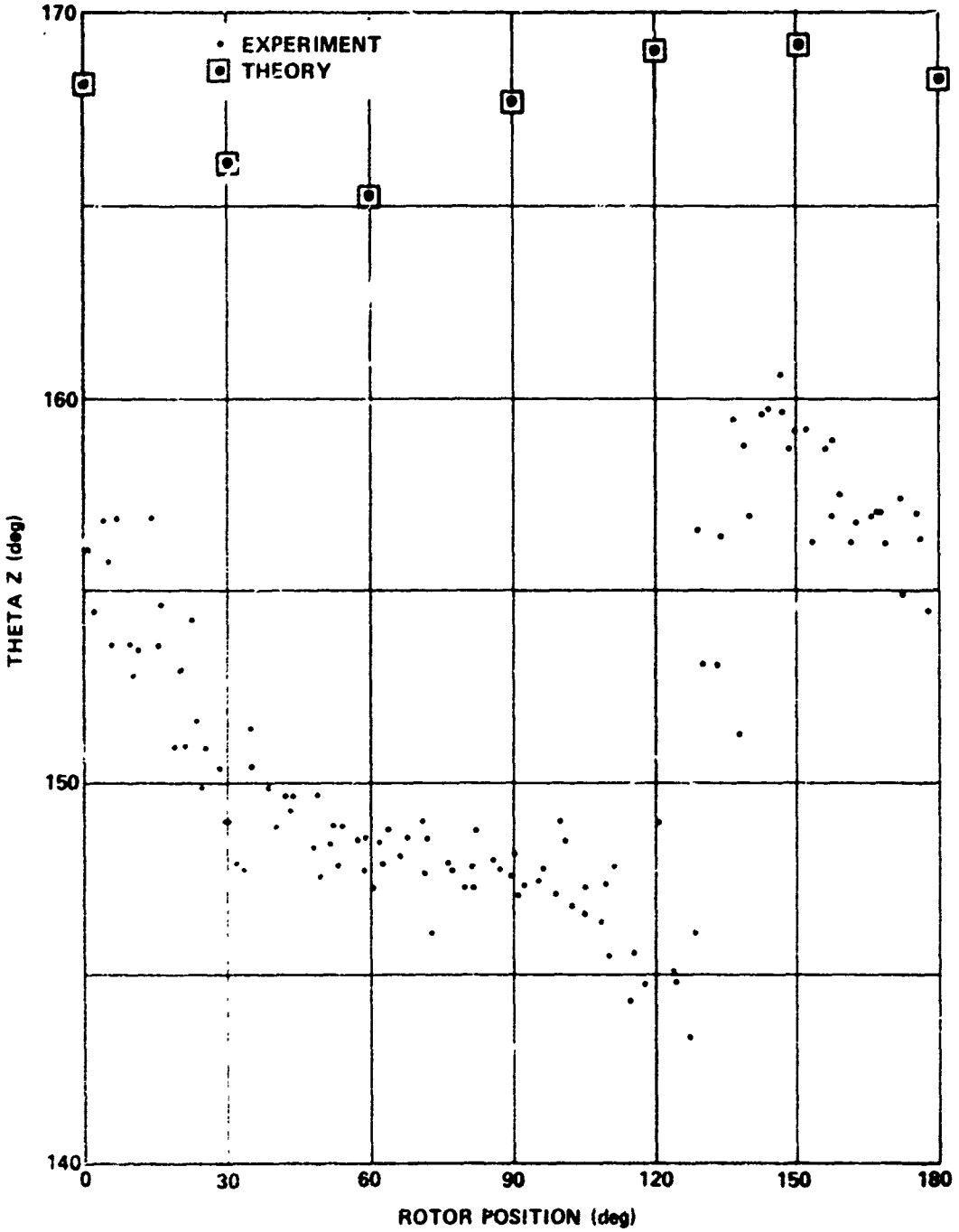

Figure 70. Folded comparison - flight record 13, sensor No. 4, and trial period 0.094500.

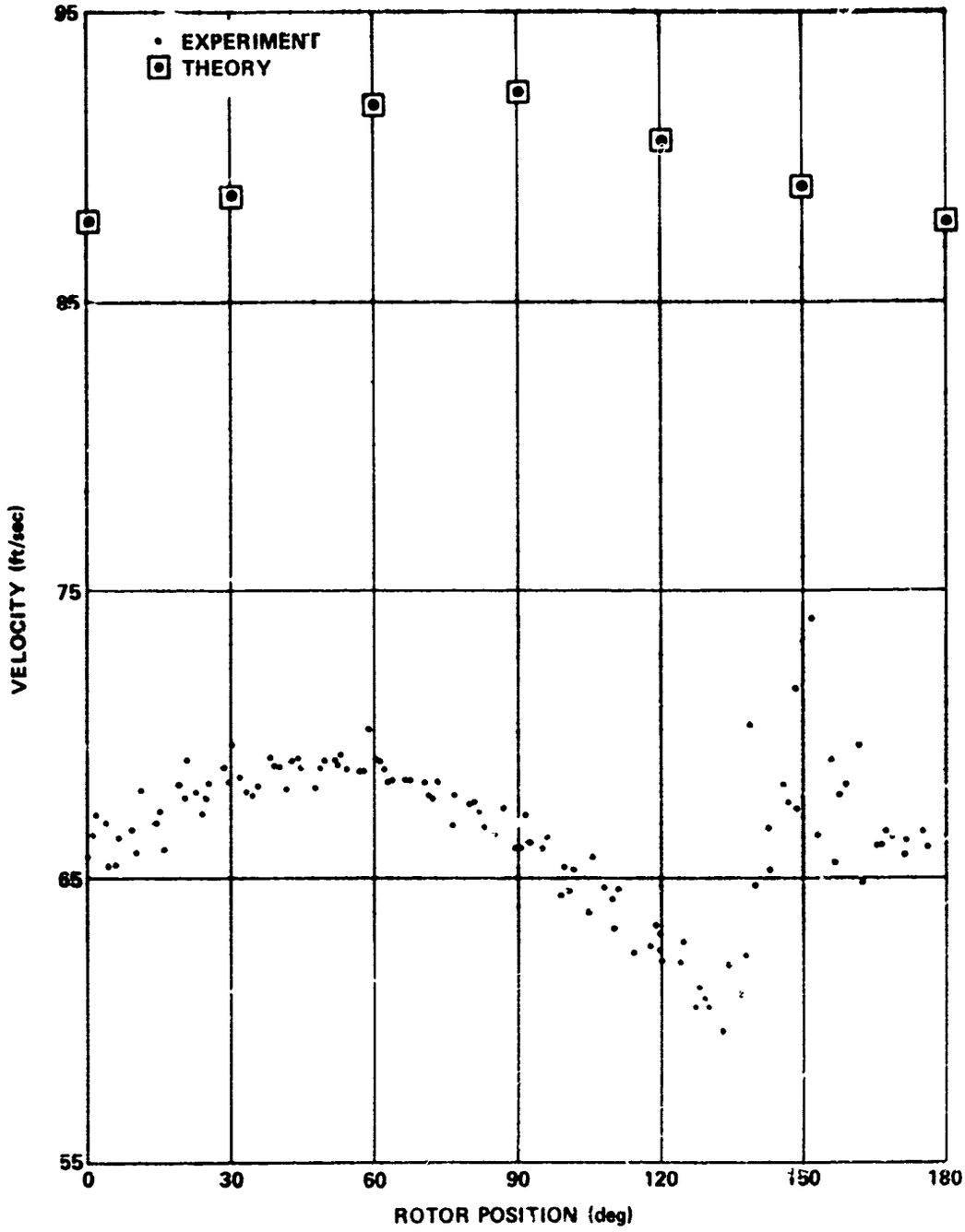

Figure 71. Folded comparison - flight record 13, sensor No. 6, and trial period 0.094500.

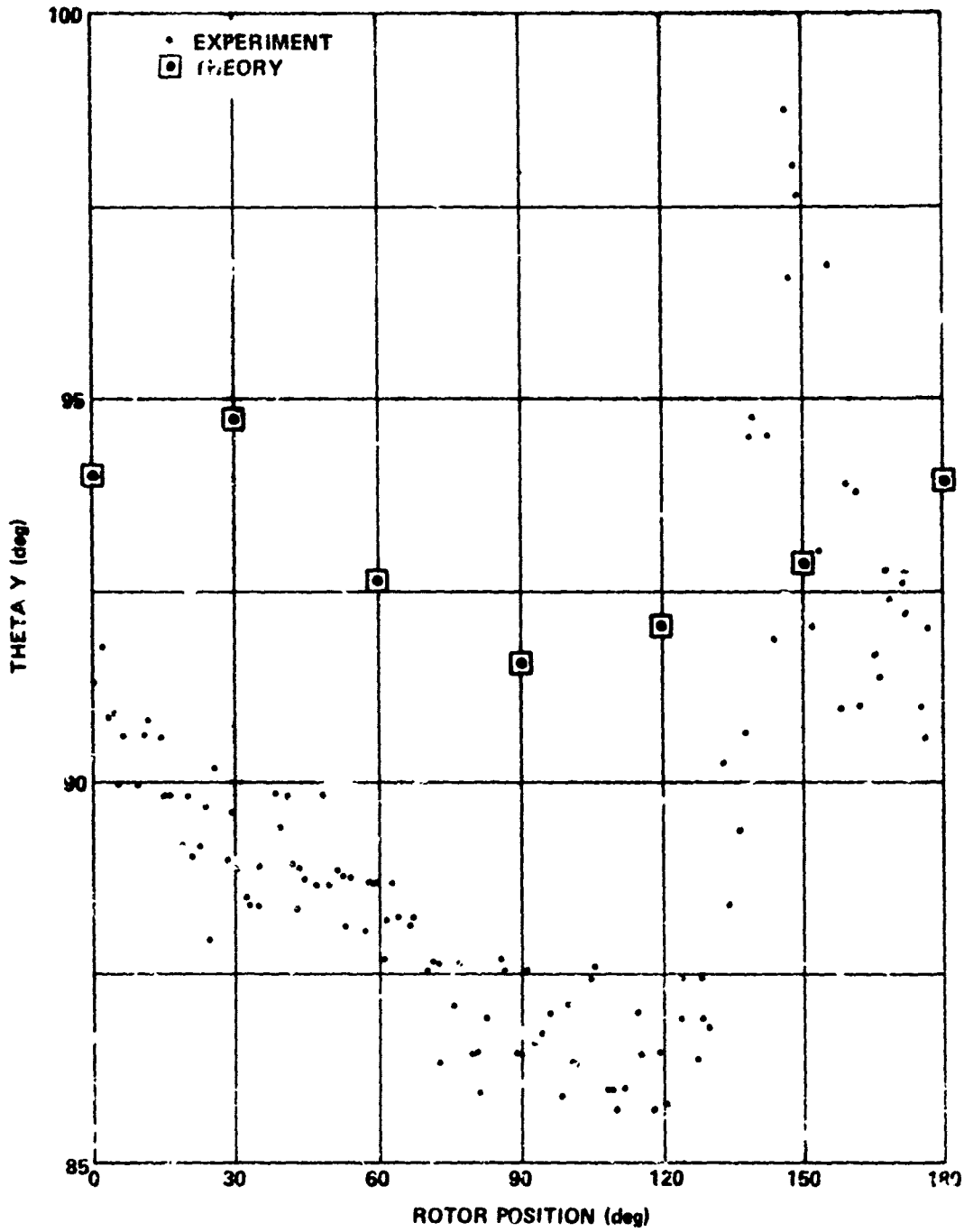

Figure 72. Folded comparison - flight record 13, sensor No. 6, and trial period 0.094500.

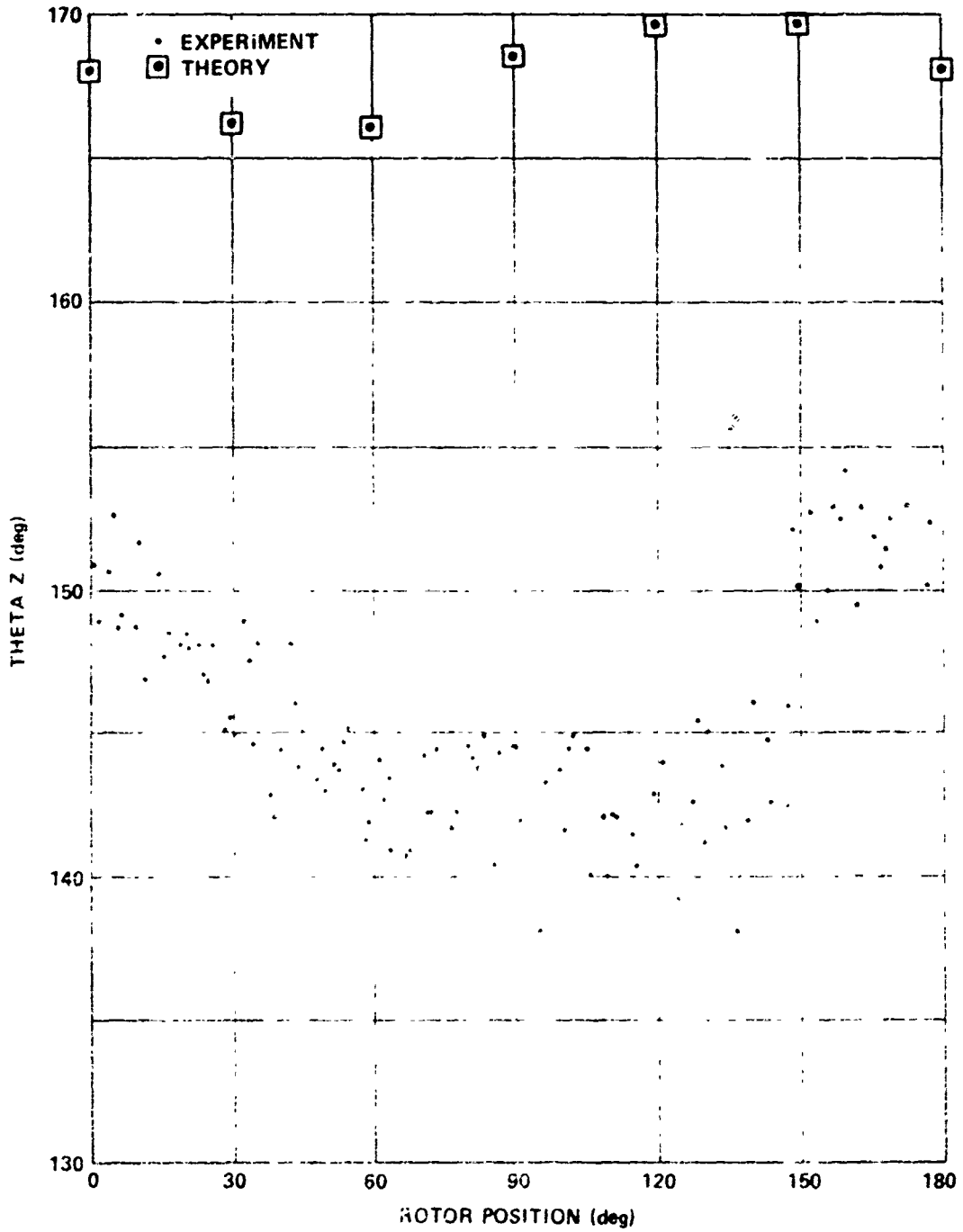

Figure 73. Folded comparison - flight record 13, sensor No. 6, and trial period 0.094500.

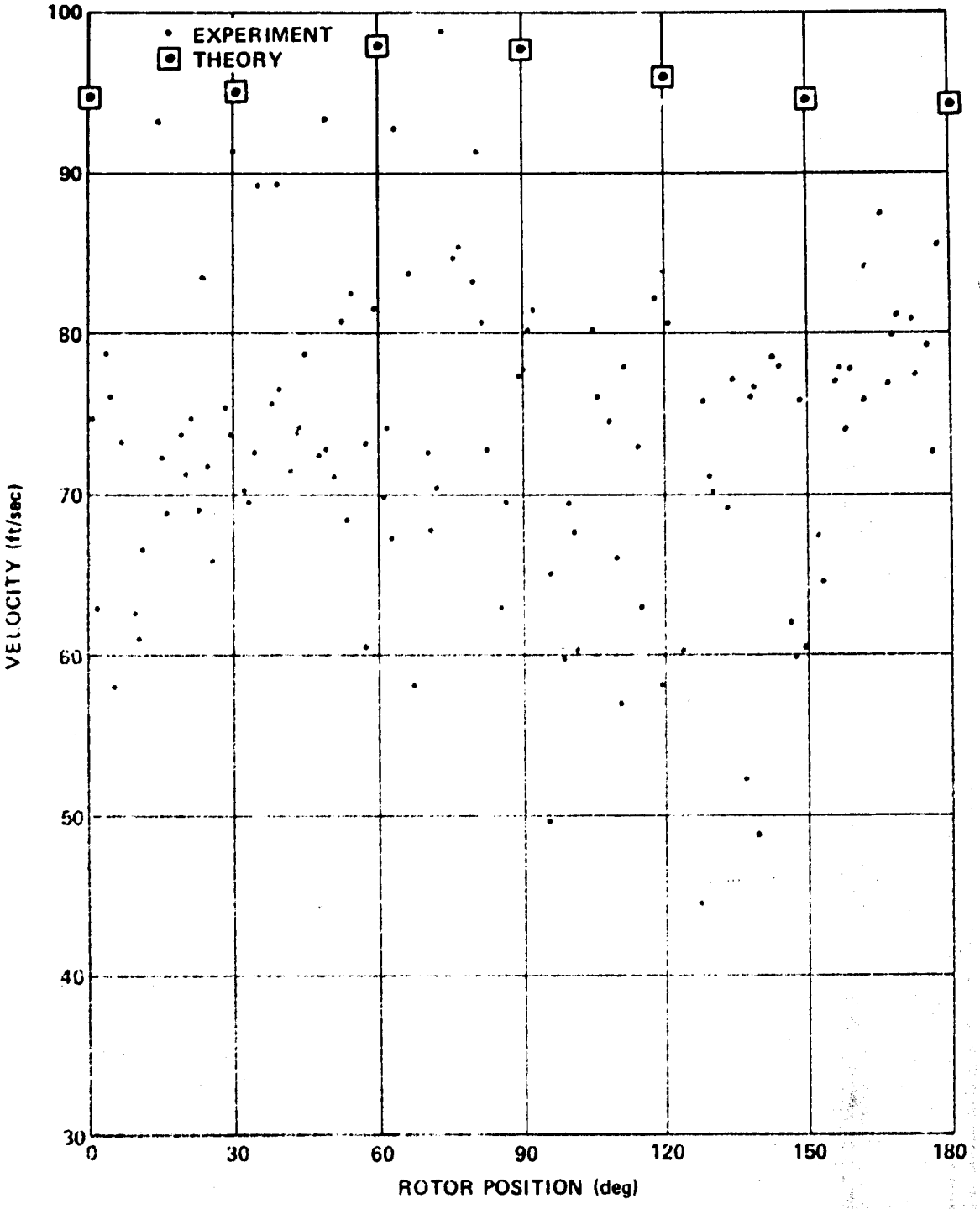

Figure 74. Folded comparison - flight record 13, sensor No. 7, and trial period 0.094500.

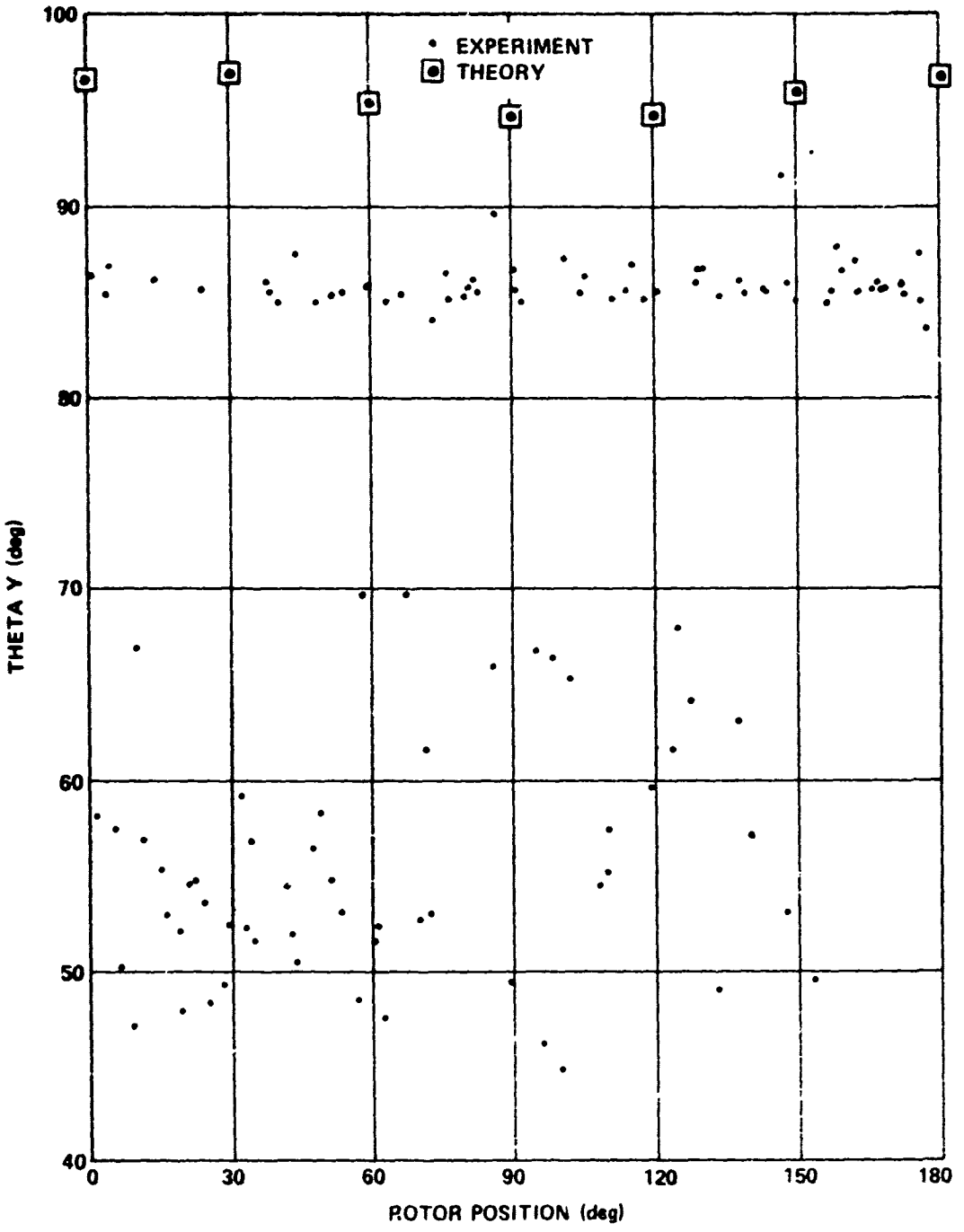

Figure 75. Folded comparison - flight record 13, sensor No. 7, and trial period 0.094500.

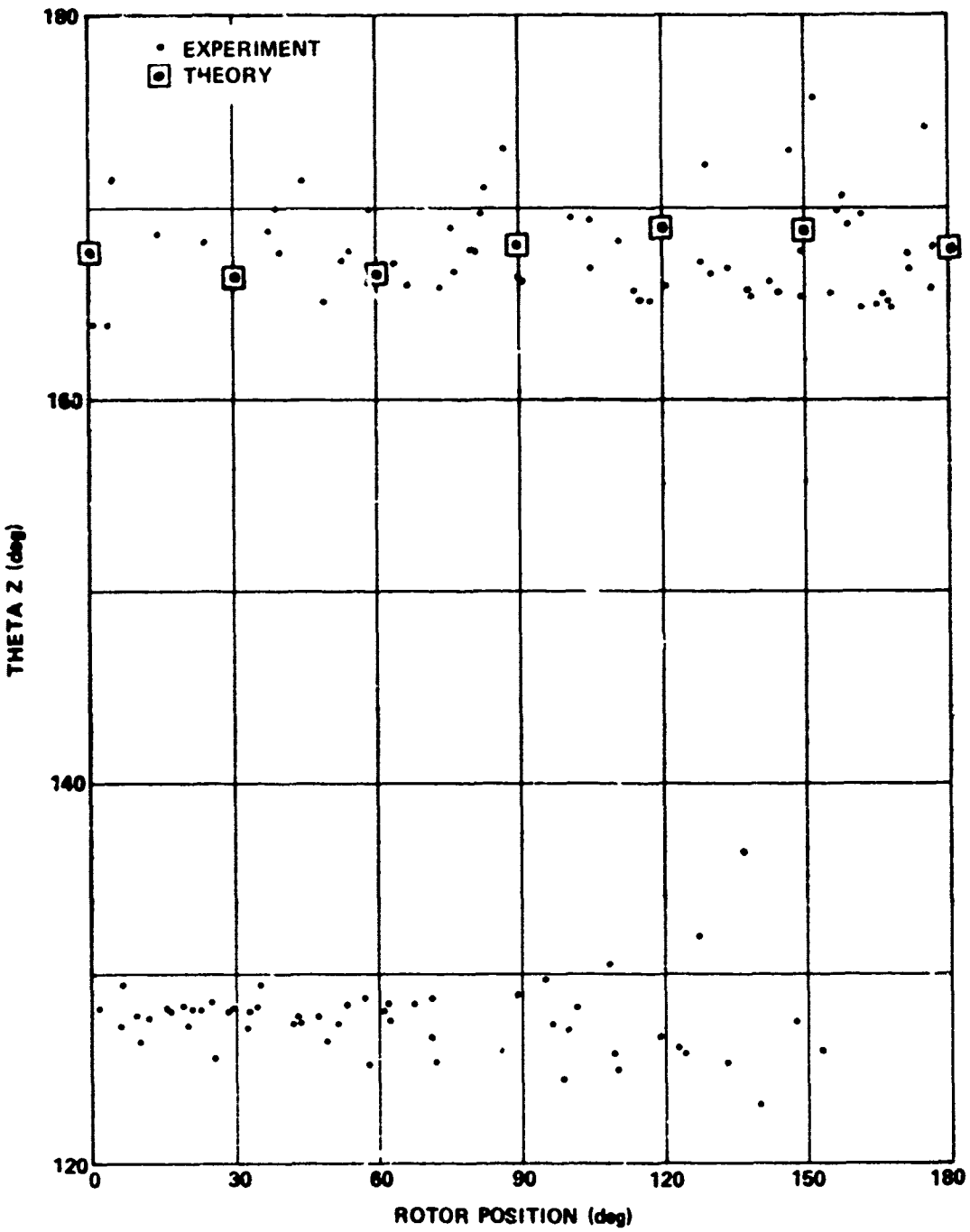

Figure 76. Folded comparison - flight record 13, sensor No. 7, and trial period 0.094500.

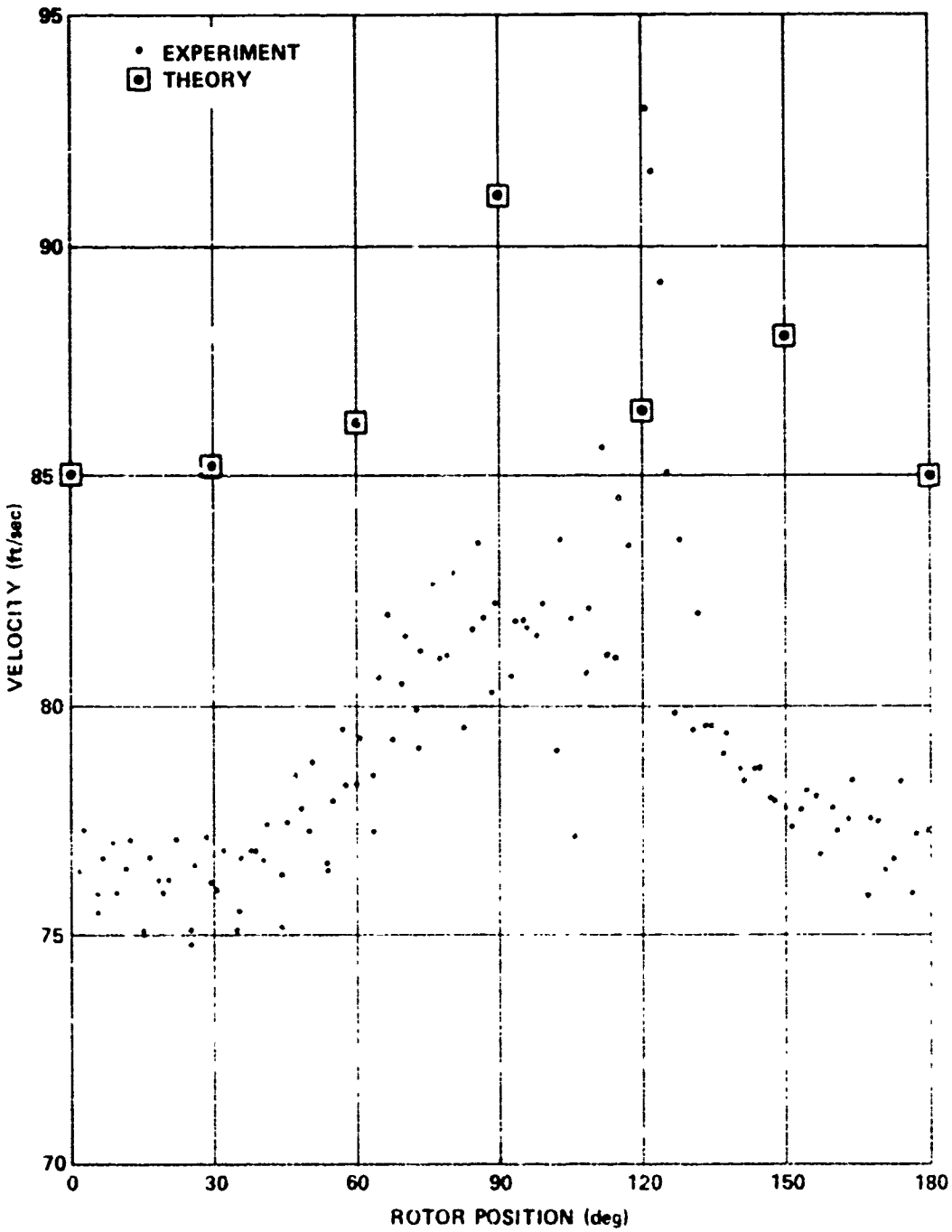

Figure 77. Folded comparison - flight record 15, sensor No. 1, and trial period 0.093500.

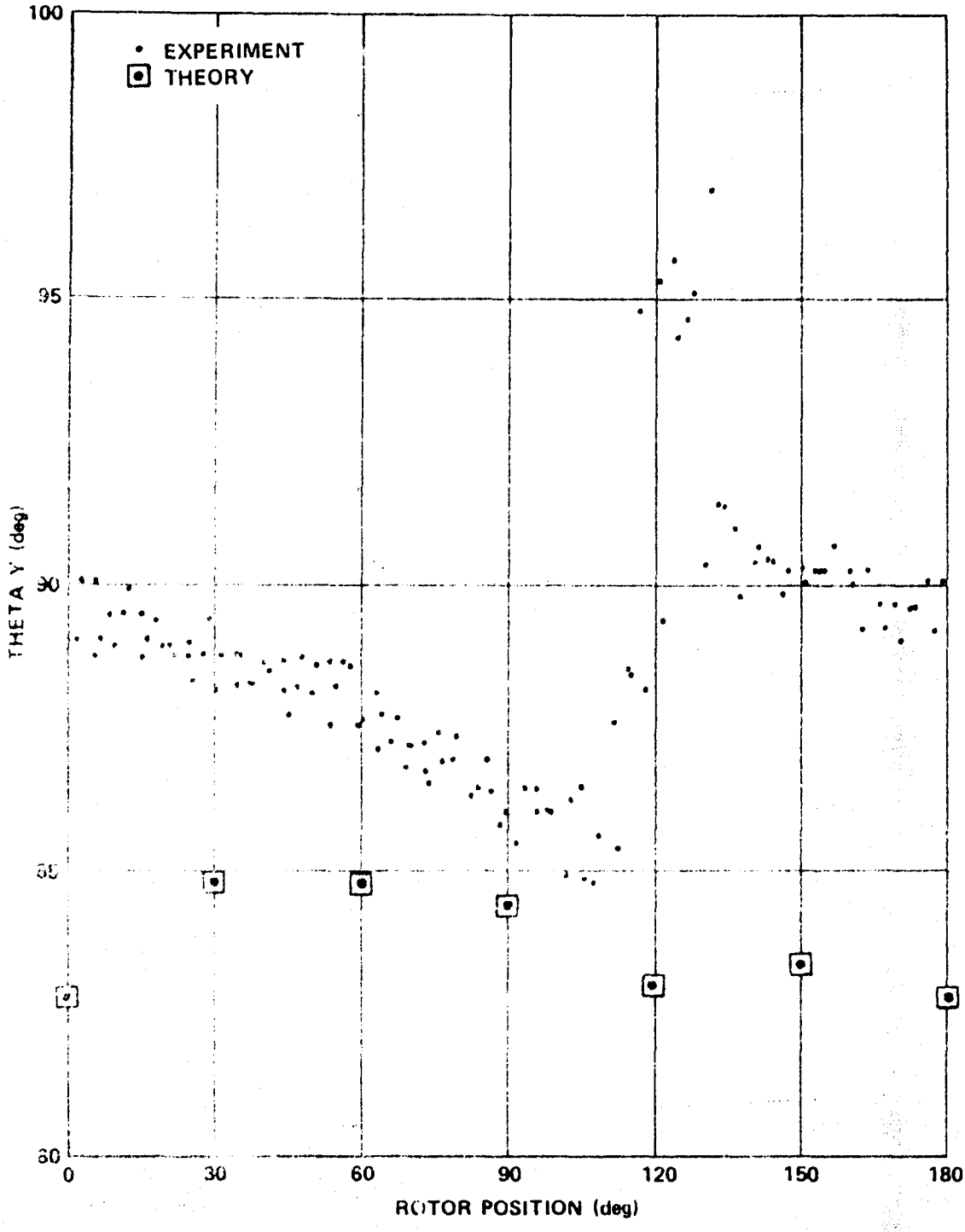

Figure 78. Folded comparison - flight record 15, sensor No. 1, and trial period 0.093500.

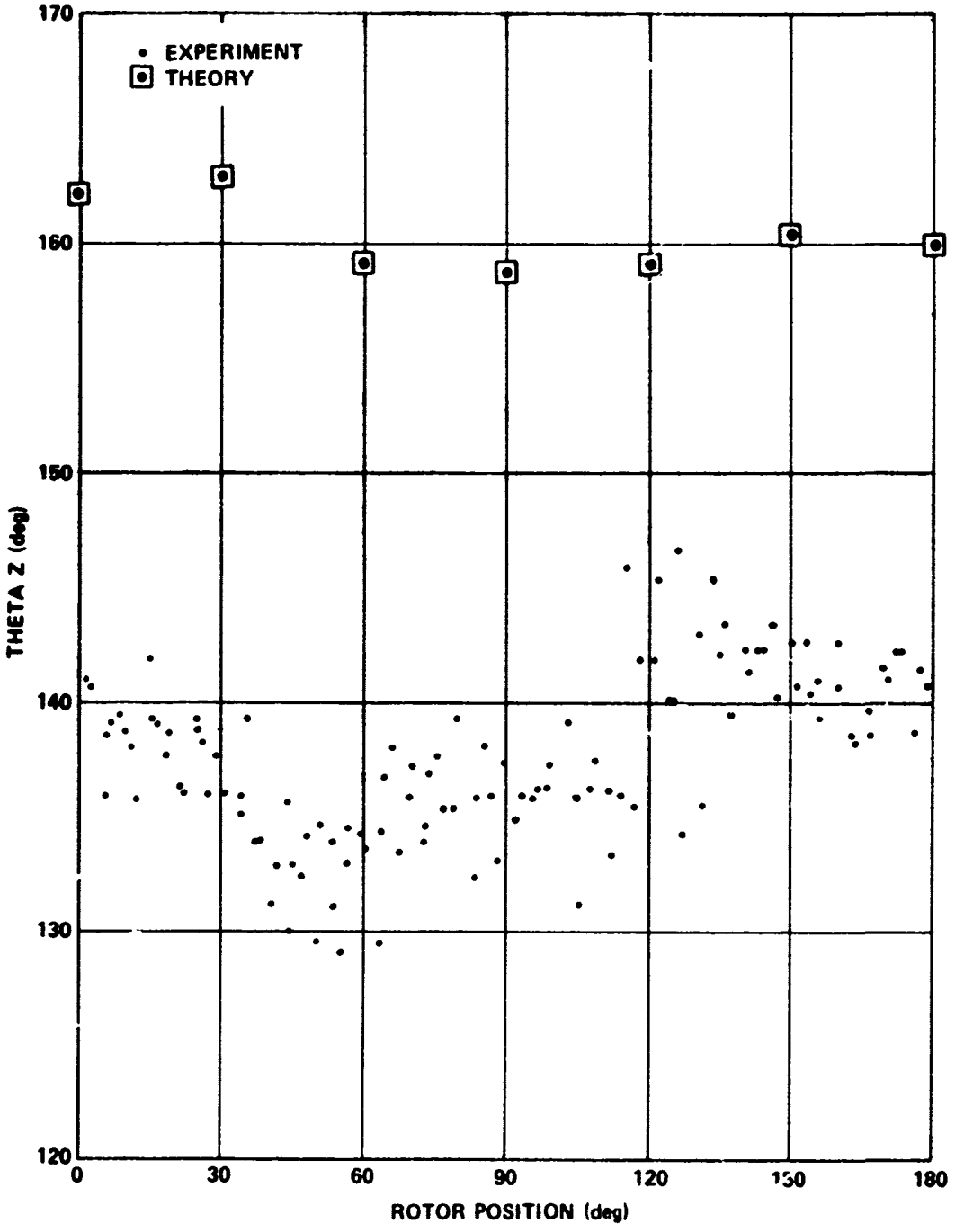

Figure 79. Folded comparison - flight record 15, sensor No. 1, and trial period 0.093500.

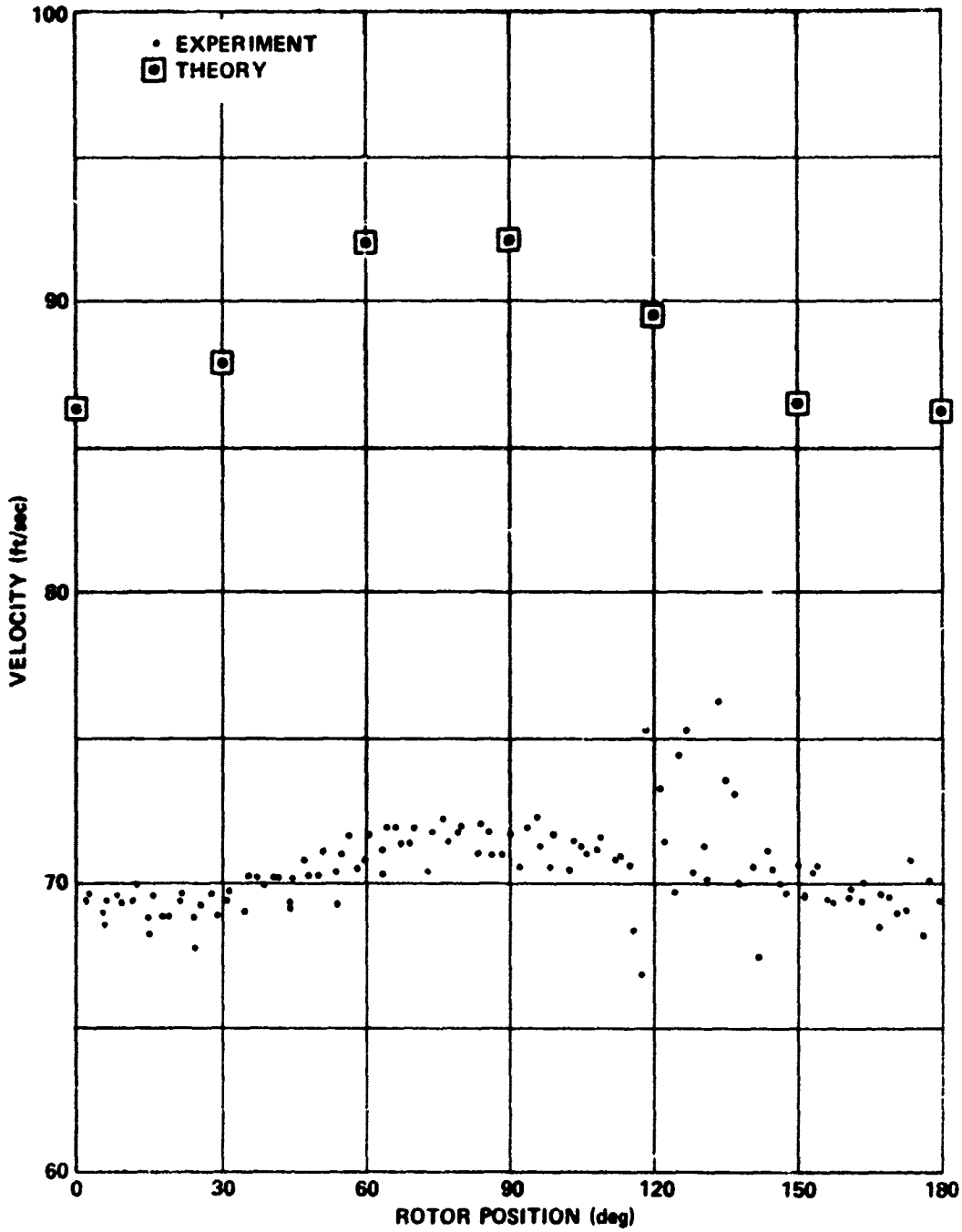

Figure 80. Folded comparison - flight record 15, sensor No. 3, and trial period 0.093500.

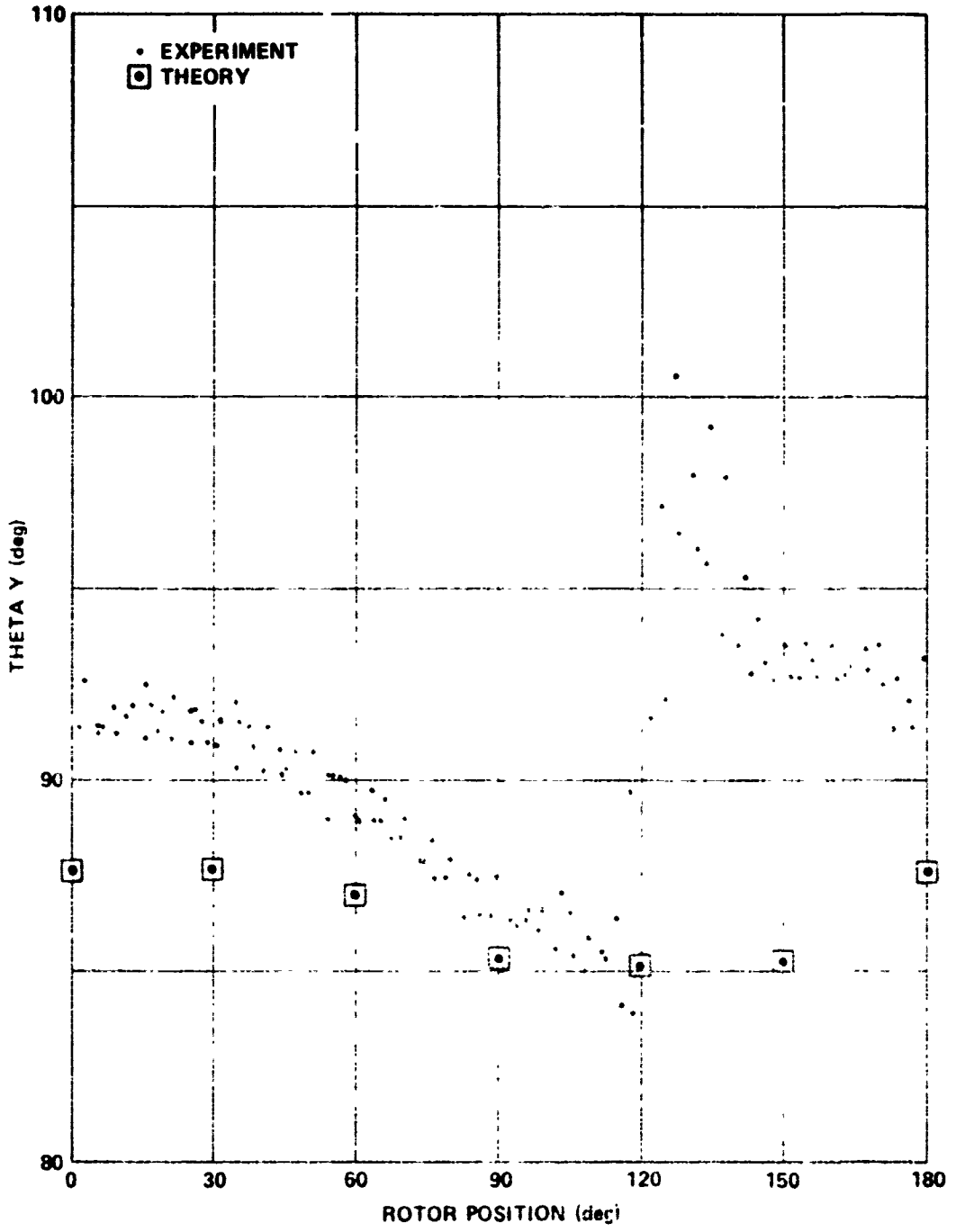

Figure 81. Folded comparison - flight record 15, sensor No. 3, and trial period 0.093500.

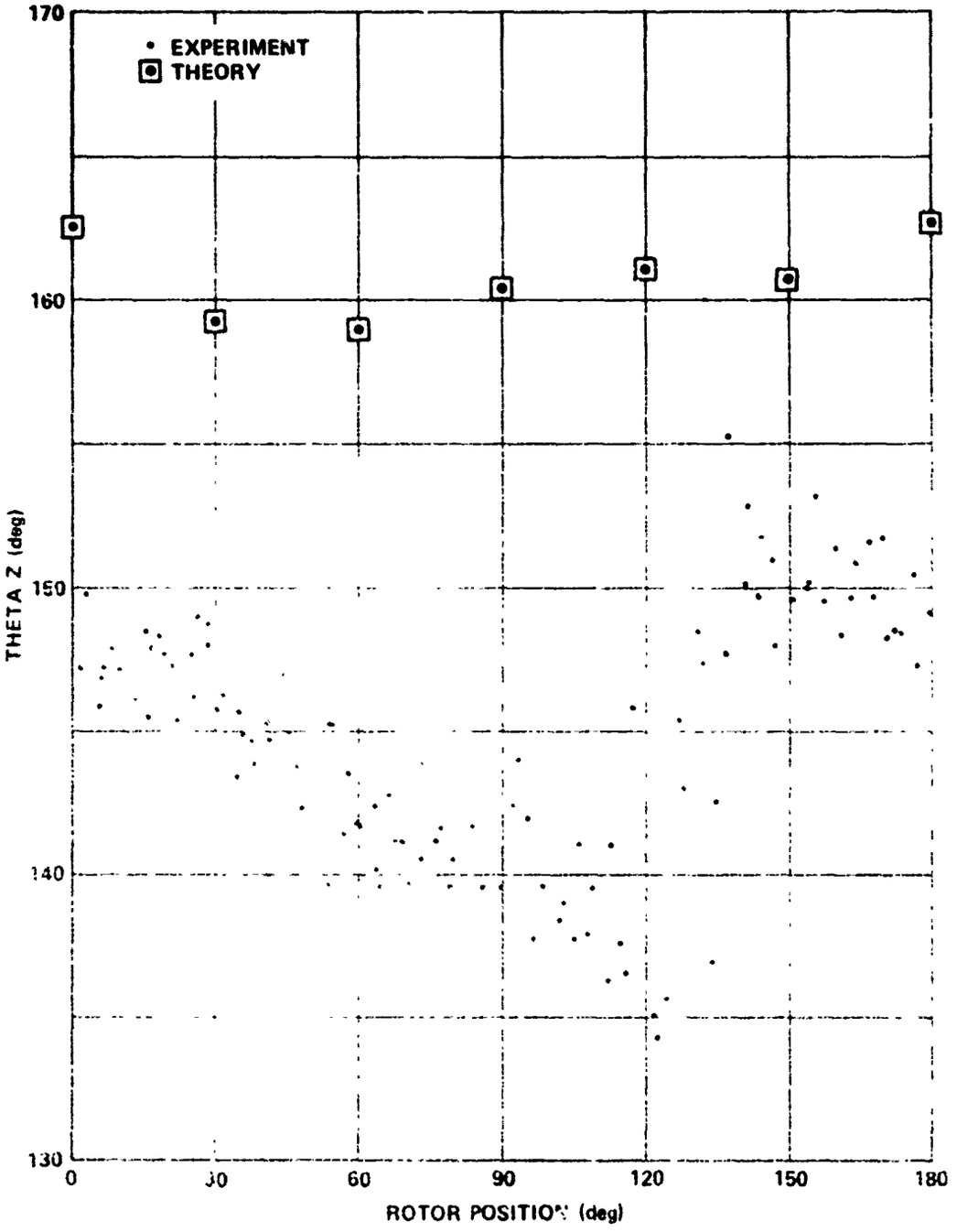

Figure 82. Folded comparison - flight record 15, sensor No. 3, and trial period 0.093500.

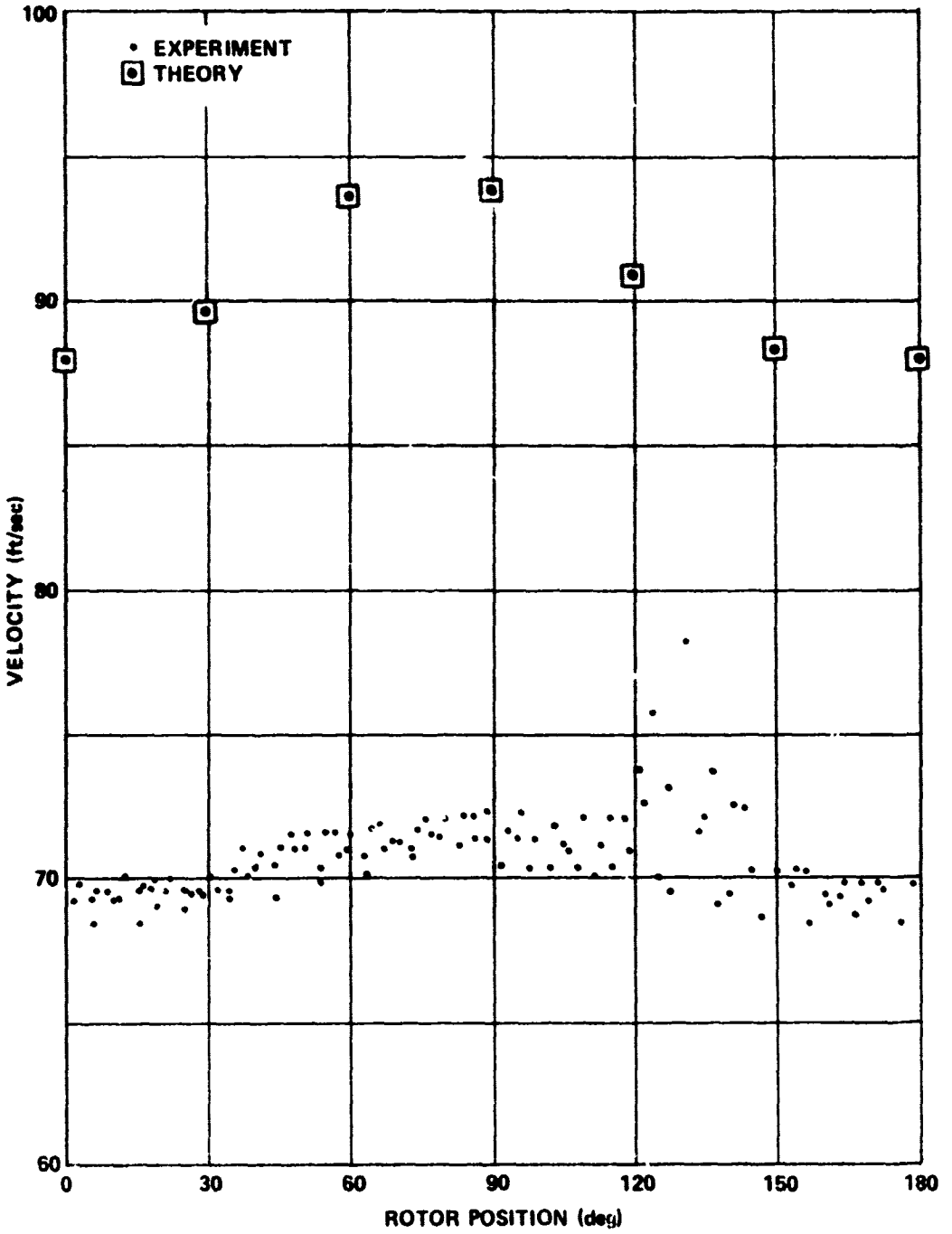

Figure 83. Folded comparison - flight record 15, sensor No. 4, and trial period 0.093500.

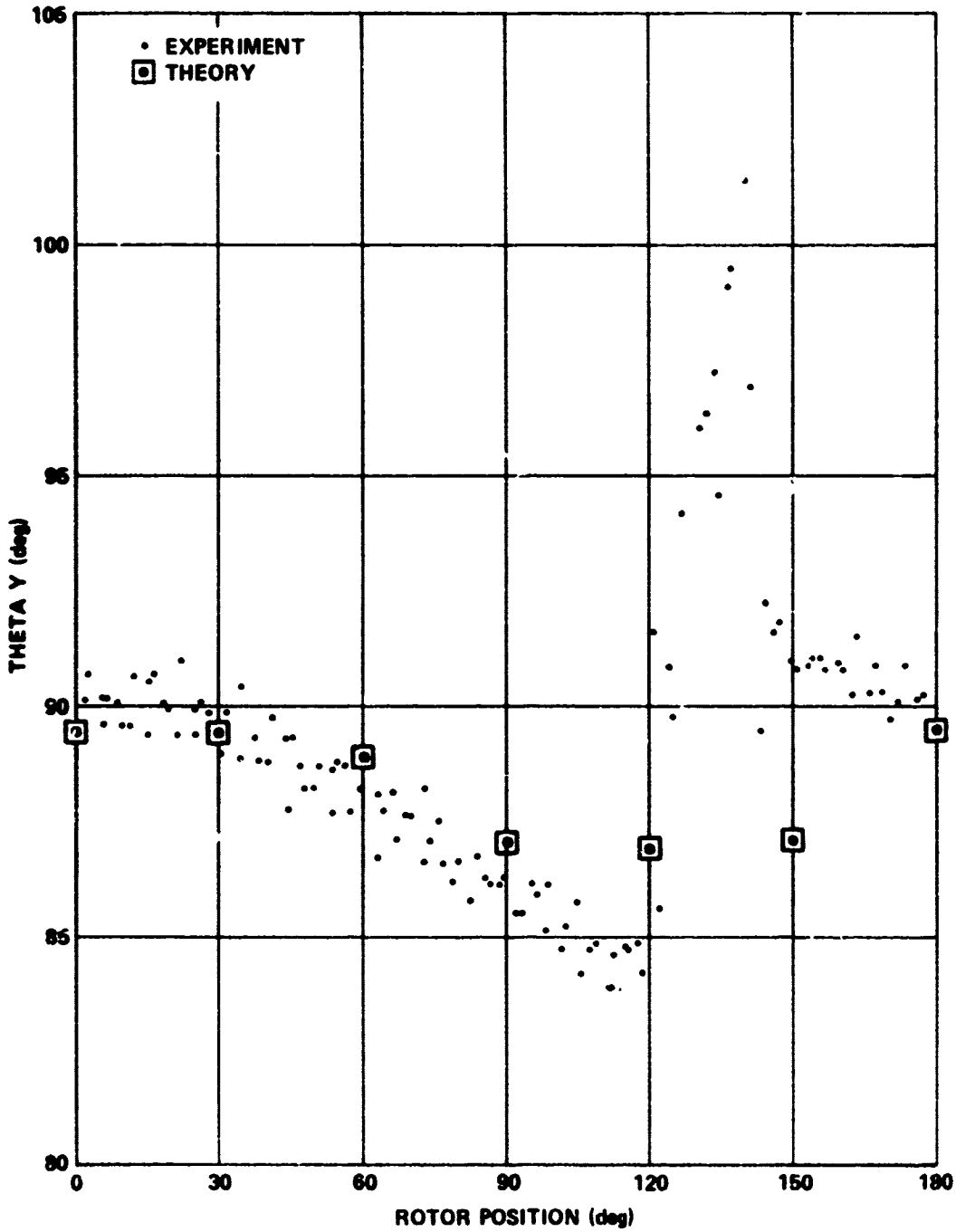

Figure 84. Folded comparison - flight record 15, sensor No. 4, and trial period 0.093500.

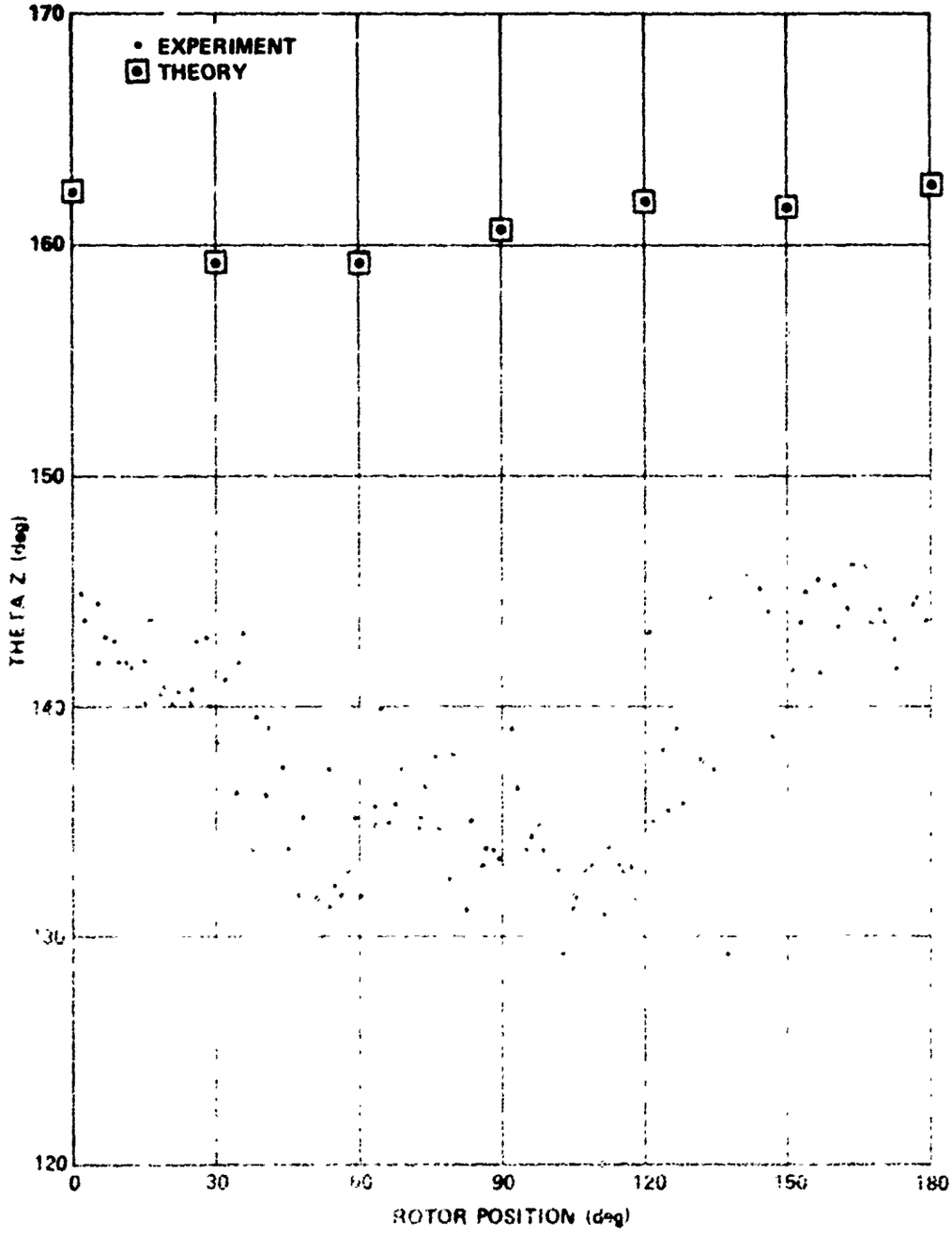

Figure 85. Folded comparison - flight record 15, sensor No. 4, and trial period 0.093500.

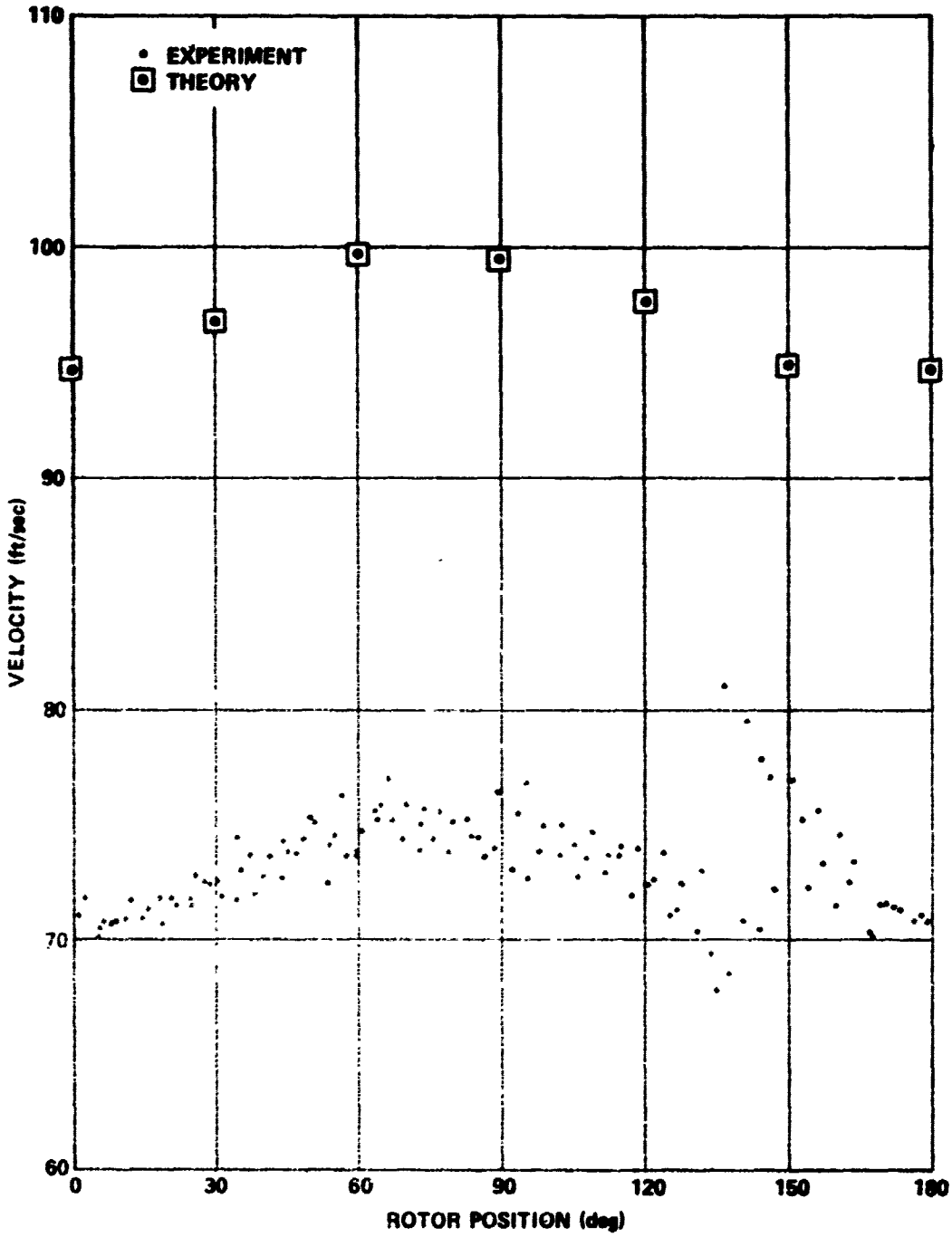

Figure 86. Folded comparison - flight record 15, sensor No. 6, and trial period 0.093500.

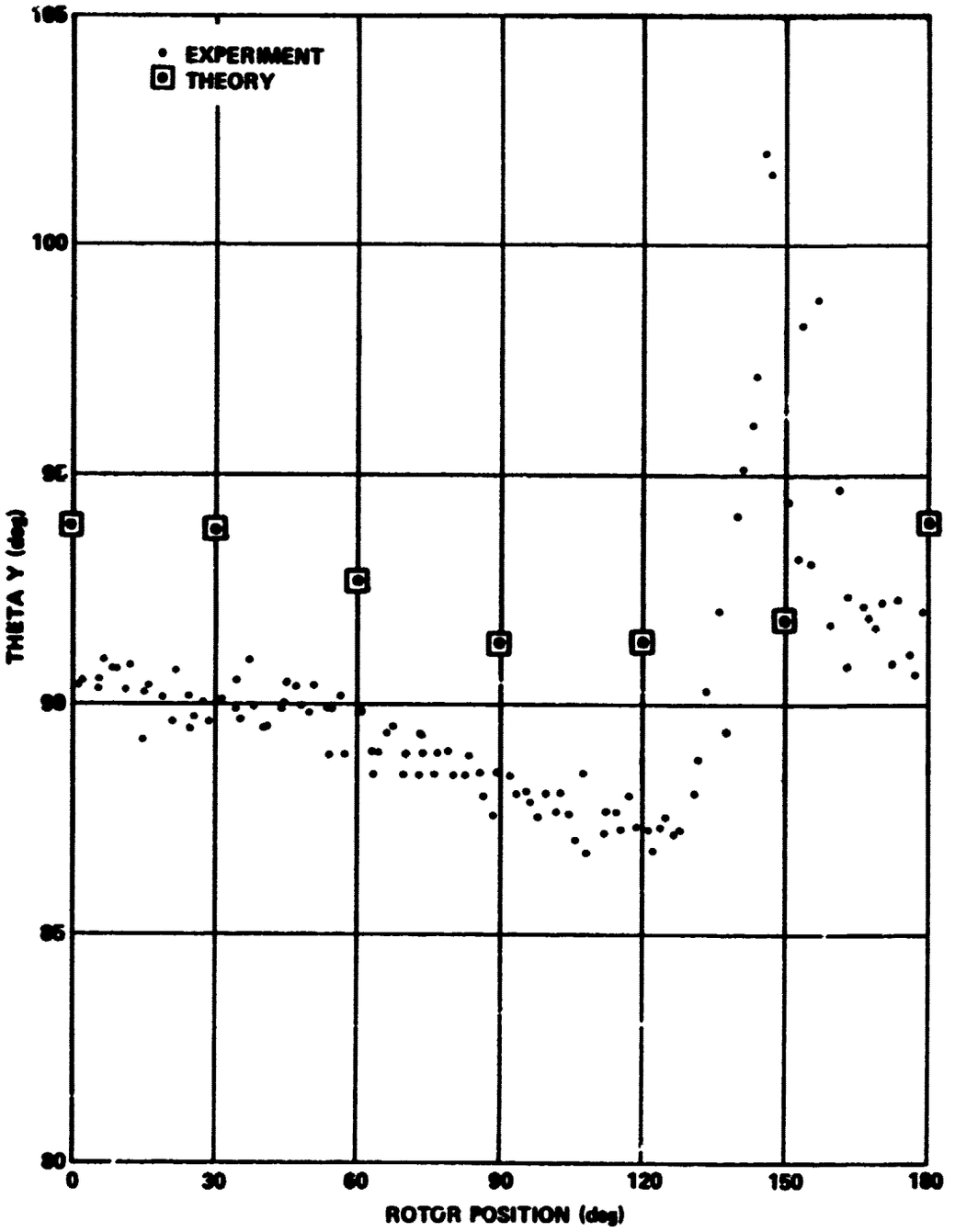

Figure 87. Folded comparison - flight record 15, sensor No. 6, and trial period 0.093500.

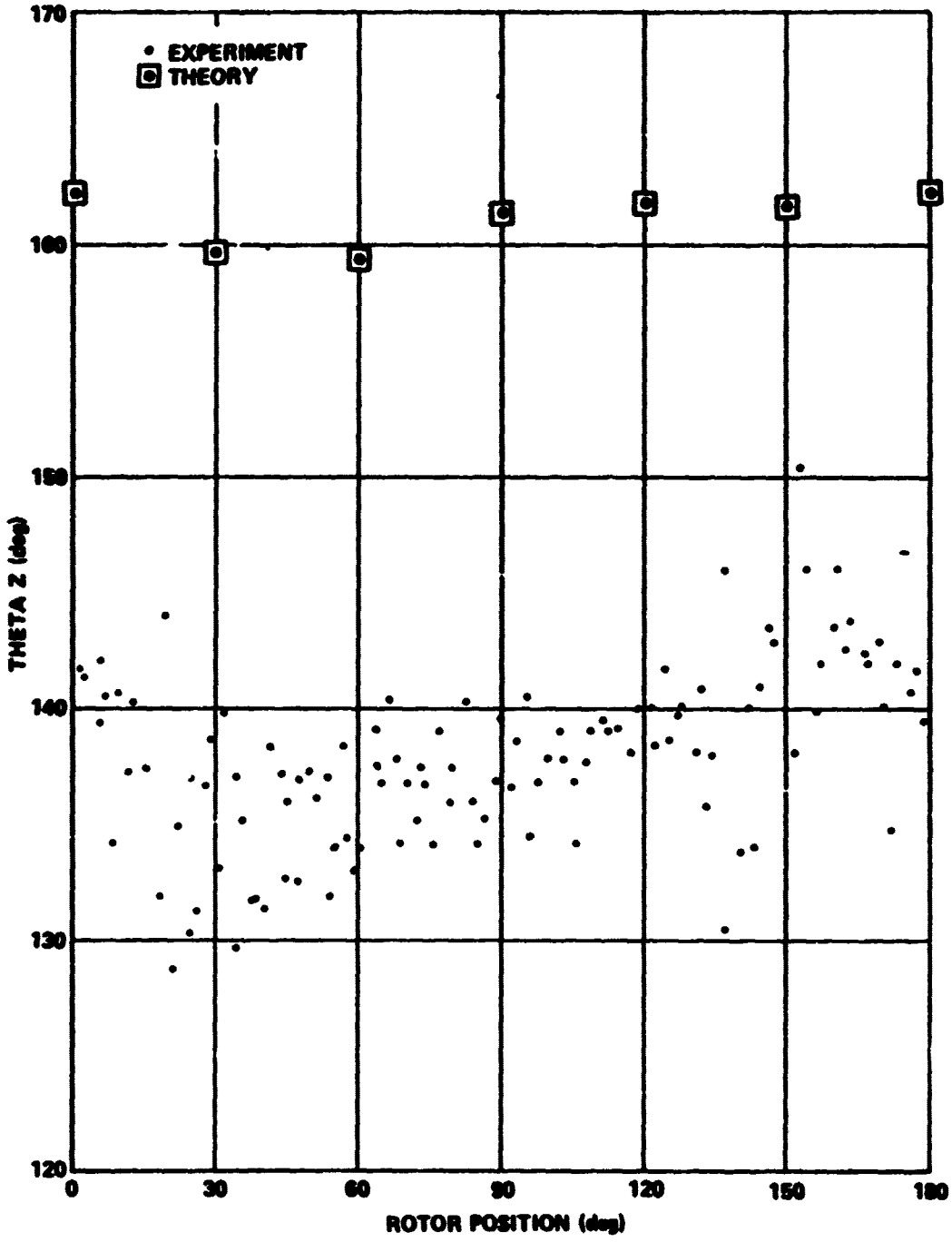

Figure 88. Folded comparison - flight record 15, sensor No. 6, and trial period 0.093500.

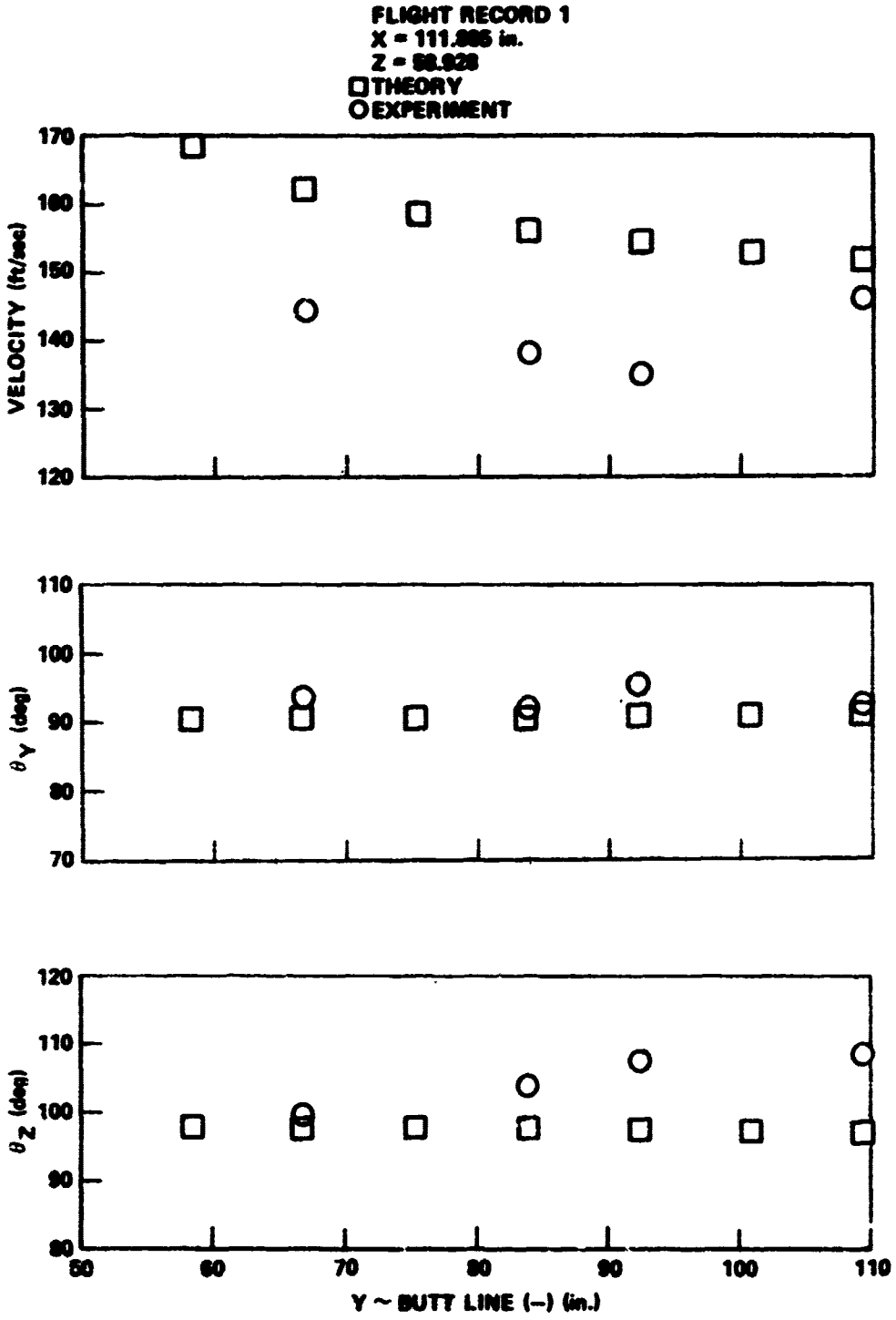

Figure 89. Comparison of time averaged velocity predictions with experiment.

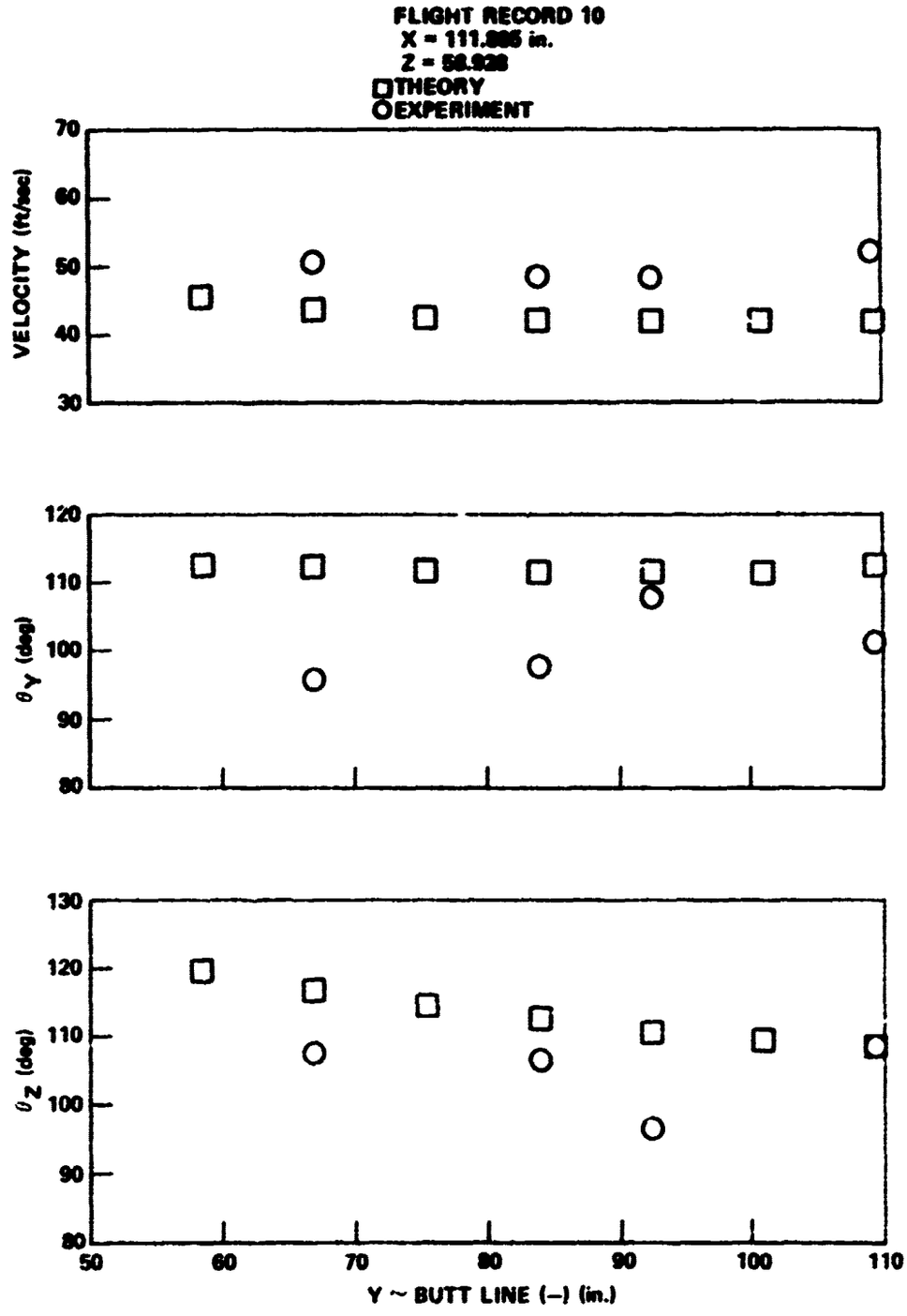

Figure 89. Continued.

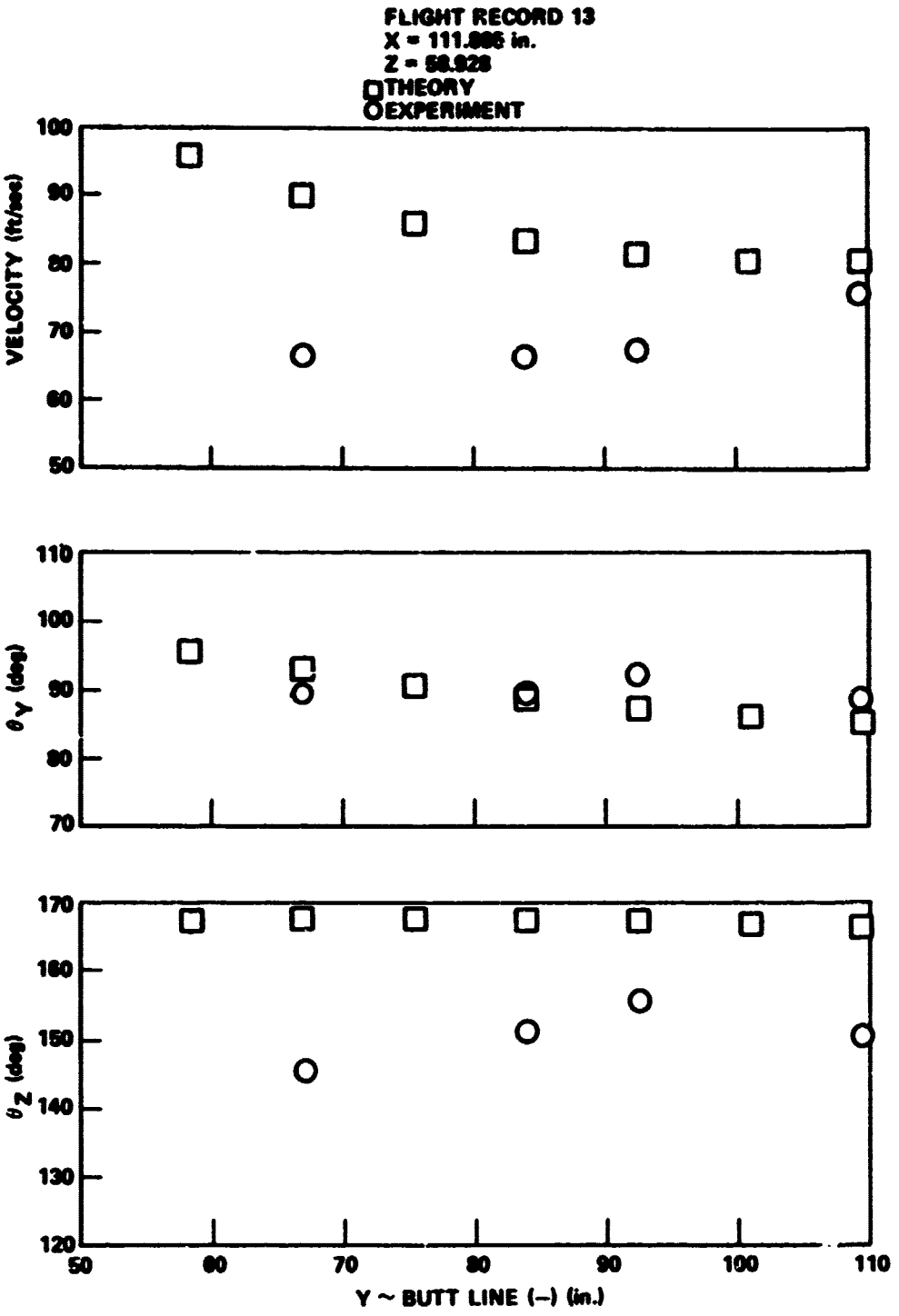

Figure 89. Continued.

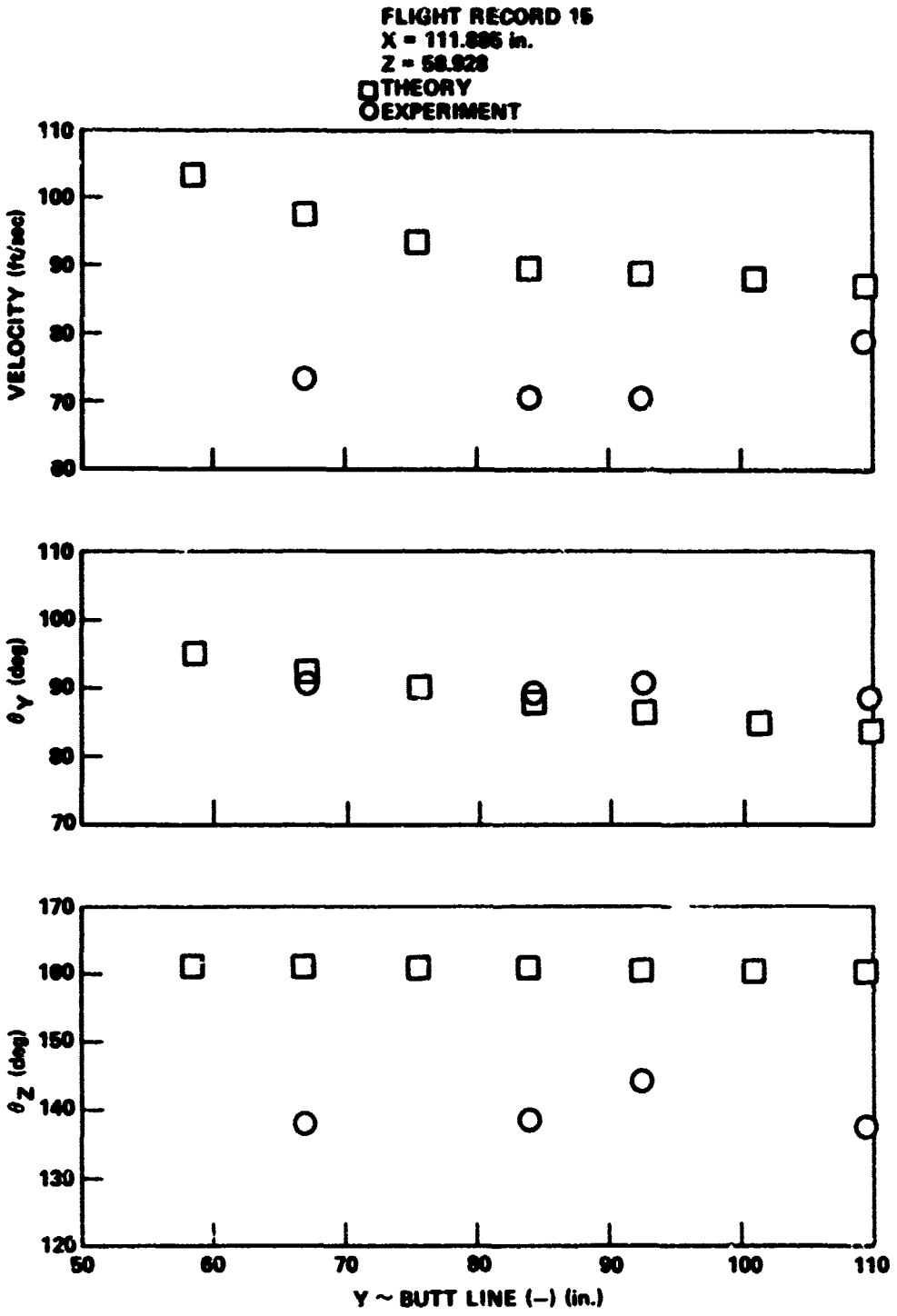

Figure 89. Concluded.

Appendix
FLIGHT TEST INSTRUMENTATION*

Flight test instrumentation were as follows:

LOCAL VELOCITY SENSING: Thermo Systems Inc. Model 1080 total vector anemometers including probes, control circuits, and chassis.

AMBIENT TEMPERATURE: Rosemount type 102AU2CK platinum resistance total temperature probe with Rosemount 510BF signal conditioning amplifier.

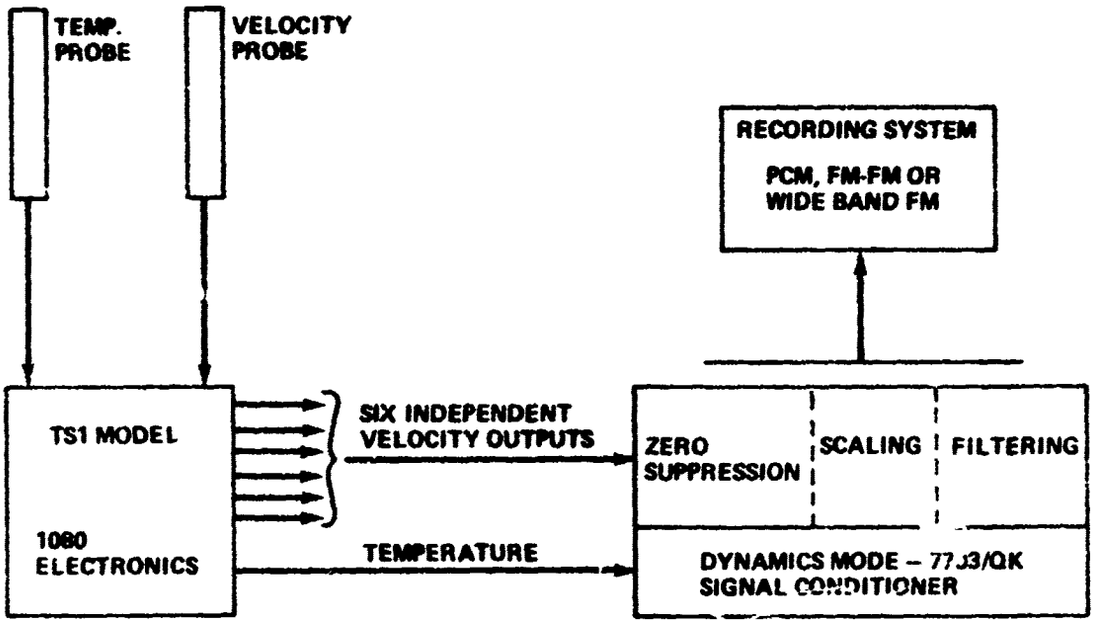

ROTOR POSITION: Defined once per revolution by a magnetic proximity sensor.

In addition, the following aircraft parameters were recorded with a state-of-the-art general purpose data system and were either measured or calculated from measured data (100 samples/second):

Angle of attack (boom)

Pitch attitude

Roll attitude

*This is a brief summary of material described in detail in reference 1.

Angle of sideslip (boom)

Yaw attitude

Pitch rate

Roll rate

Yaw rate

CG longitudinal acceleration

CG lateral acceleration

CG vertical acceleration

Rotor speed

(E) Longitudinal CAS (coarse)

(E) Longitudinal CAS (fine)

(E) Lateral CAS

(E) Total velocity

(E) Downwash velocity

(E) Vertical velocity

Calibrated airspeed

True airspeed

Pressure altitude

Density altitude

Ambient temperature

Temperature ratio

Air pressure ratio

Air density ratio

Speed of sound

Fuel used

Gross weight

Fuselage station of CG

Waterline of CG

Buttline

Main rotor tip speed

Rate of climb

Rotor tip speed ratio (advance ratio)

x component, true airspeed

y component, true airspeed

z component, true airspeed

x shaft component, true airspeed

y shaft component, true airspeed

z shaft component, true airspeed

Elliott angle of attack (sin)

Elliott angle of sideslip (sin)

Elliott angle of sideslip in A/C axis system

REFERENCES

1. Boirun, Barclay, Jefferis, Robert, and Holasek, Ronald, Rotor Flow Survey Program UH-1M Helicopter, May 1974, Final Report on USAASTA Project No. 72-05.

2. Operator's Manual, Model UH-1C/M Helicopter, Department of the Army Technical Manual, April 1971, TM 55-1520-220-10.

3. Crimi, Peter, Theoretical Prediction of the Flow in the Wake of a Helicopter Rotor, Part 1, September 1965, CAL Report No. BB-1994-S-1.

4. Crimi, Peter, Theoretical Prediction of the Flow in the Wake of a Helicopter Rotor, Part 2, September 1965, CAL Report No. BB-1994-S-2.

5. Crimi, Peter and Trenka, Andrew, Theoretical Prediction of the Flow in the Wake of a Helicopter Rotor, Addendum, August 1966, CAL Report No. BB-1994-S-3.

SYMBOLS

V - Magnitude of local air velocity = $\sqrt{VX^2 + VY^2 + VZ^2}$

VF - Airspeed of helicopter, ft/sec

VX, VY, VZ - Local air velocities relative to X, Y, Z axes, respectively, ft/sec

X, Y, Z - Cartesian coordinates relative to shaft axis system (moving with aircraft)

X = Fuselage station - inches
Y = Buttline - inches
Z = Waterline - inches
} see Figure 1

α_T - Inclination of tip path plane to freestream (equal to negative of angle of attack relative to shaft axis coordinates)

θ_X, θ_Y, θ_Z - Angles between local air velocity vector and X, Y, and Z axes, respectively

$\theta_X = \cos^{-1}(VX/V)$ etc

ρ/ρ_0 - Ratio of density at test altitude to reference density (0.002378 lb sec^2/ft^4)